MIT/WHOI

Massachusetts Institute of Technology
Woods Hole Oceanographic Institution

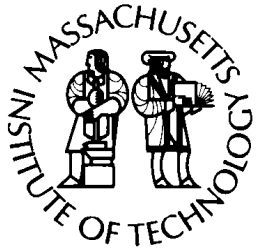

Joint Program in Oceanography/ Applied Ocean Science and Engineering

---

MASTER OF SCIENCE THESIS

Investigation of the Effect of a Circular Patch of Vegetation on Turbulence Generation and Sediment Deposition Using Four Case Studies

by

Alejandra C. Ortiz

June 2012

Investigation of the Effect of a Circular Patch of Vegetation on Turbulence Generation and Sediment Deposition Using Four Case Studies

By

Alejandra C. Ortiz

B.A., Wellesley College, 2010

Submitted in partial fulfillment of the requirements for the degree of

Master of Science

at the

MASSACHUSETTS INSTITUTE OF TECHNOLOGY

and the

WOODS HOLE OCEANOGRAPHIC INSTITUTION

JUNE 2012

Signature of Author……

Joint Program in Marine Geology & Geophysics
Massachusetts Institute of Technology
and Woods Hole Oceanographic Institution
May 11, 2012

Certified by……

Heidi M. Nepf
Thesis Supervisor

Accepted by……

Rob Evans
Chair, Joint Committee for Geology & Geophysics
Woods Hole Oceanographic Institution

Accepted by……

Heidi M. Nepf
Professor of Civil and Environmental Engineering
Chair, Departmental Committee for Graduate Students
Massachusetts Institute of Technology

Investigation of the Effect of a Circular Patch of Vegetation on Turbulence Generation and Sediment Deposition Using Four Case Studies

by

Alejandra C. Ortiz

Submitted in partial fulfillment of the requirements for the degree of Master of Science at the Massachusetts Institute of Technology and the Woods Hole Oceanographic Institution June 2012.

Abstract

This study describes the spatial distribution of sediment deposition in the wake of a circular patch of model vegetation and the effect of the patch on turbulence and mean flow. Two different types of vegetation were used along with two different stem densities totaling four different case studies. The spatial location of enhanced deposition correlated with the steady wake zone, which has length, L_1. The steady wake zone only occurred downstream of the rigid emergent patches of vegetation and was not seen downstream of the flexible submerged patches of vegetation. The enhanced deposition occurred when both turbulence and mean velocity was below the upstream, initial values. The enhanced deposition occurred when the mean velocity was less than or equal to half of the initial velocity. For the four cases studied, these parameters of low velocity and low turbulence were primarily met within the steady wake region immediately downstream of the two rigid emergent patches of vegetation. In all four cases, large coherent structures are created in the flow due to the patch. Lateral vortices are formed downstream of the patch in a von-Karman vortex street that meets at the center of the flow a distance, L_w, downstream of the patch. For the flexible submerged cases, streamlines reattach to the bed of the flume a distance, L_v, downstream of the patch. In addition, for the flexible submerged cases, secondary circulation is generated with flow moving laterally away from the patch at the surface and toward the centerline of the patch at the bed.

Thesis Supervisor: Heidi Nepf

Title: Professor of Civil and Environmental Engineering

Acknowledgements

First, I offer my sincerest gratitude to my advisor, Heidi Nepf, for her advice and help with my project. She has been invaluable with her patience and expertise on this project. I would also like to thank my advisor, Andrew Ashton, for his help and advice on this project. I would also like to thank him for his support for this science master.

Several students have been very generous with their support and advice over the last year. I would like to thank Elizabeth Follett, Natasha Maas, and Mara Orescanin. I would also like to thank Lijun Zong for her instruction and time. Finally, I would like to thank ZB Chen for his help in the lab and with the experiments.

Lastly, I give my most sincere thanks to my family and friends for all of their love and support. I also thank my mother for her editing and my friends for their unstinting encouragement.

This material is based upon work supported by the National Science Foundation under Grant Nos. EAR 0738352 and OCE 0751358. Any opinions, findings, and conclusions or recommendations expressed in this material are those of the authors and do not necessarily reflect the views of the National Science Foundation

Table of Contents

List of Figures

List of Tables

Nomenclature

H	height of water
x,y,z	streamwise, lateral, and normal directions
t	time
u_i	time averaged velocity components
u_i'	instantaneous velocity components
$u_{i,rms}$	intensity of turbulence fluctuations components
TKE	turbulence kinetic energy
U	total horizontal velocity
U_o	upstream velocity
U_e	exit velocity
U_1	steady wake velocity
L_o	upstream adjustment length
L_1	steady wake length
L_2	wake recovery length
L_w	length to maximum turbulence
L_v	vertical reattachment length
n	dowels per bed area
d	dowel diameter
h	height of canopy
a	frontal area per volume
D	diameter of patch
C_D	drag coefficient
C_o	initial sediment concentration
C_e	final sediment concentration
p	probability of sediment deposition
s	specific weight of sediment
S_*	non-dimensional fall velocity
r	sediment diameter
g	gravity
f	frequency
w_s	fall velocity
h_{meas}	depth of measurements
m	mass of sediment deposited
$C(t)$	concentration of sediment over time
C_f	bed friction coefficient
Re	Reynolds number

Greek Letters

ϕ	solid volume fraction
ψ	Shield's parameter
ν	kinematic viscosity
ρ	density

Chapter 1 Introduction

Biogeomorphology is the study of how feedbacks between vegetation and Earth surface processes affect the form and shape of landscapes. It analyzes the complex feedbacks and readjustments that exist between landforms, and physical and biotic processes (Corenblit et al., 2007). Fluvial systems have complex interplays between the land, the flow, and biota. The linkages in fluvial systems between vegetation and physical processes are conceptualized in the fluvial biogeomorphic succession model (Corenblit et al., 2007; Schnauder and Moggridge, 2009). This research aims to understand the feedbacks between aquatic plants, flow, and sediment deposition in fluvial systems, by investigating the relative importance of turbulence and mean flow on sediment deposition. We examine how porous patches of vegetation affect flow conditions, and consequently change depositional patterns.

River types can be strongly influenced by the presence of riparian vegetation. Vegetation consolidates and stabilizes riverbanks, allowing for meandering rivers to develop instead of braided streams (Murray and Paola, 2003; Rominger et al., 2010; Tal and Paola, 2007). Vegetation also grows within the channel as well as along the banks. In fluvial systems, in-channel aquatic vegetation typically exists in non-continuous patches (Corenblit et al., 2007; Naden et al., 2006). Aquatic vegetation modifies flow hydraulics (Schnauder and Moggridge, 2009). Vegetation found in rivers range from emergent reeds to submerged grasses. It affects water quality by

nutrient uptake, decreasing turbidity, and even heavy metal sequestration (Christiansen et al., 2000; Hendriks et al., 2008; Naden et al., 2006).

Within fluvial systems, the flow entrains and transports sediment. Alluvial rivers transport sediment in two different methods as bed load, sediment in contact with the bed, and suspended load, sediment independent of the bed (Church, 2006; Dade and Friend, 1998; Engelund and Fredsoe, 1976). Typically, transport as suspended sediment comprises 50-90% of the total sediment load in the river (Anderson and Anderson, 2011; Dade and Friend, 1998). Any sediment carried within the flow as suspended sediment is strongly affected by changes in flow characteristics. Sediment deposition patterns are spatially related to flow characteristics within a river. Usually, sediment deposition is considered dependent on the mean flow rather than turbulence (Bos et al., 2007; Christiansen et al., 2000; Rodrigues et al., 2006). There is controversy over the role turbulence plays in sedimentation. Some studies claim turbulence is important for sediment deposition while others suggest mean velocity is more important for sediment deposition (Boyer et al., 2006; Church, 2006; Nelson et al., 1995; Williams et al., 1989). Previous work in our lab group has focused on the spatial distribution of sediment deposition around a patch of vegetation where the primary transport is bedload rather than suspended load (Follett and Nepf, 2012). We specifically investigate suspended sediment transport and deposition.

1.1. Background

Aquatic vegetation is viewed as beneficial in fluvial restorations because it decreases near-bed velocity and stabilizes the sediment at the bed (Pollen and Simon, 2005). Vegetation also provides a heterogeneous habitat by creating different flow regimes (Kemp et al., 2000). Research has focused on the hydrodynamics of a continuous segment of vegetation (Bos et al., 2007; Ghisalberti and Nepf, 2006; Luhar et al., 2008; Murphy et al., 2007; Murphy et al., 2006; Peralta et al., 2008; Zong and Nepf, 2010). In fluvial systems, vegetation is commonly found segmented in patches (Naden et al., 2006; Sand-Jensen and Madsen, 1992; Schnauder and Moggridge, 2009). The presence of a patch of vegetation can divert the flow around the finite size such that there is enhanced flow locally on the edges of the vegetation patch, possibly inhibiting the expansion of the patch (Neumeier, 2007; Temmerman et al., 2005; Vandenbruwaene et al., 2011). This biogeomorphic feedback may limit the expansion of vegetation patches.

Previous research has emphasized the importance of different stem densities within the patch of vegetation on the flow and feedbacks with physical processes (Bos et al., 2007; Bouma et al., 2007; Rominger and Nepf, 2011; Schnauder and Moggridge, 2009). The individual plants in the patch of vegetation create a canopy, whose geometry is based on the individual plants. Given a patch of vegetation with a characteristic diameter of plants, d, and the number of stems per bed area, n, the frontal area per volume is $a = nd$. The amount of flow through the patch is based on the density of the patch described by the flow blockage value, $C_D aD$, such that high

flow blockage occurs for $C_DaD > 4$ and low flow blockage for $C_DaD < 4$. Cases of high flow blockage impose different behavior on the flow characteristics than low flow blockage patches of vegetation (Chen et al., 2012).

Recent work has focused on the flow behind patches of rigid emergent vegetation (Chen et al., 2012 ; Follett and Nepf, 2012; Zong and Nepf, 2011). The flow patterns observed in these cases differ from those for a flow behind a solid object because of the bleed flow, or flow through the patch. For a circular patch of vegetation of diameter, D, the flow blockage parameter is defined C_DaD. Given a rigid patch of vegetation composed of wooden dowels, a steady wake velocity region is observed behind the patch with a constant flow U_1 over a region a steady wake region, L_1 (Figure 1-1). The bleed flow and subsequent steady wake region delays the onset of the von-Karman vortex street, as visualized by Zong and Nepf (2012). When the von-Karman vortex street forms at the centerline of the flow, there is a peak in the turbulence production. This peak in turbulence production is located a distance L_w from the end of the patch. After the steady wake region, the velocity recovers in the wake recovery region for a distance, L2. This study investigates the different regions of flow that develop from an emergent rigid and a submerged flexible patch of vegetation and the subsequent spatial effect on sediment deposition.

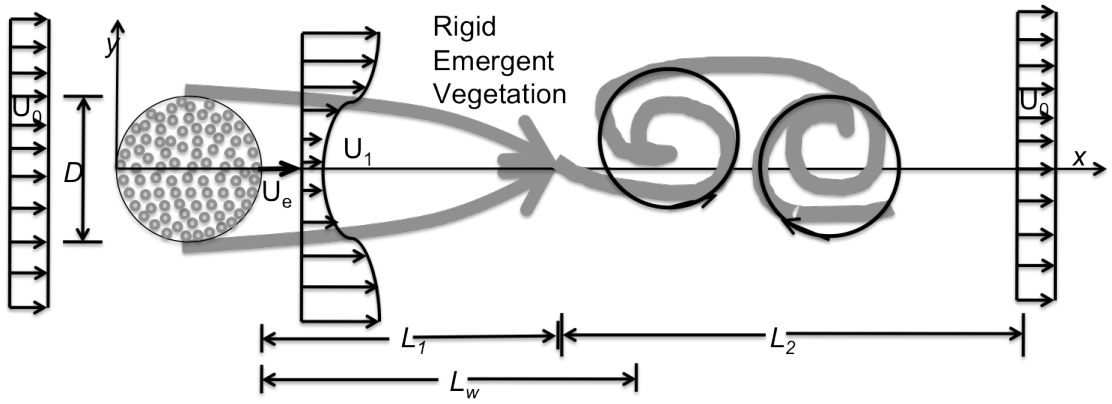

Figure 1-1. Conceptual plan-view diagram of the flow around a porous rigid emergent vegetation patch.

1.2. Outline

We focused on the effect of a single patch of vegetation (of differing rigidity and density) on flow characteristics and sediment deposition. The research examined the spatial distribution of sediment deposition, linking it to the spatial changes in mean flow and turbulence. Chapter 2 provides an in-depth summary of the different methodologies used in the experiments and subsequent data analysis. Chapter 3 details the results from each of the four case studies of varying vegetation type and density. The cases were divided by the type of vegetation studied and by the density of the vegetation patch. Chapter 4 discusses the linkages between the four cases, and, based on the data, predicts when and where enhanced sediment deposition will occur. Finally, Chapter 5 describes the conclusions of this research and recommendations for future work.

Chapter 2 Methodology

All the experiments were conducted in a flume with a patch of model vegetation. Two types of model vegetation were used to construct circular patches, with varying stem density. The experiments were run with model sediment. Velocity was measured with an Acoustic Doppler Velocimeter.

2.1. Experimental Measurements

The experiments were conducted in a 16-m long re-circulating flume; the test section is 1.2-m wide and 13-m long. A 25 hp pump was used to pump water from the tail box to the upstream head box where a large baffle dispersed flow across the width of the flume. The horizontal bed of the flume was covered with PVC baseboards, perforated with a staggered array of holes, 1 cm in depth for the length of the test section. The patch of model vegetation was constructed as a circular staggered array. Wooden dowels with a diameter d = 6.4 mm were used for the rigid emergent vegetation. The flexible vegetation was created using a piece of wooden dowel (d = 6.4 mm) 1 cm in height as a stem, with six thin blades of polyethylene film as the leaves. The model blade had a thickness of 0.2 mm, a width of 3 mm, and a length of 13 cm. The blades were attached to the wooden dowel piece with a piece of duct tape. The patch of vegetation had a diameter D = 42 cm. The projected frontal area, a, is calculated as $a = n*d$ in cm^{-1} where n is the number of dowels per bed area (cm^{-2}) and d is the dowel diameter (cm). The solid volume fraction is

calculated for each case using $\phi = n\pi d^2/4$. For each type of vegetation (flexible and rigid), two different stem densities were considered totaling four different cases studies. The two different patch densities with a solid volume fraction (SVF) were ϕ = 0.03 and ϕ = 0.10 for the stem region of each patch (Table 1). However, for the flexible blades, the SVF calculations were based on the number of blades of each plant that could be visible to the flow such that the range of SVF is ϕ = 0.04 – 0.25 and ϕ = 0.01 – 0.07 for the dense and sparse case respectively. For the rigid vegetation, the density of the patch was constant in the vertical; however, for the flexible vegetation, the density of the patch changed with the height above the bed.

Table 1. Summary of patch parameters for the four cases and two control experiments with standard deviations.

	n (cm^{-2})	a (cm^{-1})	C_DaD (cm^{-1})	SVF (%)	H (cm)	h (cm)	U_o (cm/s)
Rigid Control	-	-	-	-	13.5 ± 0.2	-	9.4 ± 0.2
Rigid Dense – Case 1	0.34 ± 0.02	0.20 ± 0.01	8.4 ± 0.4	9.6 ± 0.5	13.5 ± 0.2	14 ± 0.2	9.4 ± .2
Rigid Sparse– Case 2	0.09 ± 0.004	0.057 ± 0.03	2.5 ± 0.1	2.5 ± 0.1	13.5 ± 0.2	14 ± 0.2	9.4 ± 0.2
Flexible Control	-	-	-	-	21.5 ± 0.2	-	8.1 ± 0.2
Flexible Dense – Case 3	0.34 – 2.01 ± 0.02 - 0.1	0.134 - 0.80 ± 0.006 – 0.04	5.5 - 34 ± 0.3 – 2	4.2 – 25 ± 0.2 – 1	21.5 ± 0.2	10 ± 0.2	8.1 ± 0.2
Flexible Sparse– Case 4	0.09 - 0.57 ± 0.004 - 0.03	0.0381 - 0.23 ± 0.002 – 0.01	1.60 - 9.7 ± 0.08 – 0.5	1.20 – 7.2 ± 0.05 – 0.3	21.5 ± 0.2	8 ± 0.2	8.1 ± 0.2

The two values of SVF correspond to a high flow blockage and low flow blockage configuration. These values of SVF are representative of densities found in

different aquatic vegetation (Nepf, 2012). In mangrove systems, the SVF can be quite high, Φ = 0.45 (Mazda et al., 1997). Submerged grasses, on the other hand, tends to have lower SVF where Φ = 0.01 - 0.1 (Ciraolo et al., 2006).

The upstream flow velocity, U_o, was defined as the velocity measured on the centerline at x = -100 cm (x/D = -2.4) at the highest distance above the bed. The velocity scale, U_o, was used to normalize all the velocity data. A weir at the end of the flume controlled water depth. Two different flow depths were used to ensure velocity measurements could be taken above the top of the flexible vegetation canopy. For the flexible vegetation, the flow depth was H = 21.5 ± 0.2 cm; in the rigid vegetation cases, the flow depth was H = 13.5 ± 0.2 cm. For the flexible vegetation, the sparse case had a canopy height of h = 8.0 ± 0.2 cm; for the dense vegetation patch, the canopy height was higher due to the greater numbers of plant blades such that h = 10.0 ± 0.2 cm.

The coordinate system was defined with x in the streamwise direction, y cross-stream, and z vertical depth to the bed where x = 0 at the start of the patch; y = 0 at the center of the patch; and z = 0 at the bed (Figure 2-1). The flow characteristics were assumed to be symmetrical about the y=0 line down the center of flume. Measurements for both deposition and velocity were taken only on one half of the flume.

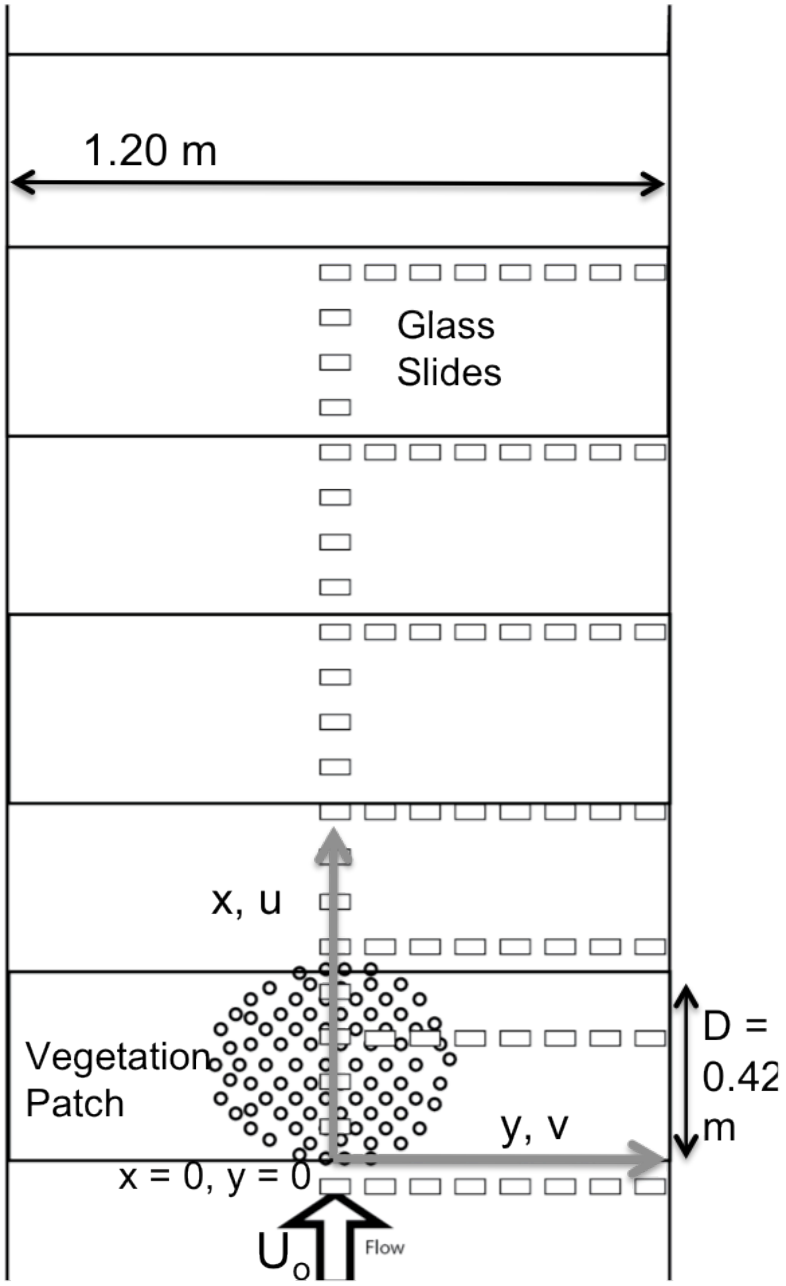

Figure 2-1. Plan-view deposition experiment setup in the flume. The large arrow shows the direction of the mean flow. The approximate locations of slides are indicated by the small rectangles on the bed of the flume. The location of the coordinate system is shown by the grey arrows, where x = 0 and y = 0 at the center and the upstream edge of the circular patch.

Velocity measurements were taken using a Nortek Vectrino acoustic Doppler velocimeter (ADV). The sampling volume of the ADV was 6 mm across and 3 mm high, and was located 5 cm from bottom of the instrument prongs (Figure 2-2 & Figure 2-3). The ADV was mounted on a movable platform above the flume, which enabled manual positioning along and across the flume with an accuracy of ± 0.5 cm in the *y* direction and ± 1 cm in the *x* direction and ± 1 cm in the *z* direction. Longitudinal transects were taken through the centerline of the flume from 1 meter upstream of the edge of the vegetation patch to 7 meters after the end of the patch (x = -2.4 – 17D). Lateral transects were also taken: upstream of the vegetation patch, in the vegetation patch, and downstream of the vegetation patch.

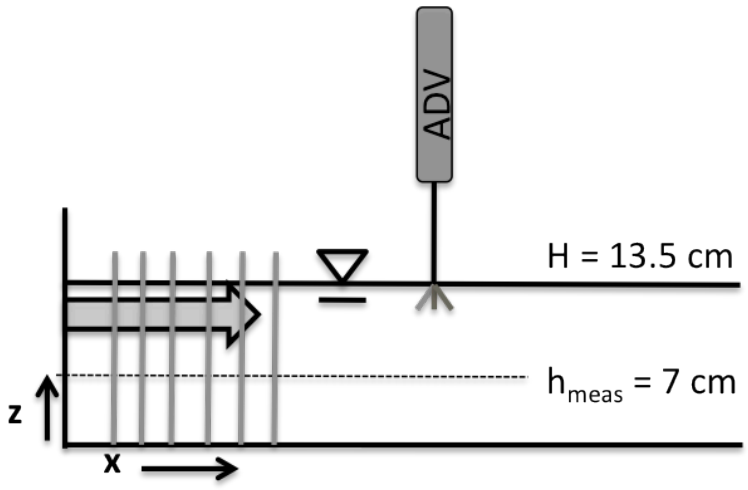

Figure 2-2. Diagram of ADV in flume for rigid emergent vegetation patch (Case 1 & 2). The grey rods represent the rigid patch. The ADV is measuring at a depth of 7 cm above the bed (h_{meas}) with a total water depth of H = 13.5cm.

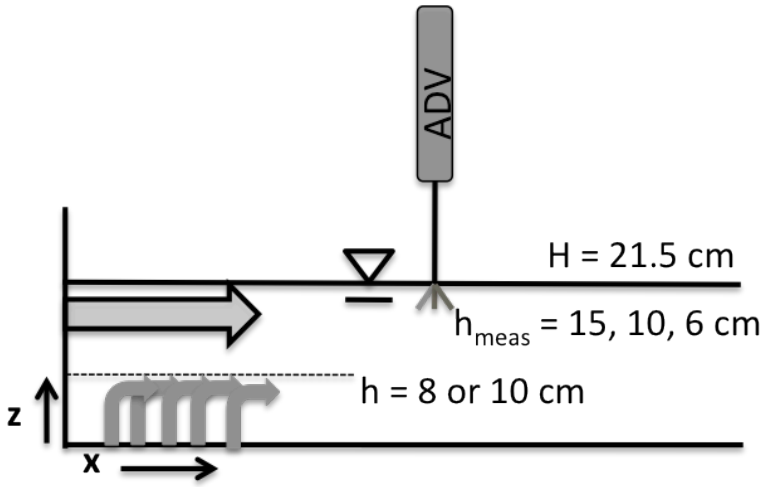

Figure 2-3. Diagram of ADV in the flume for flexible submerged sparse vegetation patch (Case 3 & 4). The flexible patch is represented by the bent grey arrows with the top of the canopy at h = 8 cm for the sparse canopy, for the dense canopy h = 10 cm. The ADV is measuring at a depth of 15, 10, and 6 cm above the bed (h_{meas}) with a total water depth of H = 21.5 cm.

2.2. Data Processing

The ADV collected instantaneous measurements of longitudinal (*u(t)*), lateral (*v(t)*), and vertical (*w(t)*) velocity at each measurement location for 240 s at a sampling rate of 25 Hz. The instantaneous velocity components were decomposed into the time average ($\overline{u}, \overline{v}, and\, \overline{w}$), where the over-bar indicates the time averaging, and fluctuating components (*u'(t), v'(t), w'(t)*) using MATLAB & Simulink Student Version, 2011b. The intensity of the turbulent fluctuations (u_{rms}, v_{rms}, w_{rms}) was estimated by the root-mean-square of the fluctuating components of velocity ($\sqrt{\overline{(u')}}$, $\sqrt{\overline{(v')}}$, and $\sqrt{\overline{(w')}}$). Finally, the turbulence kinetic energy (TKE), the kinetic energy per unit mass associated with the turbulent eddies, was calculated as the mean of the fluctuating components of velocity such that:

$$TKE = \frac{1}{2}\left(\overline{u'^2} + \overline{v'^2} + \overline{w'^2}\right) \quad (1)$$

Spectral analysis was used to analyze trends in the turbulence energy cascade. For given locations, a spectrum for each component of the velocity time series was produced utilizing MATLAB's inbuilt power spectral density with Welch's method. Given the low patch-scale Reynolds number ($Re = \frac{U_0 D}{\nu}$ = 39,000) and low stem-scale Reynolds number ($Re_{stem} = \frac{u_x d}{\nu}$ = 60 -320), the Strouhal number is equal to 0.2 (Norberg, 1994), allowing for the calculation of the expected frequency in the velocity spectra for both stem turbulence production and patch-sized turbulence production,

specifically: $$.2 = \frac{f_{stem} d}{U_x} \quad or \quad .2 = \frac{f_{patch} D}{U_o} \quad (2)$$

where f_{stem} was the frequency associated with the turbulence produced from the stem; and f_{patch} was the frequency associated with the turbulence produced from the patch itself in the form of a von Karman vortex street. In addition, *d* was the size of the stems (wooden dowels, *d*= 6 mm) and *D* was the patch diameter (*D* = 42 cm). However, for a Reynolds number close to 100 (i.e. Re_{stem} = 60 for Case 1), there is a deviation of the Strouhal number and the alternating vortices are not formed.

The deposition experiments were conducted separately from the ADV measurements. Numbered slides were placed along the bed of the flume, as shown in Figure 2-1. Net deposition was estimated by weighing each slide before and after

a deposition experiment. The slides (7.5 x 2.5 cm) were cleaned, numbered, and weighed prior to their use in the experiments. The flume was filled to the desired water depth, dependent on the vegetation type, with the circular patch of vegetation in the flume. The slides were placed perpendicular to the flow direction along the bed of the flume every 10 cm on the centerline in a longitudinal transect starting 1 meter before the patch (x/D = -2.4) and ending 6-8 meters (x/D = 14.3 – 19.0) after the patch (Figure 2-1). The flume was filled with water before the slides were placed to prevent the slides from being moved out of position by the infilling water.

Lateral slide transects were also placed upstream and downstream of the vegetation patch. Depending on the density of the vegetation patch, a different configuration of slides was placed within the patch itself. For the sparse patch (ϕ = 0.03), the regular-sized slides were placed every 2-3 cm along the centerline of the patch without any removal of plants. For the dense patch (ϕ = 0.10), five small slides (2.5x2.5 cm) were placed within the patch by removing a single plant at each location.

Once the slides were placed, the pump was started up slowly until the initial upstream flow velocity was reached (U_o) so that the slides would not move out of position. Spherical glass beads (made by Potters Industry with a diameter of 12 μm, a density of 2.5 g/cm^3, and a settling velocity of 0.01 cm/s) were used as the sediment in the deposition experiments. A total of 650 grams of the sediment was vigorously mixed with water in small containers before being poured into the flume upstream of the patch. Within a minute, the sediment was well mixed in width and

depth across the flume. The initial concentration in the flume was *Co* = 105 g/m^3 and 75 g/m^3 for the rigid and flexible vegetation cases respectively. *Co* was calculated by estimating the total volume of water within the flume, given the measured dimensions of the flume, the water height in each area of the flume, and dividing by the amount of sediment released. The flume was left to run for four hours. At the end of four hours, the flow was slowly decreased to prevent scour and to decrease the possibility of backwash from a sudden drop in velocity moving the slides. Once the flow was stopped fully, the flume was drained. This entire stopping process took around 20 minutes compared to a four-hour experiment.

The slides were then left to dry in the flume for 2-3 days until the sediment had formed a dry white coating on the slides and the rest of the flume was dry. The slides were carefully removed from the flume and put into a drying oven at 50° C for 2-4 hours to remove all excess moisture. The slides were reweighed to determine the amount of sediment deposited on each slide. The net deposition was calculated for each location by the difference in weight for each slide before and after the experiment divided by the area of the slide.

Each deposition study was run in triplicate for each plant case (i.e. rigid dense – Case 1, rigid sparse – Case 2, flexible dense – Case 3, and flexible sparse – Case 4). The variance among triplicates at each measurement position was used as an estimate of uncertainty for that position. In addition, for each water depth–velocity combination, a control deposition experiment was run with the flume empty of vegetation but otherwise with the same setup (i.e. PVC baseboards

covering the bed and slides used to determine net deposition). The control experiment indicated the background deposition without vegetation for the given initial flow U_0 = 9.4 ± 0.2 cm/s or U_0 = 8.1 ± 0.2 cm/s and water height H = 13.5 ± 0.2 cm or H = 21.5 ± 0.2 cm.

The deposition data showed high variability between the replicates in the cases of the flexible vegetation within the patch. The large variance within and around the flexible patch was due in part to the plant blades falling onto the slides while drying and wiping off sediment. Attempts were made to decrease this occurrence as the flume was drained, but these were limited by concerns of disturbing the sediment off the slides while still wet. This issue only occurred with the flexible blades; therefore, all values that were affected by the blades were removed from the analyses.

Mean total deposition was estimated for each of the deposition cases and the two control experiments. The net deposition was taken from the longitudinal transect along the centerline of the flume for each slide measurement. The net deposition measured for each slide was then used as the net deposition for a larger area around the slide. The area covered half the distance streamwise until the next slide and from the center to 21 centimeters laterally (x/D = 0.5) (~ 210 cm^2). The sum of the net deposition from the center to 21 centimeters laterally and from 1 meter upstream of the patch to 8 meters downstream of the patch was divided by the bed area of the flume covered by the deposited sediment. This value was then recorded as the net mean deposition for the given experiment.

2.3. Data Analysis

An advective-deposition model was used to analyze the spatial deposition patterns for each of the four vegetation cases and the two control experiments. The model (Zong and Nepf, 2010) was used to estimate the total sediment accumulation per unit area on the bed of the flume as a function of x (longitudinal or streamwise distance), such that

$$m(x) = p\, w_s \int_0^T C(t)dt \tag{3}$$

Where w_s is the calculated fall velocity for the spherical glass particles (w_s = 0.01 cm/s) (Madsen). C(t) is the suspended sediment concentration in the flow over time estimated from knowing the initial concentration, based on the amount of sediment poured into the flume and volume of water, and extrapolating the final concentration of sediment in the flow ($C_e = C(4\ hours)$) by extrapolating the total amount of sediment deposited on the bed of the entire flume. This is then integrated over the total duration of the experiment. Finally, p is a probability function of sediment depositing in the flow based on the Engelund-Fredsoe Equation (Engelund and Fredsoe, 1976). This equation predicts whether or not sediment will be deposited using the probability based on the critical shear stress: as flow decelerates, the local friction velocity, u_*, decreases and the probability that sediment will deposit increases until ψ equals ψ_{cr}.

The non-dimensional shields parameter is estimated from:

$$\psi = \frac{u_*^2}{(s-1)gr} \tag{4}$$

where s is the specific weight of the sediment (ρ_s/ρ_w = 1.25*)*; g is gravity 981 cm/s^2, r is the sediment diameter (r = 0.0012 cm); and $u_*(x)$ is the friction velocity estimated from $u_* = U\sqrt{C_f}$. C_f is the bed friction coefficient previously measured for flow over the PVC boards to be 0.006 (Zong and Nepf, 2010). U was calculated as the total horizontal velocity measured at each location in x such that $U = \sqrt{\overline{u}^2 + \overline{v}^2}$. The specific sediment weight is s = 2.5. Finally, ψ_{cr} is calculated using the modified Shield's diagram such that $\psi_{cr} = .1S_*^{-2/7}$ (Madsen and Grant, 1976). S_* is the non-dimensional value that is a function of the fluid and sediment properties such that $S_* = \frac{r}{4\nu}\sqrt{(s-1)gr}$ where ν = 0.01 cm^2/s is the kinematic viscosity for fresh water at a temperature of 20°C. The estimated non-dimensional ψ_{cr} = 0.25. Though, the Shield's value can be unrealistic at very low Re$_*$ values (where the sediment size is small), given that the glass spheres were well mixed before and were perfectly spherical, clumping and flocculating were assumed to be minimal (Madsen; Madsen and Grant, 1976). Thus, the use of the extended Shield's parameter at low values was valid. For $\psi < \psi_{cr}$, the probability function is set to p = 1. For $\psi > \psi_{cr}$, the probability that sediment will be deposited is less than unity due to initiation of motion because the shear stress is above the critical shear stress.

The above deposition model did not take into account a change of bed roughness and equivalent u^* values within the patch. It also assumed that $C(t)$ was a

linear decrease over time, and well mixed over depth and width throughout the experiment. Visually, this did seem to be a valid assumption. After the four hours of the experiment, the sediment was still well mixed laterally and vertically. Previous work with this model fit the resultant curves to the actual deposition data by varying the estimated fall velocity w_s; in this study, this was not done as the model was used purely to estimate trends in the data set (Zong and Nepf, 2010).

Chapter 3 Results

3.1. Control Experiments

A control deposition experiment was run for both the h = 13.5 cm (equivalent to the rigid emergent patch of vegetation Case 1 & 2) and the h = 21.5 cm (equivalent to the flexible submerged patch of vegetation Case 3 & 4). These two deposition experiments were run to estimate the variability in spatial deposition along the flume. The control for the rigid emergent cases has a mean deposition of 0.0025 ± 0.0001 g/cm^2 where the error is estimated from the variability inherent in both the longitudinal profile along the centerline and the variability along the lateral transects that mirrored each other (Figure 3-1). The control for the flexible plant cases has a mean deposition of 0.0026 ± 0.0002 g/cm^2 where the error is calculated the same as for the other control experiment (Figure 3-2). The mean net deposition for the rigid control experiment is 0.0025 ± 0.0003 g/cm^2. The mean net deposition for the flexible control experiment is 0.0027 ± 0.0003 g/cm^2.

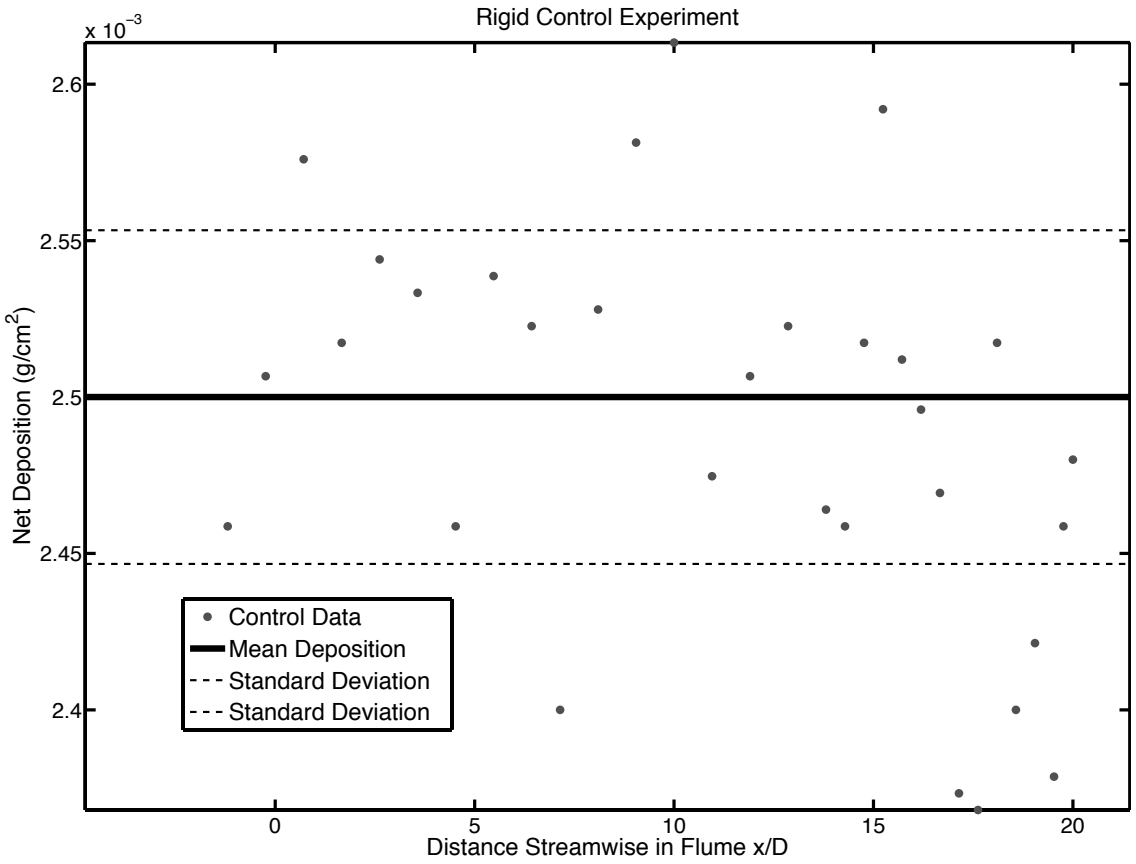

Figure 3-1. Net deposition along centerline of flume for control experiment where H = 13.5 cm with plotted mean and standard deviation of net deposition.

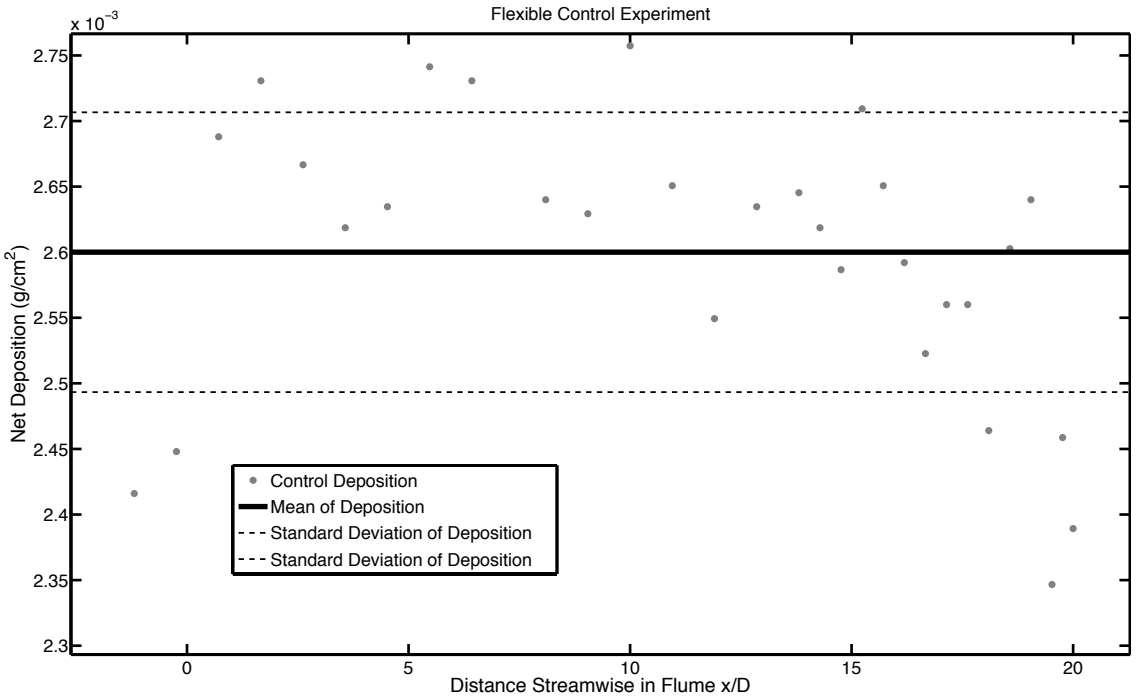

Figure 3-2. Net deposition along centerline of flume for control experiment where H = 21.5 cm with plotted mean and standard deviation of net deposition.

3.2. Rigid Emergent Vegetation

Case 1 and Case 2 were specifically chosen such that they fell into the high flow blockage ($C_D aD$ = 8.4) and low flow blockage ($C_D aD$ = 2.5) cases respectively (Table 2). Upstream of the patch, flow is affected by the patch a distance, L_o, the upstream adjustment length, which is proportional to the diameter of the patch, D (Figure 3-3 & Figure 3-4). Different flow regimes develop based on the flow blockage, where the high flow blockage experiences decreased flow through the patch itself and has very low flow, $U_1 \sim= 0.05U_o$, immediately downstream of the patch and an area of recirculation (Table 2 & Figure 3-3). The low flow blockage case has increased flow through the patch compared to the high flow blockage case such that the flow immediately downstream of the patch, $U_1 = 0.5U_o$, with no area of

recirculation (Table 2 & Figure 3-4). The area of low flow, U_1, lasts for the steady wake region, L_1. Within the steady wake region, there is both low velocity and low turbulence. The shear layers converge on the centerline of the flume at the distance, L_1, creating the von-Karman vortices. The presence of the von-Karman vortices increases turbulence and velocity, and the peak in TKE is at a distance, L_w. The velocity increases in the wake recovery zone, L_2, till by the end of L_2 the flow has recovered back to initial upstream velocity.

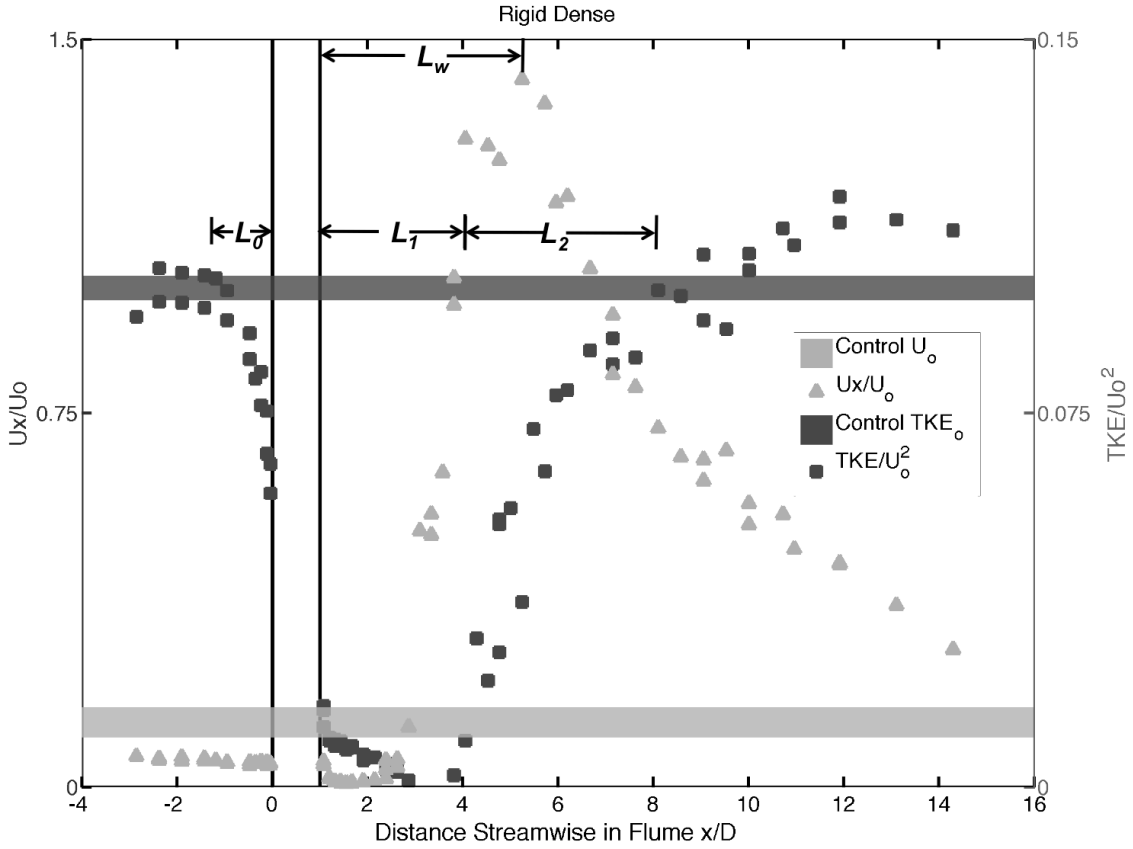

Figure 3-3. Mean velocity and turbulence along the centerline of the flume for Case 1. Mean velocity normalized to U_o on primary axis. *TKE* normalized on secondary axis. The x-axis is streamwise distance normalized *D*. The control velocity with standard deviation is plotted as the solid black line. The control turbulence with standard deviation is plotted as the solid grey line on the secondary axis. The different flow regimes seen in the conceptual diagram, **Figure 1-1**, are labeled by the parameters L_o, L_1, L_w, L_2 (**Table 2**).

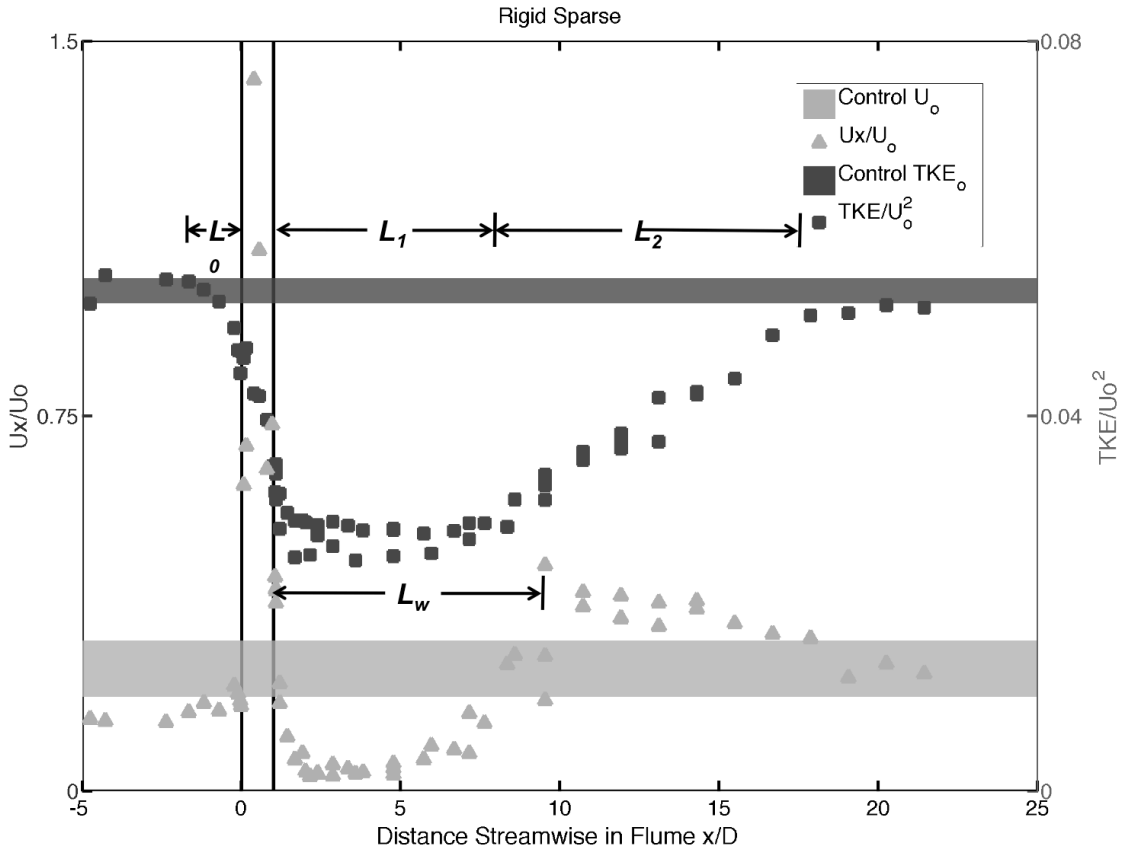

Figure 3-4. Mean velocity and turbulence along the centerline of the flume for Case 2. Mean velocity normalized to U_o on primary axis. *TKE* normalized on secondary axis. The x-axis is streamwise distance normalized *D*. The control velocity with standard deviation is plotted as the solid black line. The control turbulence with standard deviation is plotted as the solid grey line on the secondary axis. The different flow regimes seen in the conceptual diagram, **Figure 1-1**, are labeled by the parameters L_o, L_1, L_w, L_2 (**Table 2**).

Table 2. Summary of measured flow parameters with calculated standard deviation for rigid emergent patch of vegetation (Case 1 & 2).

	C_DaD	H	h	U_o	U_1	L_1	L_w	L_2	Mean Total Deposition (g/cm²)
Rigid Control	-	13.5 ± 0.2	-	9.4 ± 0.2	-	-	-	-	0.0025 ± 0.0003
Rigid Dense – Case 1	8.4 ± 0.4	13.5 ± 0.2	14 ± 0.2	9.4 ± 0.2	$0.05U_o$ ± $.06U_o$	2.8D ± 0.5D	4.2D ± 0.5D	4.3D ± 0.5D	0.0022 ± 0.0004
Rigid Sparse– Case 2	2.5 ± 0.1	13.5 ± 0.2	14 ± 0.2	9.4 ± 0.2	$0.53U_o$ ± $.05U_o$	6.6D ± 0.7D	8D ± 2D	10.2 D ± 0.7D	0.0026± 0.0004

3.2.1. Case 1 – Rigid Dense

Velocity measurements are taken at 7 cm above the bed of the flume. These measurements are used to visualize the flow characteristics around the patch of vegetation (Figure 3-5). The flow is strongly diverted around the patch laterally at x = 0 – 1.5 D, and the velocity increases locally (u_x = 1.6U_o) by the diversion around the patch. The flow is then directed back towards the center of flume where the flow is back to initial flow (within 10% of U_0) by 4 meters from the patch (x = 9.5D, L_2 = 4.3D) (Figure 3-3). In addition, measurements directly downstream of the patch demonstrate the marked decrease in velocity. This effect of the patch on the flow creates a zone of very low velocity known as the steady wake region, L_1 = 2.8D. There is also a section of recirculation along the centerline starting at x = 3.1 – 3.8 D from the start of the patch (Figure 3-6). The velocity measurements along the centerline are not pointed purely in the streamwise direction due probably to instrument position error, i.e. the ADV was not facing exactly perpendicular to flow.

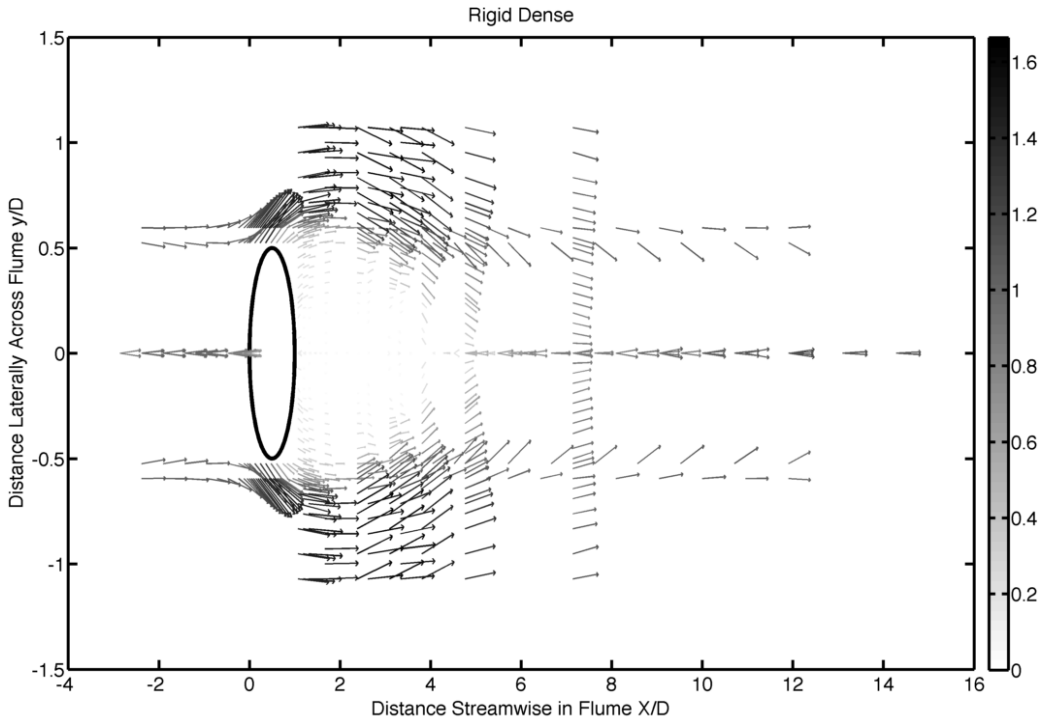

Figure 3-5. Quiver plot of the flume in plan view for Case 1, where the length of the arrows and the color of the arrows indicate the horizontal velocity magnitude.. The colorbar on the right shows the total horizontal velocity relative to the U_0. The location of the patch is shown by the black ellipsoid.

To visualize the change in velocity and deposition, data collected along the centerline of the patch are graphed (Figure 3-6). The velocity measurements are normalized by the upstream velocity, U_o, as calculated from the control experiments (Table 2 & Table 3). In addition, the y-axis limits are set such that the dashed black line is located at the measurement from the control experiments (i.e. in the rigid control experiment, u_{rms}/U_o = 0.13 ± 0.3 cm/s). The secondary y-axis plots the mean deposition values relative to the control mean deposition, by subtracting the mean deposition from the local deposition. The dark gray shaded line is the measured standard deviation from the three replicates, where the middle of the grey area

marks the mean value of the three replicates. The dashed black line also denotes the zero deposition relative to the control (i.e. anything below that line is deposition that is less relative to the control, while anything above the zero line indicates enhanced deposition relative to the control experiment). The location of the vegetation patch is shown by the thick black vertical lines located at x= 0D & 1D.

Deposition upstream of the patch is highly variable between the three replicates, as indicated by the high variance (Figure 3-6). Downstream of the patch, the deposition increases relative to the control experiment for 1 meter behind the patch (till x = 3D). From x > 3.5D, the deposition is lower than the control, and it stays lower to the end of the measurement section (x = 21D). The decrease in deposition, relative to the control, corresponds to the positions with an increase in u_{rms} and TKE. The peak in TKE and u_{rms} at x = 5D corresponds to where the von-Karman vortex street begins, L_w = 4.2D (Table 2).

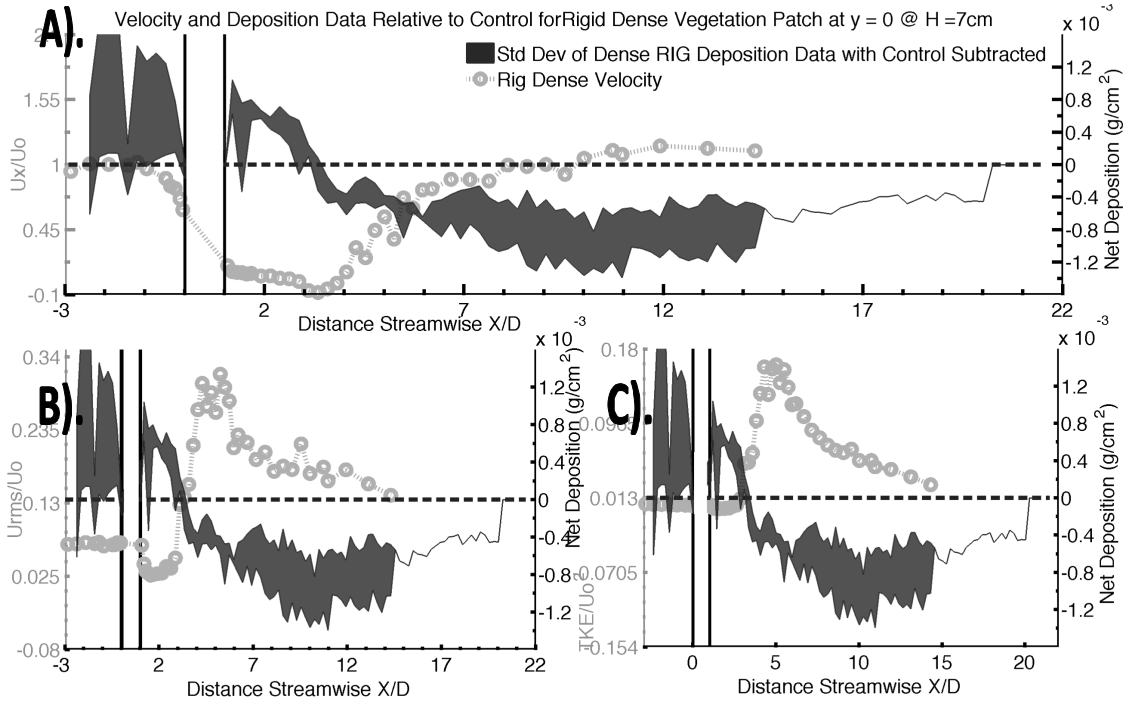

Figure 3-6. Deposition and velocity along centerline of the flume for Case 1. The x-axis is normalized by the patch diameter, *D*. The secondary y-axis is the net deposition relative to the control experiment (g/cm²). The location of the patch in the streamwise direction is indicated by the black vertical lines on each graph. A) U/U_0 on the primary y-axis and the mean deposition of the three replicates with the standard deviation of the replicates indicated by the edges of the polygon fill on the secondary y-axis. B) u_{rms}/U_0 on the primary y-axis. C) TKE/u_o^2 on the primary y-axis.

The lateral velocity transects indicate the lateral extent of patch influence on the flow(Figure 3-7). Directly downstream of the patch at x = 1.2D, flow is strongly depressed to 0.05U_o, but a large increase in velocity to 1.5U_o is visible at the lateral edge of the patch (x = 0.5D). At half a meter behind the patch (x = 2.4D), the lateral transect is still similar in structure to that measured directly behind the patch. By three meters from patch (x = 7.14D), the flow is laterally uniform. Directly downstream of the patch, there is a peak in u_{rms} that increases strongly at 1 meter from the patch (x = 2.4D). Even though the u_{rms} remained high along the centerline

of the flume after the peak at x = 6D (Figure 3-6), it is much less than the u_{rms} spikes at x = 1.2D and 2.4D.

Directly downstream of the patch, there is a spike in *TKE* at the lateral edge of the patch (y = 0.5D), and this elevated region of TKE moves laterally inwards towards the center moving downstream (x = 2.4D). This is associated with the shear layer forming at the edges of the wake and growing inward over distance (Figure 3-7). However, by three meters from the patch (x = 7.1D), the *TKE* is significantly elevated over the entire lateral transect corresponding to the presence of the large coherent turbulent structures of the von-Karman vortex street, L_w = 4.2D (Figure 1-1).

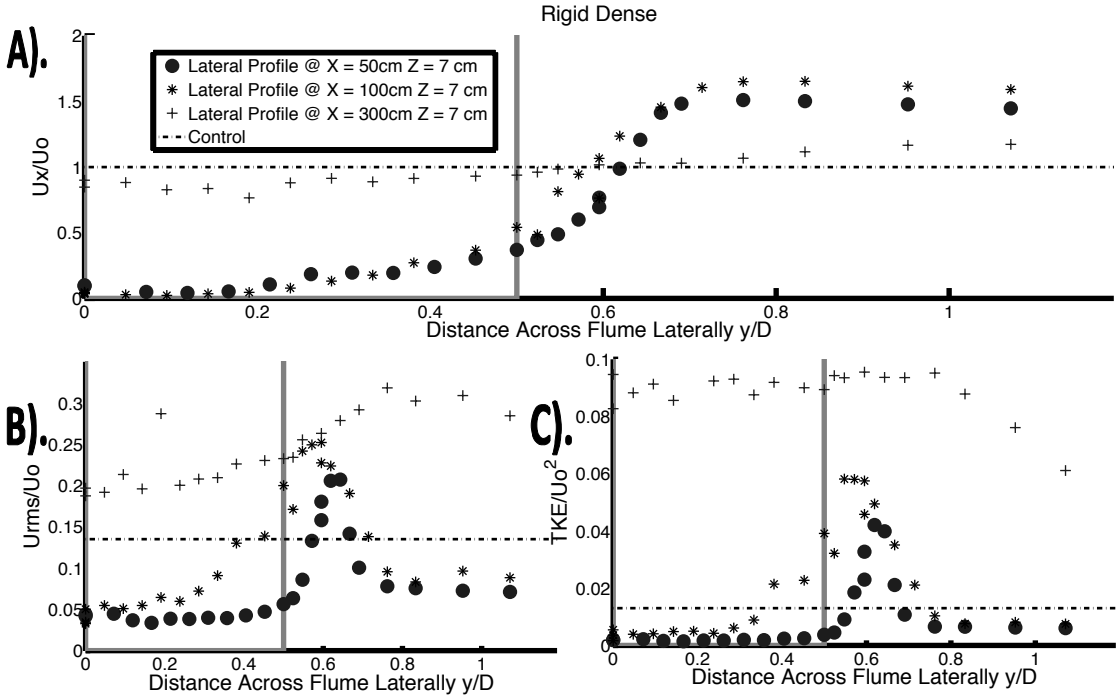

Figure 3-7. Lateral transects of normalized A) velocity, B) urms, and C) TKE for Case 1. The horizontal axis is the distance across the flume from the center of the flume (y = 0), normalized by the patch diameter.

Spectral analyses of the velocity measurements taken along the centerline indicate the varying production terms of turbulence (Figure 3-8). Upstream of the patch of vegetation (x = -2.4D), the spectra have no distinctive peaks indicating a lack of a specific length scale to turbulence production. Downstream of the patch (x = 2.6D), the largest peak in S_{vv} is observed to correspond with the turbulence associated with the length scale of the entire patch of vegetation f = 0.05 Hz using the upstream initial velocity. There is no peak observed in turbulence associated with the length scale of the individual dowel stems because the stem Reynolds's number is around 60, thus there is no vortex shedding (Norberg, 1994).

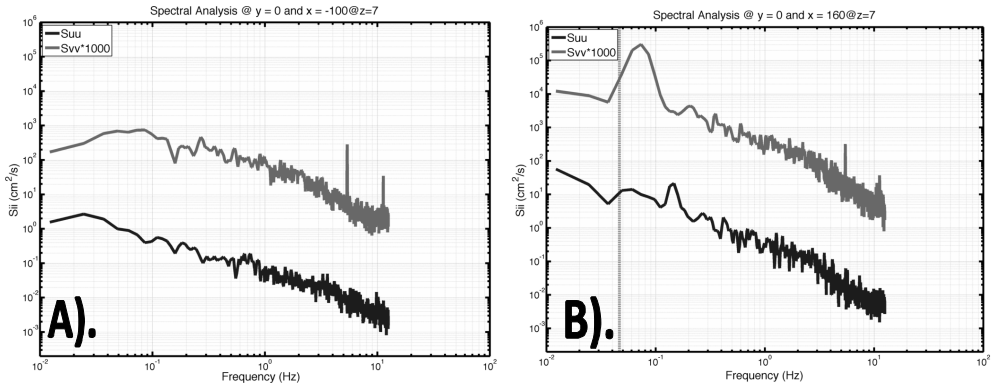

Figure 3-8. Spectral analysis of velocity data taken along centerline of flume at 7 cm depth for Case 1, where x = -2.4D and 2.6D (A and B). The x-axes are the frequency (Hz) and the y-axes are the spectra in cm^2/s. Each graph has two curves plotted; the black line is the spectra in the x-component (Suu) and the grey line is the y-component (Svv). B), the vertical grey line marks the turbulence production based on the size of the entire vegetation patch (see **Methodology** for calculation).

3.2.2. Case 2 – Rigid Sparse

The rigid emergent sparse vegetation patch affects the flow characteristics for 7 meters (x = 16.8D). The flow is diverted laterally around the patch (x = 0 – 1 D), accelerating around the outer edge (u_x = 1.1U_o) (Figure 3-9). The flow is decreased downstream of the patch; the decreased flow lasts for 6 meters from the start of the

patch (x = 14.2D). The magnitude of flow retardation and acceleration is less than that for the rigid emergent dense patch of vegetation where U_1 = 0.05U_o and U_1 = 0.5U_o in Cases 1 and 2, respectively (Table 2). However, the distance of the steady wake zone is longer for Case 2 than Case 1 (i.e. L_1 = 2.8D and L_1 = 6.6D for Cases 1 and 2, respectively). In addition, the wake recovery is longer for Case 2 than Case 1 (L_2 = 4.3D and L_2 = 10.2D for Cases 1 and 2, respectively). There is no recirculation zone for Case 2 as it is a low flow blockage case (Chen et al., 2012 ; Rominger and Nepf, 2011; Zong and Nepf, 2011).

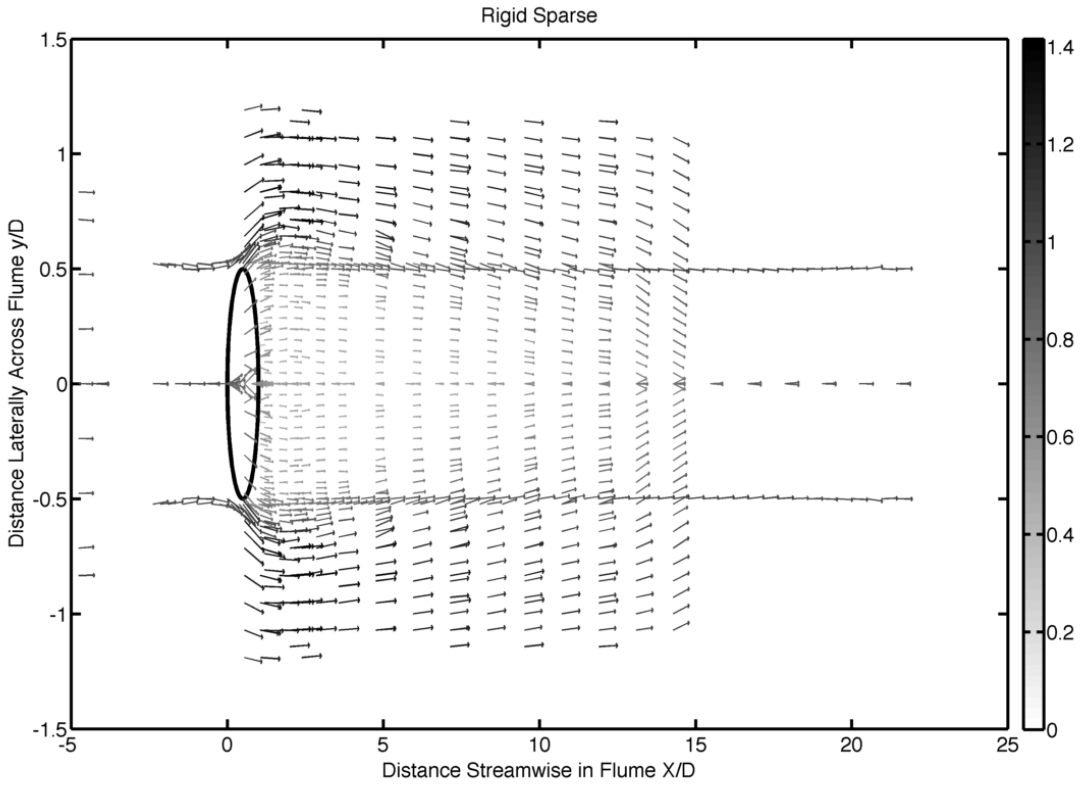

Figure 3-9. Quiver plot of the flume in plan view for Case 2, where the length of the arrows and the color of the arrows indicate the horizontal velocity magnitude**.** The colorbar on the right shows the total horizontal velocity relative to the U_0. The location of the patch is shown by the black ellipsoid**.**

The deposition upstream of the patch is only slightly elevated above the control deposition (Figure 3-10). Downstream of the patch, however, there is enhanced deposition relative to the control deposition for 3 meters ($x = 8D$), which corresponds to the steady wake region ($L_1 = 6.6D$). This trend follows the decreased mean flow, u_x, and the depressed u_{rms} and *TKE*. After 4 meters (x = 9.5D), the deposition is no longer elevated relative to the control, and both u_{rms} and *TKE* are also elevated. The mean flow, u, does not increase back to the initial flow until around 6-7 meters, $L_2 = 10.2D$, (x = 14.2D). Within the patch, both the u_{rms} and *TKE* are elevated. In addition, there is decreased deposition within the patch relative to the control, and relative to the deposition immediately downstream of the patch. The spike in u_{rms} and *TKE* is highest within the patch compared to the rest of the flume (Figure 3-10 & Figure 3-11).

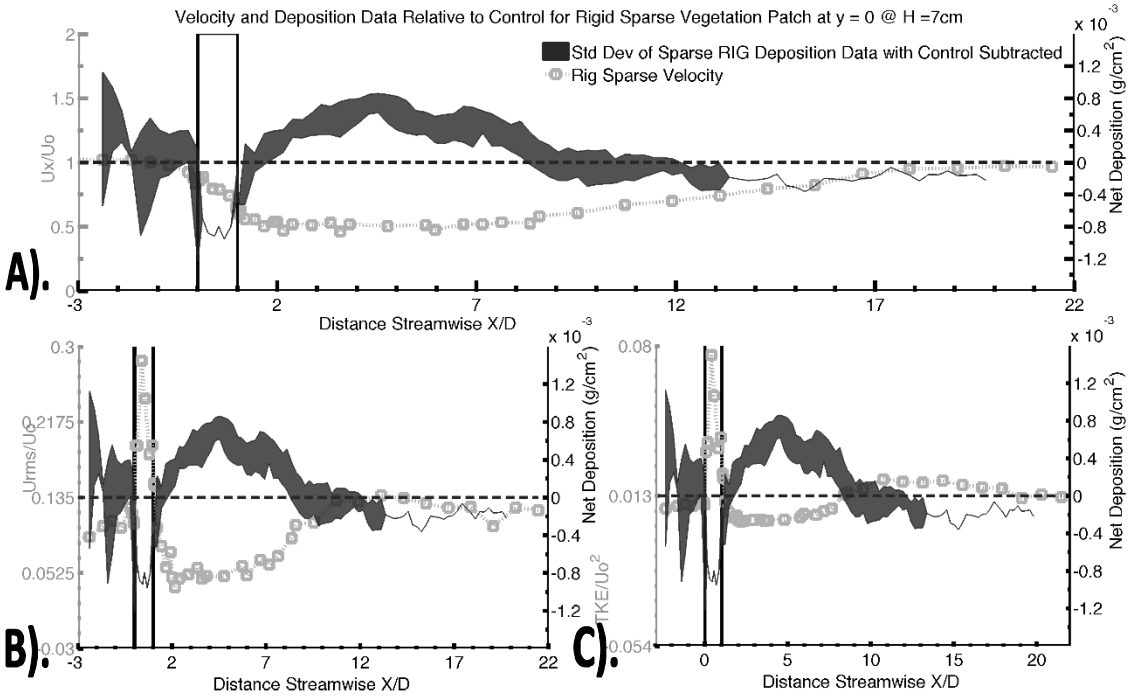

Figure 3-10. Deposition and velocity along centerline of the flume for Case 2**.** The secondary y-axis is the net deposition relative to the control experiment (g/cm^2). The location of the patch in the streamwise direction is indicated by the black vertical lines on each graph. A) U/U_0 on the primary y-axis and the mean deposition of the three replicates with the standard deviation of the replicates indicated by the edges of the polygon fill on the secondary y-axis. B) u_{rms}/U_0 on the primary y-axis. C) TKE/u_o^2 on the primary y-axis.

Upstream of the patch, the mean flow is laterally uniform within uncertainty of the measurements (Figure 3-11). Downstream of the patch, the flow is depressed on the centerline ($u_x = 0.5U_o$); but elevated outside the patch wake ($u_x = 1.4U_o$). Moving downstream from the patch, the mean flow gradually becomes laterally uniform until by $x = 14.3D$, ($u_x = 0.8 – 1.1\ U_o$). Upstream of the patch, both u_{rms} and TKE are relatively low; it is 0.8 of the measured open channel flow from the control experiment. Immediately downstream of the patch, there is a peak in u_{rms} and TKE at the lateral edge of the patch ($y = 0.5D$). Further downstream, u_{rms} and TKE remain elevated compared with both the upstream flow and the open channel flow from the

control experiment. In addition, while elevated overall, the *TKE* is not laterally uniform; the u_{rms} is laterally uniform. Both of the values remain elevated above the open channel flow due to initiation of the von-Karman vortex street at the center of the flume, L_w.

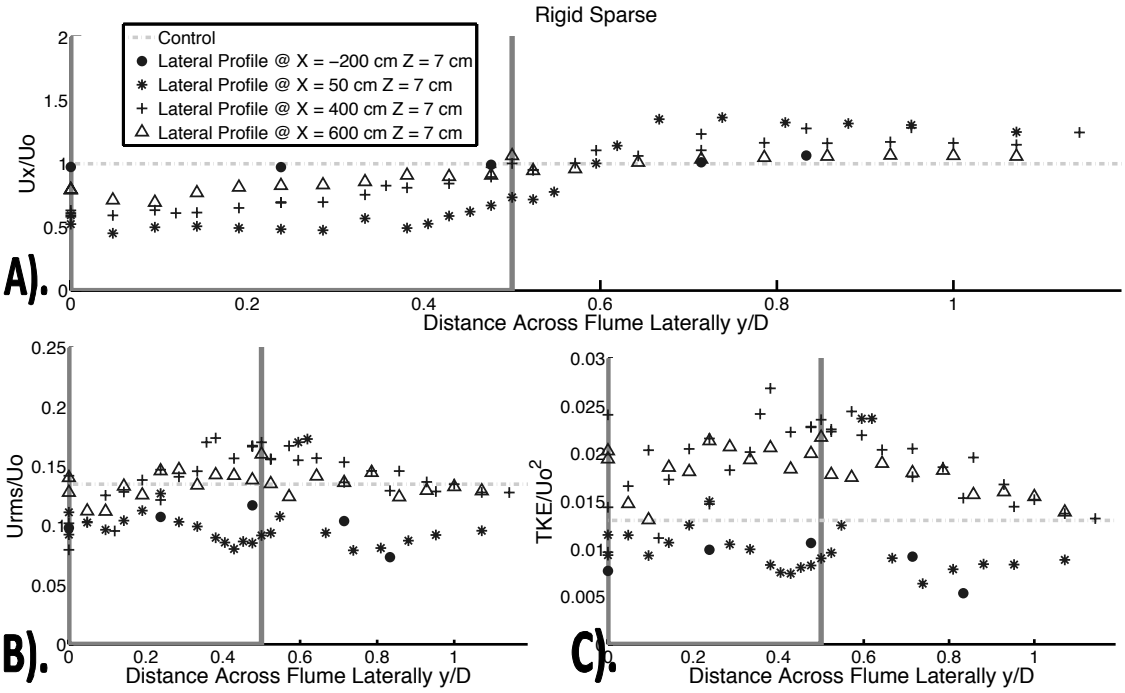

Figure 3-11. Lateral transects of normalized A) velocity, B) urms, and C) TKE for Case 1. The x-axis is the distance across the flume from the center of the flume (y = 0), normalized by the patch diameter.

Within the patch of vegetation and immediately downstream of the patch of vegetation, there is a peak in the turbulence energy cascade linked to the individual wooden dowel stem (Figure 3-12) the grey vertical line marks the predicted frequency for the individual stems, f_{stem} = 2.5 Hz (as calculated in Methodology). For the sparse case, the Re_{stem} = 320, thus the predicted presence of vortices off of the dowel is expected unlike in Case 1, where $Re_{stem} \sim 60$. Further downstream where there are peaks in u_{rms} and *TKE*, the largest peak in the power spectra is linked to the

von-Karman vortices created by the diameter of the patch of vegetation, f_{patch} = 0.04 Hz (where the vertical grey line marks the predicted frequency for the length scale of the patch).

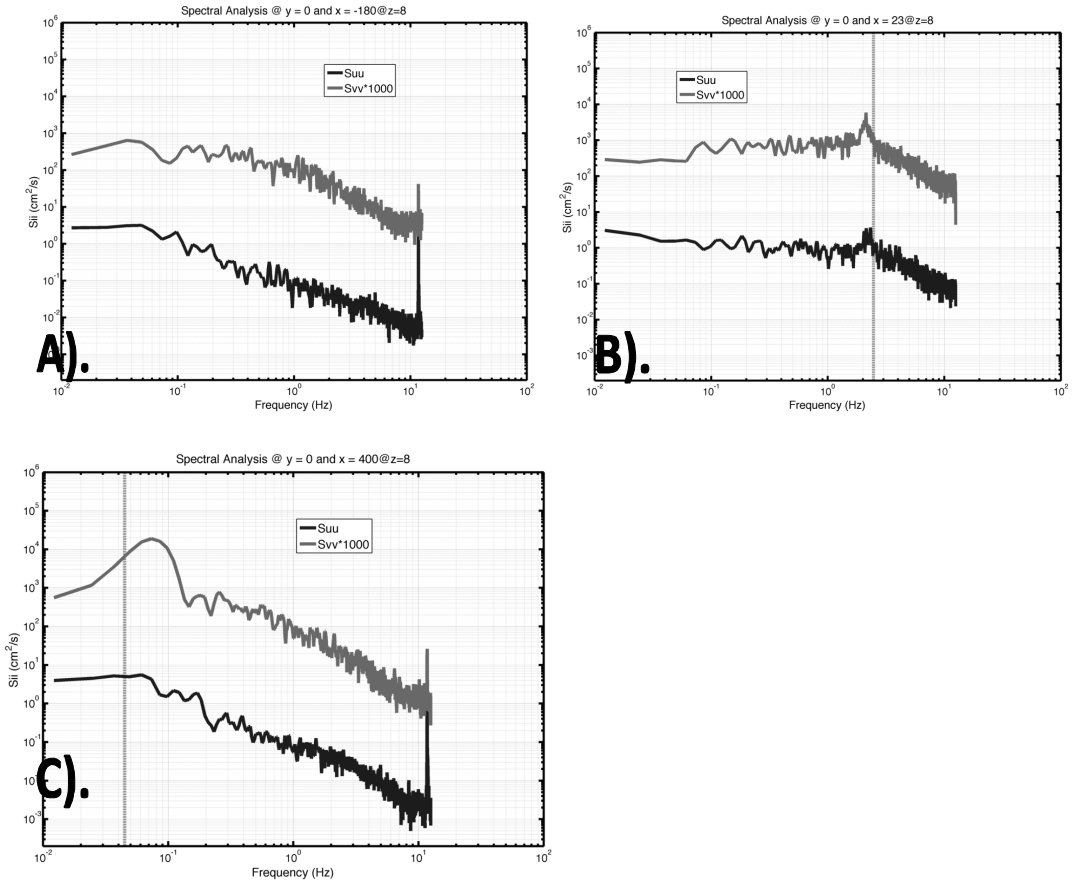

Figure 3-12. Velocity Spectra measured along centerline of patch at 7 cm depth for Case 2, where x = -4.3D, 0.5D, and 9.5D (A, B, and B). The x-axes are the frequency (Hz) and the y-axes are the spectra in cm^2/s. The black line is the spectra in the x-component (Suu) and the grey line is the y-component (Svv); the light grey vertical line represents the predicted frequency for possible turbulence contribution. B), the light grey vertical line marks the expected frequency for turbulence production based on the size of a single wooden dowel. C), the vertical grey line marks the turbulence production based on the size of the entire vegetation patch (see **Methodology** for calculation).

3.3. Flexible Submerged Vegetation

The flexible vegetation of a submerged patch produces a range of different flow patterns and turbulent structures in all three dimensions. In the horizontal

plane, or "plan-view," the flow is diverted laterally around the patch similar to the rigid cases, but there is no L_1 or evidence for a von-Karman vortex street (L_w) (Figure 1-1 & Figure 3-13). The wake recovery zone lasts a distance, L_2, from the downstream edge of the patch, after which the flow is uniform again. In the vertical plane, or "side view," the flow is diverted over the top of the patch and reattaches to the bed a distance L_v (Figure 3-14). In addition, there is small recirculation area downstream of the patch. Finally, there is a secondary circulation pattern that develops visible in the view normal to flow (Figure 3-15). Vertical vortex tubes develop alongside the lateral patch caused by the lateral shear. The vortex tubes are tipped forward by the mean flow shear. This creates a component of vorticity with an axis in the streamwise direction. The resulting circulation is directed away from the patch centerline at the free surface, and towards the patch centerline at the bed.

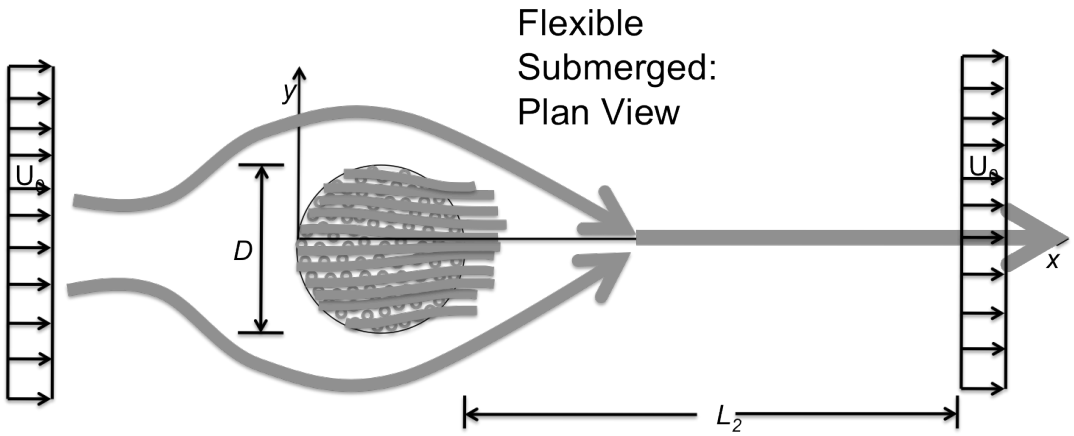

Figure 3-13. Conceptual diagram of plan view of the flow around porous flexible submerged patch of vegetation.

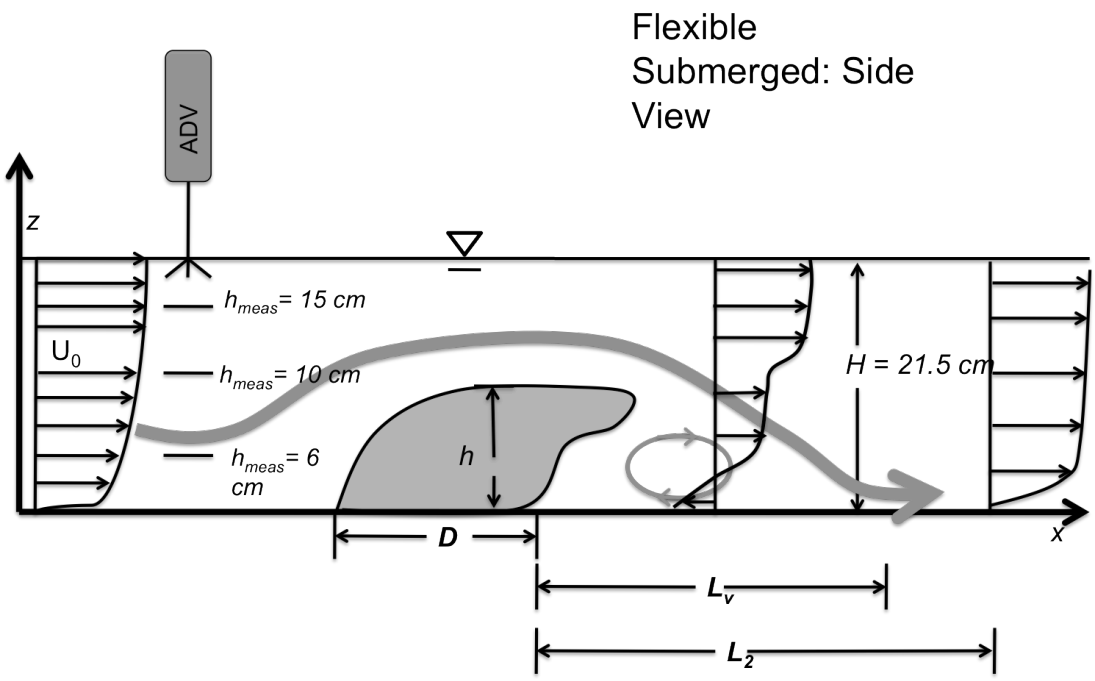

Figure 3-14. Conceptual diagram of side view of the flow over submerged flexible vegetation.

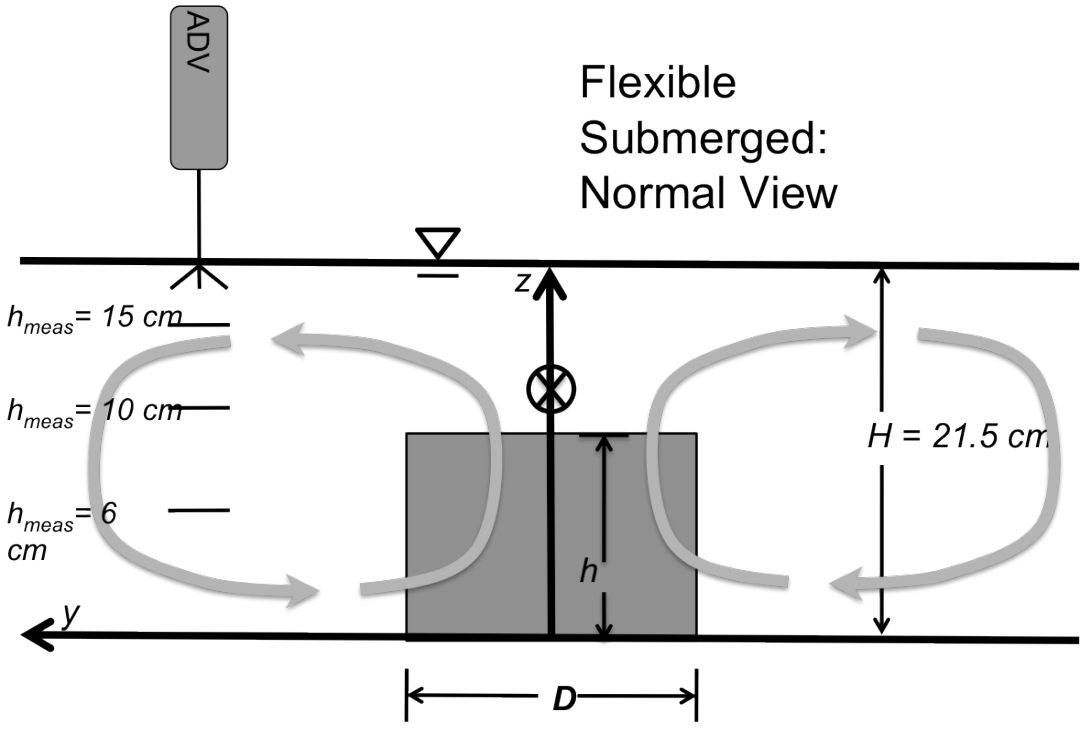

Figure 3-15. Conceptual diagram of normal view of flexible submerged patch of vegetation.

Fluvial systems contain both emergent vegetation and frequently submerged vegetation. The submerged vegetation can be both flexible and rigid, however, in this research only flexible vegetation was used for the submerged cases (Case 3 & 4). This type of model vegetation is a good mimic of grasses (Bos et al., 2007; Folkard, 2005). Sometimes flow over flexible vegetation generates monami, however, this was not seen in Case 3 or 4 (Nepf and Ghisalberti, 2008). There is no generation of monami because the patch length, *D*, is too short for a shear layer to develop and generate Kelvin-Helmholtz vortices (Nepf, 2012). The patch of flexible vegetation is slightly deformed by the flow, and has a given canopy height that differs for the two different densities (Figure 3-14 & Table 3). Previous work looked at the hydrodynamic effect of a patch of vegetation on flow by investigating the flow fields around the patch and the distribution of Reynolds stresses (Folkard, 2005). However, this work had a patch that extended across the width of the entire flume.

Table 3. Summary of measured flow parameters with calculated standard deviation for flexible submerged patches (Case 3 & 4) with standard deviation.

	C_DaD	C_Dah	H	h	U_o	L_2	L_v	Mean Total Deposition (g/cm^2)
Flexible Control	-	-	21.5 ± 0.2	-	8.1 ± 0.2	-	-	0.0027 ± 0.0003
Flexible Dense – Case 3	5.5 - 33.6 ± 0.4	1.3 – 8.0 ± 0.4	21.5 ± 0.2	10.0 ± 0.2	8.1 ± 0.2	11.4 ± 0.5D	1.4D ± 0.5D	0.0025 ± 0.0005
Flexible Sparse– Case 4	1.6 - 9.7 ± 0.1	0.3 – 1.8 ± 0.1	21.5 ± 0.2	8.0 ± 0.2	8.1 ± 0.2	12.8 ± 0.5D	1.5D ± 0.5D	0.0026 ± 0.0005

3.3.1. Case 3 – Flexible Dense

Measurements taken near the surface show the diversion of flow laterally around the patch (Figure 3-16). The velocity is accelerated both laterally around the patch and vertically over the top of the patch. The velocity is then slowed to half the initial velocity a meter and a half downstream of the patch (x/D = 5), an effect which lasts for another 2 meters. Measurements taken at mid depth are exactly at the top of the canopy of the patch of vegetation. The flow is diverted laterally away from the center. The velocity is slowed to half of the initial flow half a meter behind the patch for 3 meters (x/D = 2.2 – 5). Measurements taken near the bed are 4 cm below the top of the canopy (almost mid canopy). The flow is slightly diverted laterally away from the center of the flume at the upstream edge of the patch. Return flow is visible in the half meter behind the patch (x/D = 2.4). Overall, the flow is strongly decreased to almost zero flow downstream of the patch, and then recovers slowly staying around half of the initial flow for four meters (x = 9.5D).

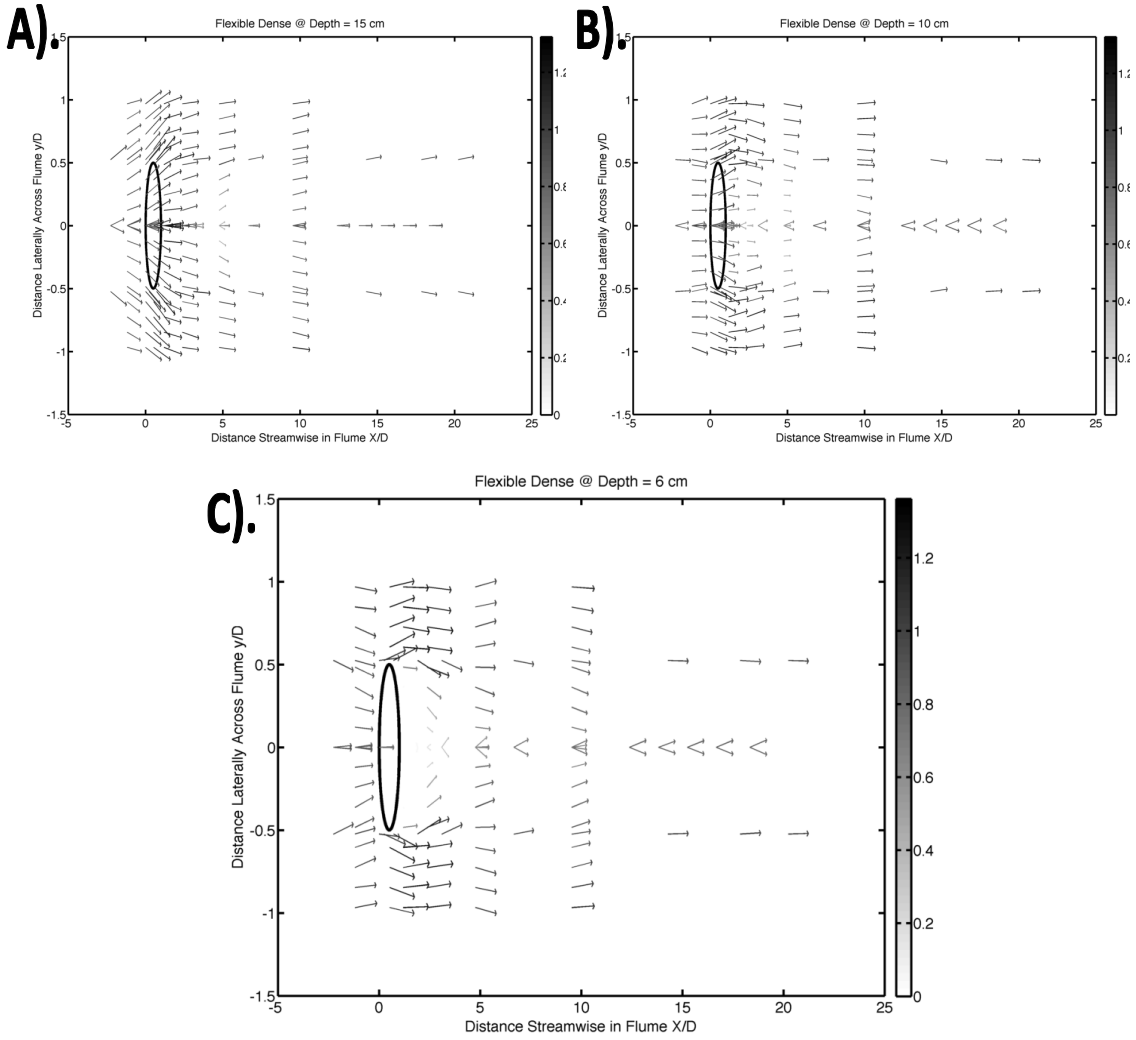

Figure 3-16. Quiver plot of the flume in plan view for Case 3, where the length of the arrows and the color of the arrows indicate the horizontal velocity magnitude. The x-axis is the position streamwise in the flume relative to the location of the patch; the y-axis is the position laterally across the flume. The colorbar on the right shows the total horizontal velocity relative to the U_0. The location of the patch is shown by the black ellipsoid. A) quiver at depth = 15 cm. B) quiver at depth = 10 cm. C), quiver at depth = 6 cm.

Secondary circulation is visible throughout the measured sections of the flume (Figure 3-17). Half a meter upstream of the patch, the flow is directed away from the patch centerline at the surface, and then returns to the center of the flume near the bed. While the secondary circulation does seem to diminish in magnitude

throughout the flume to three quarters of the initial value, the flow pattern remains visible for at least 3.5 meters behind the patch (x = 10D).

In addition to the secondary helical flow that is created, the flow is diverted over the top of the patch, and reattaches to the bed half a meter behind the patch (Figure 3-14). This accounts for the return flow in the near bed measurements behind the patch. It also accounts for the flow directed towards the bed in the center of the flume at x = 100 cm. As seen in Figure 3-16 downstream of the patch, the flow is slowed near the bed, and then directed back towards the patch.

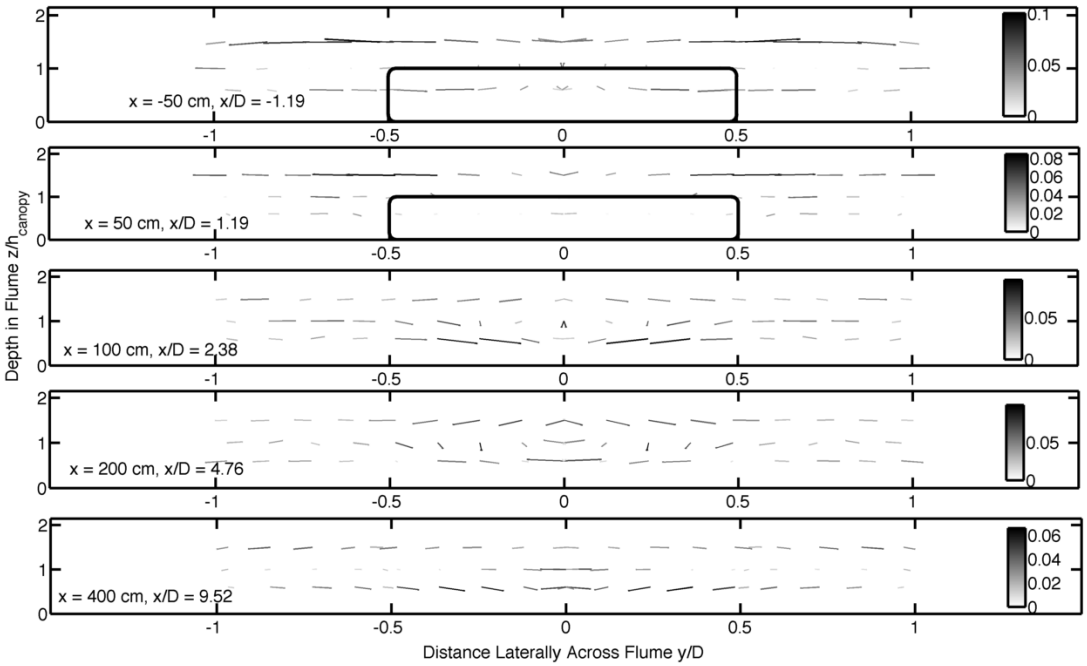

Figure 3-17. Vertical-lateral quiver slices taken in y and z throughout the flume from x = -50, 50, 100, and 400 cm, respectively for Case 3 (x/D = -1.2, 1.2, 2.4, 4.8, and 9.5). The length of the arrows and the color of the arrows indicate the horizontal velocity magnitude. The x-axis is the position laterally across the flume; the y-axis is the depth above the bed flume. The colorbar on the right shows the total horizontal velocity relative to the U_0.

Velocity is accelerated over the top of the patch near the surface (Figure 3-18). Downstream of the patch, flow is decreased to at least half of the initial

velocity for all three depths. Within four meters (x = 9.5D), the flow recovers back to the initial velocity. Mean flow measurements taken near the bed show highly decreased flow (almost zero) that recovers quickly to half of the initial velocity within one meter (2.4D). Both u_{rms} and TKE have peaks immediately downstream of the patch, with a smaller peak above the patch. The deposition upstream of the patch has a large standard deviation compared to the standard deviation for the rest of the transect. The area of large standard deviation of net deposition corresponds to the upstream flow adjustment length scale, L_o. Downstream of the patch, the deposition is decreased relative to the control experiment. Within one meter from the end of the patch, deposition increases slightly and stays relatively constant, but below the control experiment.

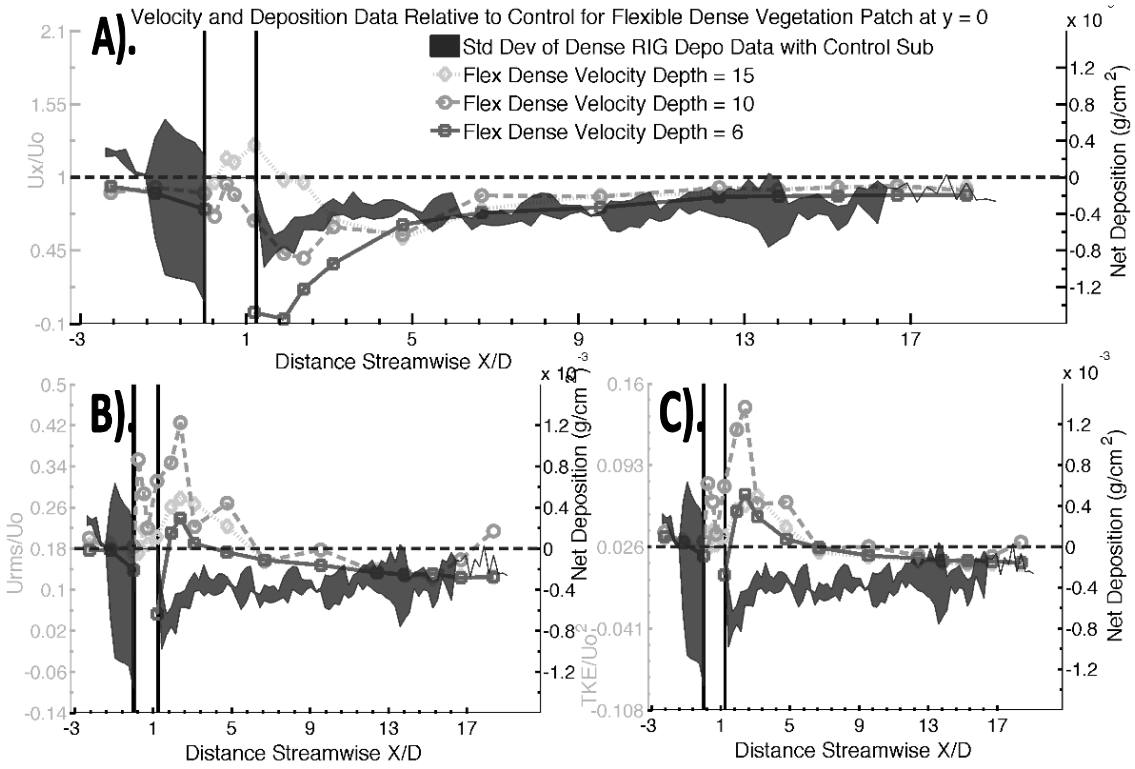

Figure 3-18. Deposition and velocity along centerline of the flume for Case 3. The x-axis is the streamwise position along the flume normalized by the patch diameter, *D*. The secondary y-axis is the net deposition relative to the control experiment (g/cm^2). The location of the patch in the streamwise direction is indicated by the black vertical lines on each graph. A) U/U_0 on the primary y-axis at three depths and the mean deposition of the three replicates with the standard deviation of the replicates indicated by the edges of the polygon fill on the secondary y-axis. B) u_{rms}/U_0 on the primary y-axis at three depths . C) TKE/u_o^2 on the primary y-axis at three depths.

The lateral transect taken upstream of the patch indicates that the flow is relatively uniform across the flume width (Figure 3-19). Immediately behind the patch, the flow is depressed very strongly to almost zero, but increases to one and half times the initial flow moving laterally away from the center of the patch. Within 4 meters (x/D = 9.5), the flow is almost uniform laterally. Both u_{rms} and TKE show similar trends to each other. They are uniform laterally upstream of the patch. Behind the patch, there is damping due to the patch with a peak at the edge of the patch from the local shear due to the velocity gradient at the lateral edge of the

patch. There is a large peak in both u_{rms} and *TKE* half a meter behind the patch (x = 2.4D). This peak, strongly pronounced in *TKE*, is possibly due to the streamlines that flow over the patch and reconnect to the bed. By four meters from the patch (x/D = 9.5), all the flow parameters are nearly uniform laterally across the width of the flume

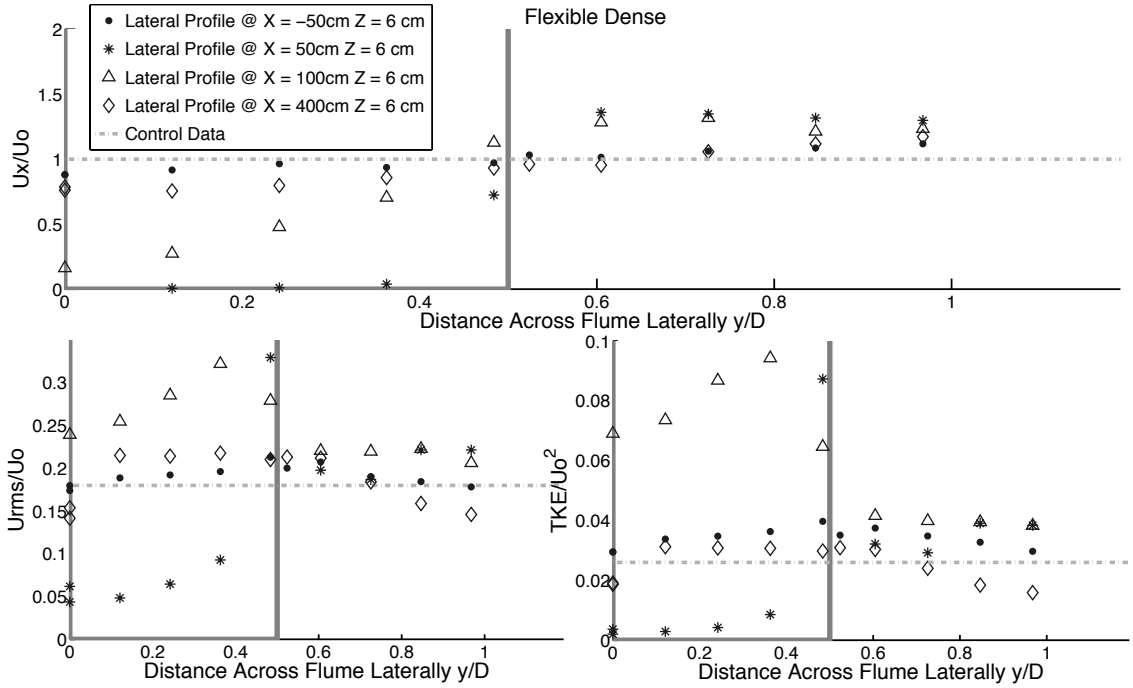

Figure 3-19. Lateral transects of normalized A) velocity, B) urms, and C) TKE for Case 1. The x-axis is the distance across the flume from the center of the flume (y = 0), normalized by the patch diameter.

The intensity of turbulence fluctuations along the centerline of the flume has a peak in all three components half a meter downstream of the end of the patch (x = 2.4D) recorded at all three depths (Figure 3-20). This distance is the vertical reattachment length, L_v = 1.4D, where the flow is diverted over the top of the canopy reattaches to the bed (Figure 3-14). For flow over a submerged cube, the vertical reattachment length, L_v, is 1.5-2.2D *(Hussein and Martinuzzi, 1996; Ratnam and*

Vengadesan, 2007). However, for a submerged hemisphere, the vertical reattachment length, L_v, is smaller around $0.6 - 0.75D$ (Savory and Toy, 1986). Flow over a submerged patch of flexible vegetation of more than twice the patch diameter in this research, D = 1 m, has a vertical reattachment length, $L_v = 1.4D$ (Folkard, 2005). The measured vertical reattachment length, $L_v = 1.4D$, agrees with previous research.

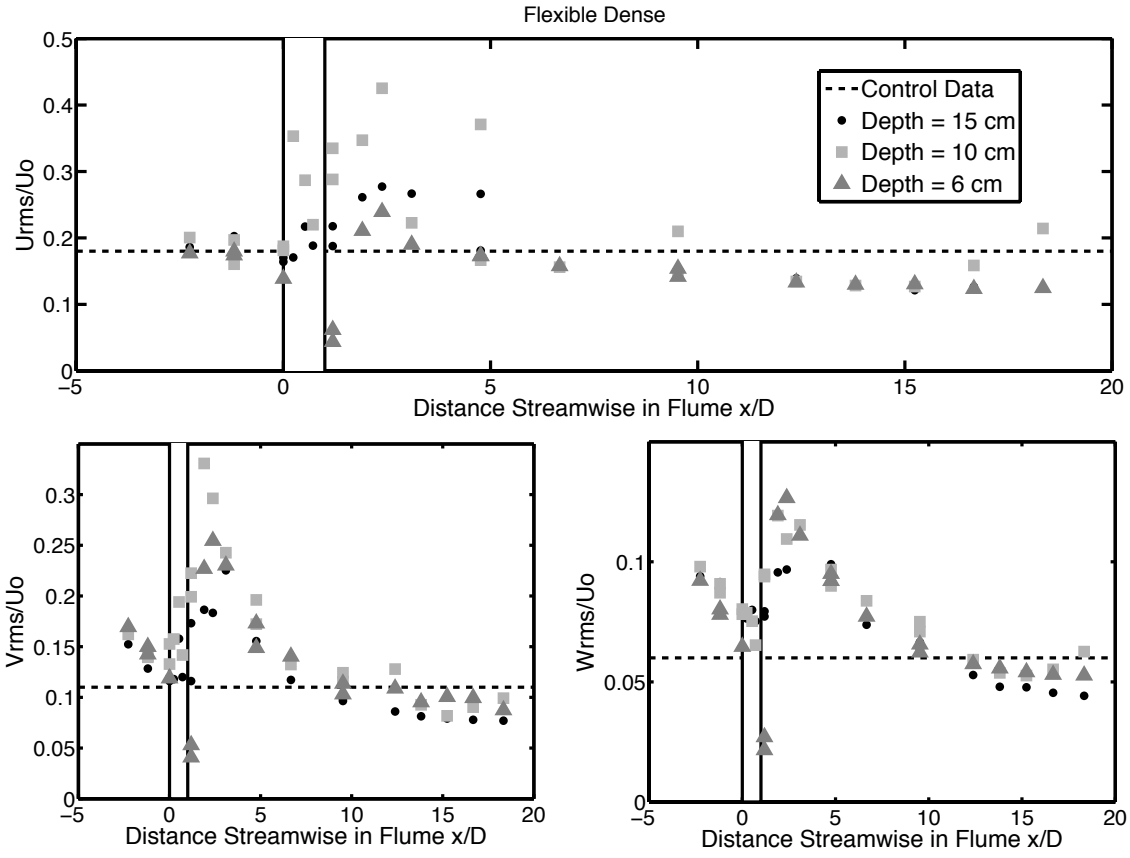

Figure 3-20. Normalized intensities of turbulence fluctuations along centerline of flume at three depths for Case 3. The x-axis is the distance streamwise normalized by the patch diameter; the y-axes are the intensity of turbulence fluctuations normalized by the upstream velocity. The solid vertical black lines indicate the patch location. The control value for a given fluctuation is the dashed black line.

3.3.2. Case 4 – Flexible Sparse

Measurements taken at 15 cm above the bed are 7 cm above the top of the canopy of the flexible sparse vegetation (Figure 3-21). The flow is diverted away from the center for 4 meters behind the patch (x/D = 9.5); there is acceleration on the lateral edges of the patch. Measurements taken 10 cm above the bed are 2 cm above the top of the canopy of the flexible sparse vegetation. The flow is reduced to three quarters of the initial velocity 1 meter downstream of the patch and continuing for 2 meters (x/D = 2.2 – 4.8). At a depth of 6 cm above the bed, measurements are taken 2 cm below the top of the canopy. The flow is primarily directed towards the center of the flume for four meters behind the patch (x/D = 9.5). The velocity is significantly slowed immediately downstream of the patch to almost zero, and remains decreased at half of the initial flow for 4 meters (x/D = 9.5).

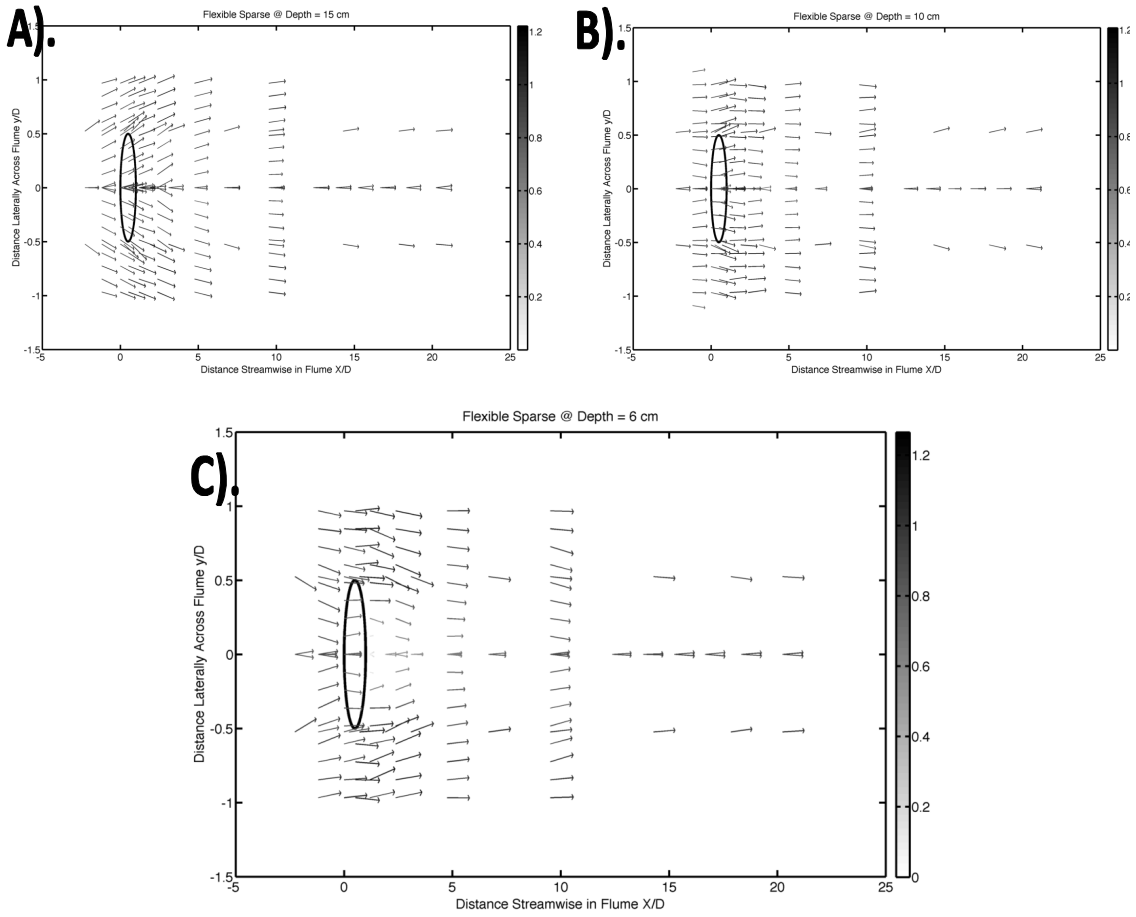

Figure 3-21. Quiver plot of the flume in plan view for Case 3, where the length of the arrows and the color of the arrows indicate the horizontal velocity magnitude. The x-axis is the position streamwise in the flume relative to the location of the patch; the y-axis is the position laterally across the flume. The colorbar on the right shows the total horizontal velocity relative to the U_0. The location of the patch is shown by the black ellipsoid. A) quiver at depth = 15 cm. B) quiver at depth = 10 cm. C), quiver at depth = 6 cm.

Vertical quiver slices taken throughout the flume highlight the secondary flow circulation (Figure 3-22). Immediately before the start of the patch, the flow is diverted above and over the patch. Secondary circulation is seen in the flow directed away from the centerline at the free surface and back towards the center of the flume at the bed. Behind the patch, the secondary circulation is still visible with the same pattern of flow away from the centerline at the surface and back towards the

center at the bed. By 4 meters from the patch, the secondary circulation is no longer present where the velocity orthogonal to flow is more than half the values upstream of the patch.

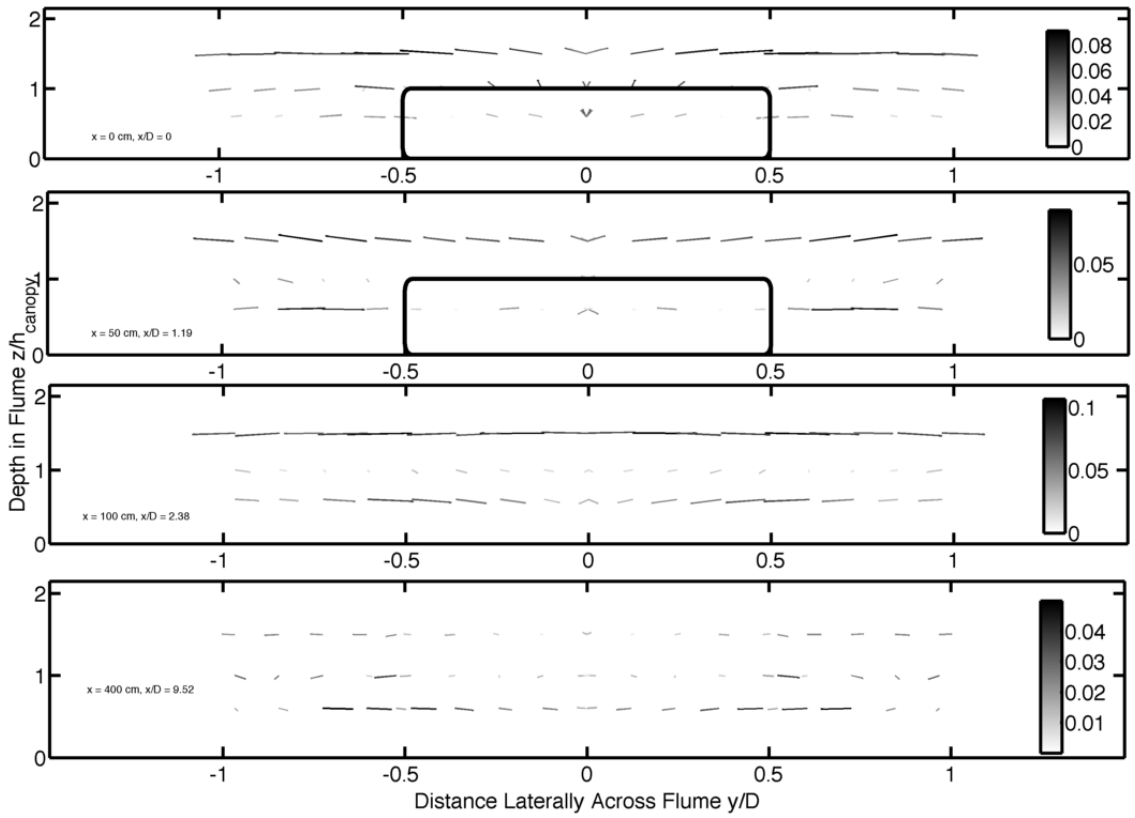

Figure 3-22. Vertical-lateral quiver slices taken in y and z for Case 4 throughout the flume from x = 0, 50, 100, and 400 cm, respectively (x/D = 0, 1.2, 2.4, and 9.5). The length of the arrows and the color of the arrows indicate the horizontal velocity magnitude. The x-axis is the position laterally across the flume; the y-axis is the depth above the bed flume in centimeters. The colorbar on the right shows the total horizontal velocity relative to the U_0. The black rectangle is the patch of vegetation.

The deposition pattern along the centerline of the flume is highly variable in front of the patch, but appears to be equivalent to the control experiment (Figure 3-23). Downstream of the patch, the mean deposition is below the deposition from the control experiment but still within standard deviation of the control experiment

for the length of the transect. Velocity measurements taken at three depths along the centerline highlight the overall lack of change in velocity. Directly downstream of the patch, the flow at the bed is reduced to less than a quarter of the initial flow, but it doubles within a meter. Within $7D$, flow is recovered to initial flow. Both the u_{rms} and TKE have the highest peak above the patch, and a secondary peak in all three depths 0.5 meters behind the patch.

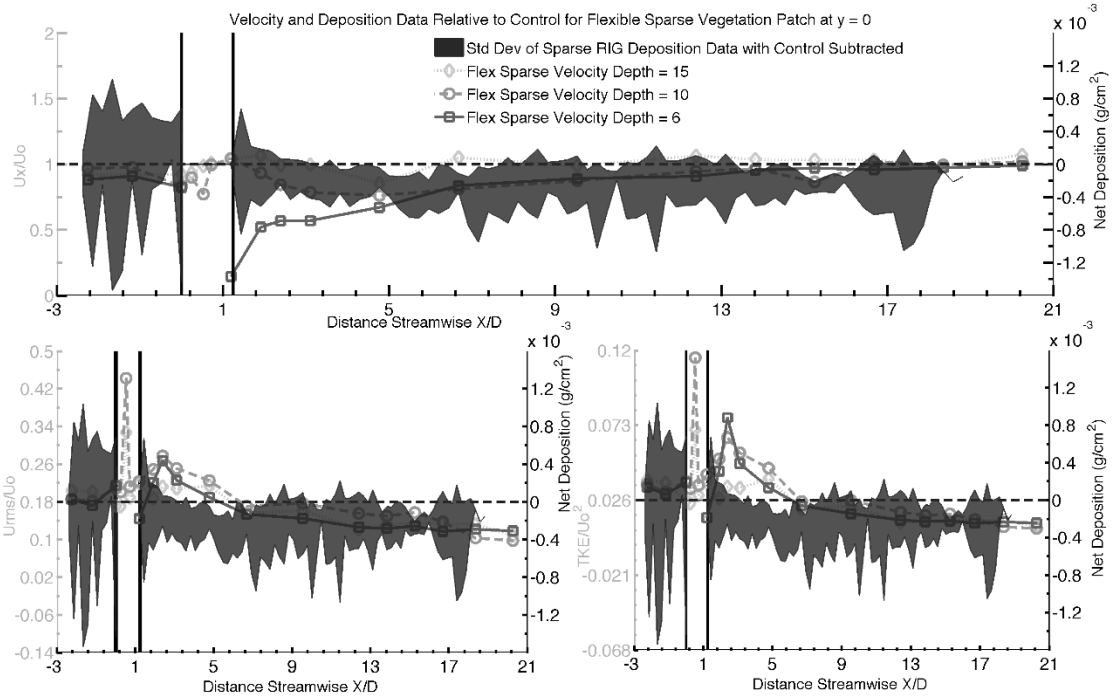

Figure 3-23. Deposition and velocity along centerline of the flume for Case 3. The x-axis is the streamwise position along the flume normalized by the patch diameter, *D*. The secondary y-axis is the net deposition relative to the control experiment (g/cm^2). The black vertical lines on each graph indicate the location of the patch in the streamwise direction. A) U/U_0 on the primary y-axis at three depths and the mean deposition of the three replicates with the standard deviation of the replicates indicated by the edges of the polygon fill on the secondary y-axis. B) u_{rms}/U_0 on the primary y-axis at three depths . C) TKE/u_o^2 on the primary y-axis at three depths.

Lateral velocity transects taken near the bed have the largest variability throughout the flume. Upstream of the patch, the mean flow is uniform laterally

(Figure 3-24). Downstream of the patch, the mean flow is depressed directly behind the middle of the patch, but increases moving laterally. Further downstream behind the patch, the mean flow increases back to uniform in the lateral, such that by 4 meters from the patch flow is uniform. There is relatively little change laterally in the u_{rms} throughout the flume for each transect. The peak in the u_{rms} directly behind the patch is due to the shear that develops in the velocity difference at that transect between the depressed mean flow behind the patch and the flow increasing laterally.

There is the peak in *TKE* directly downstream of the patch from the contribution of the peak in u_{rms}. One meter from the patch, the *TKE* is elevated behind the patch overall and decreases moving laterally. This contribution might come from the vertical flow component that is seen in Figure 3-15. This indicates the presence of a large vertical structure of flow over the patch that returns to the bed of the flume about 0.5 meters behind the patch. Overall, *TKE* is elevated compared to the control experiment where $TKE/u_o^2 = 0.015$ (increasing laterally to 0.02).

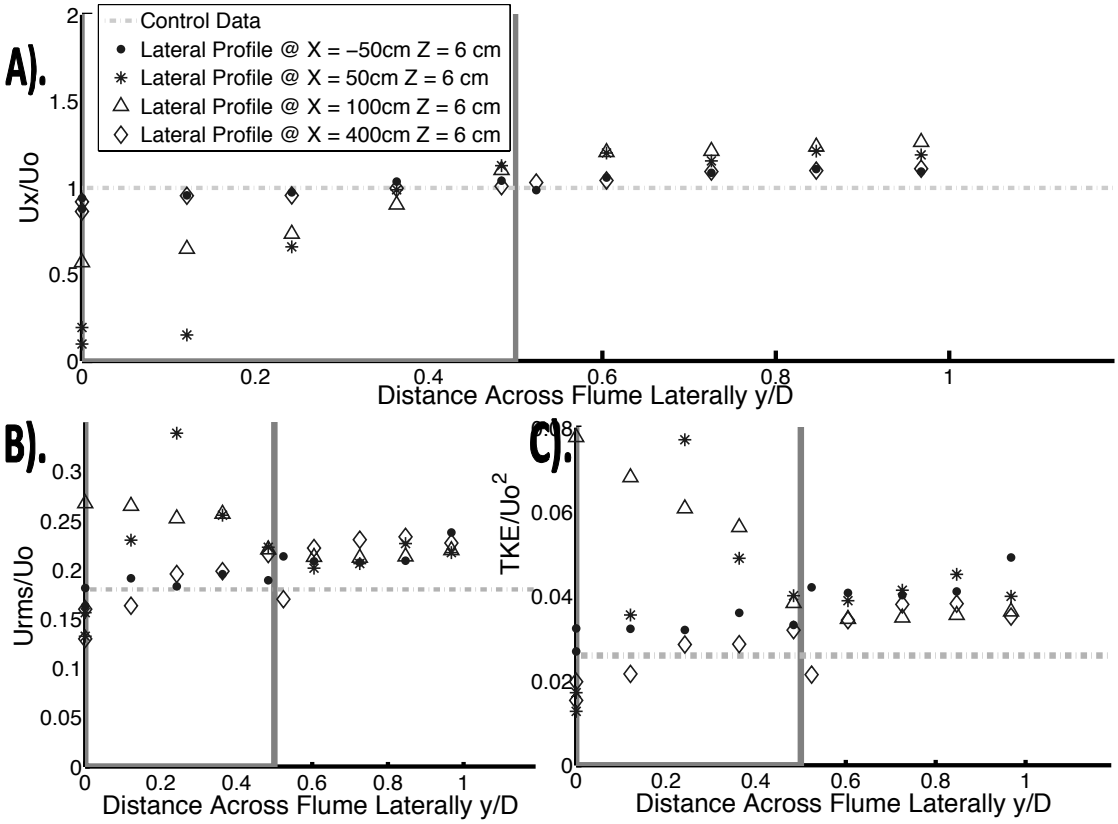

Figure 3-24. Lateral transects of normalized A) velocity, B) urms, and C) TKE for Case 1. The x-axis is the distance across the flume from the center of the flume (y = 0), normalized by the patch diameter.

The intensity of turbulence fluctuations along the centerline of the flume has a peak in all three components half a meter downstream of the end of the patch (x = 2.4D) recorded at all three depths (Figure 3-25). This distance is the vertical reattachment length, L_v, where the flow that is diverted over the top of the canopy reattaches to the bed. The measured vertical reattachment length (L_v = 1.5D) agrees with previous research (Folkard, 2005; Manhart, 1998; Ratnam and Vengadesan, 2007; Savory and Toy, 1986). There is a slight increase in the measured L_v, for Case 4 compared to Case 3, which is probably due to the increased flow through the

sparse patch (Case 4) than through the dense patch (Case 3). This would be similar to the effect of the bleed flow delaying the formation of the von-Karman vortex street with the emergent patches of vegetation (Case 1 & 2) (Zong and Nepf, 2011).

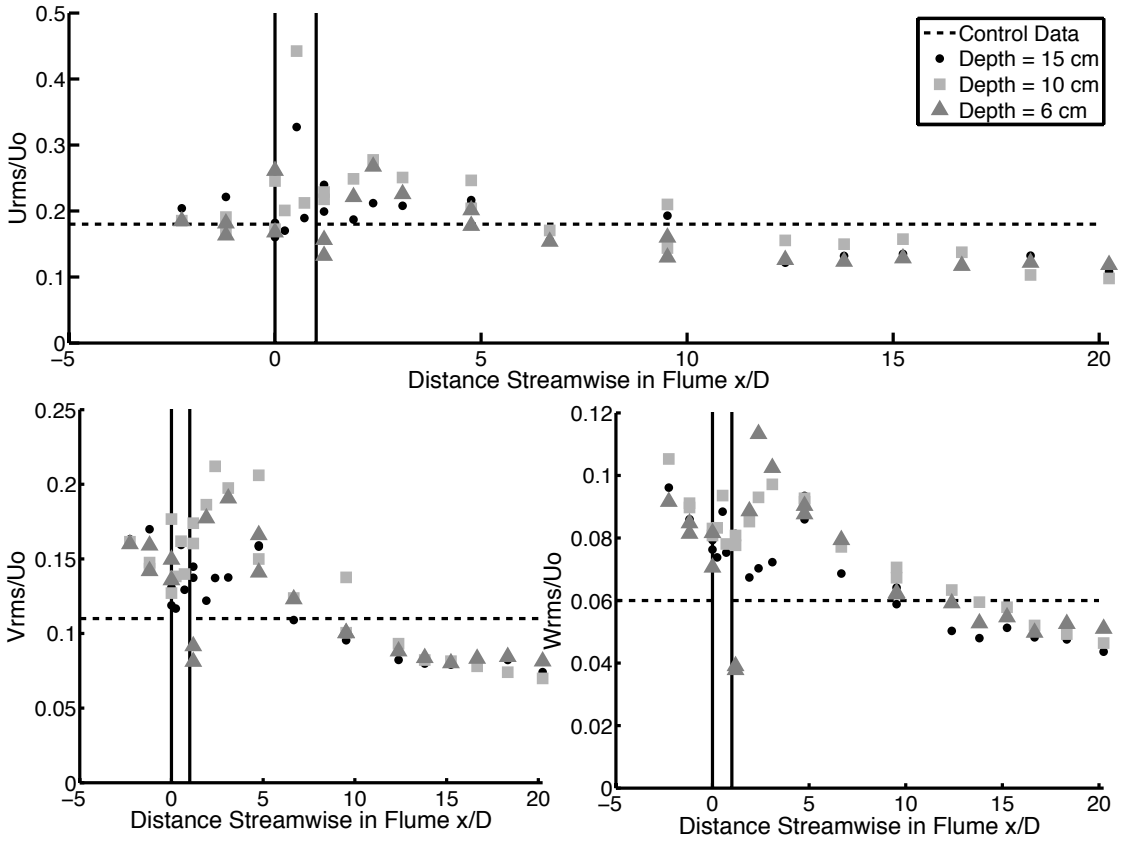

Figure 3-25. Normalized intensities of turbulence fluctuations along centerline of flume at three depths for Case 4. The x-axis is the distance streamwise normalized by the patch diameter; the y-axes are the intensity of turbulence fluctuations normalized by the upstream velocity. The solid vertical black lines indicate the patch location. The control value for a given fluctuation is the horizontal dashed black line.

Chapter 4 Discussion

The rigid emergent patch of vegetation affects the flow and subsequent sediment deposition differently depending on the density of the patch. Downstream of the dense patch, Case 1, the steady wake flow, U_1, is 2% of the initial flow, U_o, and lasts for $L_1 = 2.8D$ from the end of the patch (Figure 3-3 & Table 2). Downstream of the sparse patch, Case 2, the steady wake flow is U_1, is 50% of the initial flow, U_o, and lasts for $L_1 = 6.6D$ from the patch (Figure 3-4 & Table 2). Deposition is increased relative to the control experiment over the steady wake region, L_1, for both the dense and sparse patch (Figure 3-6 & Figure 3-10). In the dense patch (Case 1), the wake recovery is $L_2 = 4.3D$, but for the sparse patch (Case 2), $L_2 = 10.2D$ (Table 2). The length until the maximum turbulence, L_w, is very different for the two cases, $L_w = 4.2D$ for Case 1 and $L_2 = 8D$ for Case 2 (Table 2). The von-Karman vortex street converges on the centerline at this distance L_w.

The flexible submerged patch of vegetation has a very different affect on the flow pattern with little difference between the different densities. There is no steady wake region downstream from the patch, $L_1 = 0$ (Figure 3-13, Figure 3-16, and Figure 3-21). Instead, the wake recovery region is $L_2 = 11.4D$ for Case 3 and $L_2 = 12.8D$ for Case 4 (Table 3). In addition, the streamlines that were diverted over the patch upstream of the patch re-attach to the bed at $L_v = 1.4D$ Case 3 and $L_v = 1.5D$ Case 4 (Table 3). For both flexible cases (Case 3 & 4), the deposition remains near

constant throughout the flume within the standard deviation of the control experiment (Figure 3-18 & Figure 3-23).

For all four cases, there is a location of maximum fluctuation of turbulence (the root mean square variables), which corresponds to the presence of a large-scale coherent vortex. These coherent turbulent structures vary in formation. For the rigid experiments (Case 1 & 2), the coherent turbulence structure is the von-Karman vortex street (Figure 1-1) (Zong and Nepf, 2011). For the flexible experiments (Case 3 & 4), the coherent structure is the reattachment of the streamline that flows over the top of the submerged canopy (Figure 3-14) (Hussein and Martinuzzi, 1996; Ratnam and Vengadesan, 2007; Tal and Paola, 2007). For both the rigid emergent and flexible submerged cases, the maximum value of fluctuations ($7.7V_{rmso}$ for Case 1 and $3V_{rmso}$ for Case 3) in turbulence occurs for the dense experiment (Case 1 & 3) compared to the sparse experiments (Case 2 & 4) (Table 4). The reason for the maximum occurring in the two different dense cases is because the sparser the patch is, the lower the flow blockage, and the larger the bleed flow through the patch itself. The bleed flow delays the onset of the coherent turbulence structures: $L_w = 8D$ for Case 2 (almost twice the distance for the dense experiment, Case 1, $L_w = 4.2D$) and $L_v = 1.5D$ for Case 4 (Table 2 & Table 3). In addition, the bleed through effect decreases the magnitude of the turbulence, the peaks in all three components of the intensity of turbulence fluctuations is always larger for the dense experiments than for the sparse experiments (Table 4).

Table 4. Summary of peak of intensities of turbulent fluctuations for each case along centerline of flume with standard deviation.

	U_{rms} Peak (cm/s)	Locus of Peak -	Above Control -	V_{rms} Peak (cm/s)	Locus of Peak -	Above Control -	W_{rms} Peak (cm/s)	Locus of Peak -	Above Control -
Rigid Control	1.3 ± 0.3	-	-	0.6 ± 0.3	-	-	0.5 ± 0.3	-	-
Rigid Dense – Case 1	3.0 ± 0.3	L_w	$2.4U_{rmso}$	4.7 ± 0.3	L_w	$7.7V_{rmso}$	1.0 ± 0.3	L_w	$2.0W_{rmso}$
Rigid Sparse – Case 2	1.3 ± 0.3	L_w	U_{rmso}	1.4 ± 0.3	L_w	$2.4V_{rmso}$	0.6 ± 0.3	L_w	$1.7W_{rmso}$
Flexible Control	1.4 ± 0.3	-	-	0.9 ± 0.3	-	-	0.5 ± 0.3	-	-
Flexible Dense – Case 3	3.4 ± 0.3	L_v	$2.4U_{rmso}$	2.7 ± 0.3	L_v	$3.0V_{rmso}$	1.0 ± 0.3	L_v	$2.0W_{rmso}$
Flexible Sparse – Case 4	2.2 ± 0.3	L_v	$1.5U_{rmso}$	1.7 ± 0.3	L_v	$1.9V_{rmso}$	0.8 ± 0.3	L_v	$1.6W_{rmso}$

The estimated change in suspended sediment concentration was calculated for each experiment, enabling the calculation of the percent of sediment deposited (Table 5). Based on these values, both the control experiments have enhanced sediment deposition for the entire flume compared to the total sediment deposited for all four cases. Overall, the trends inherent in this calculation matches the mean total deposition calculated for each experiment and the controls as described in Data Processing (Table 2 & Table 3). The rigid sparse experiment (Case 2) has the least net deposition, the flexible dense experiment (Case 3) has the most net deposition. In both calculations, the control experiments have almost the same net

deposition for the entire flume but are enhanced slightly compared to the experiments with a patch of vegetation. Given the amount of error in these extrapolation calculations, the total net deposition for the reach of the experiment is unaffected by the presence of a patch of vegetation, rather it is merely redistributed in location. This result matches experiments done with similar patches looking at bedload sediment transport (Follett and Nepf, 2012).

Table 5. Summary of estimated sediment concentrations for each experiment for entire flume with calculated standard deviations based on 10% error.

	C_o (g/m^3)	C_e (g/m^3)	Percent Deposited %
Rigid Control	105 ± 10	30 ± 3	71 ± 7
Rigid Dense – Case 1	105 ± 10	45 ± 5	57 ± 4
Rigid Sparse– Case 2	105 ± 10	35 ± 4	67 ± 5
Flexible Control	77 ± 7	18 ± 2	77 ± 4
Flexible Dense – Case 3	77 ± 7	25 ± 3	67 ± 3
Flexible Sparse– Case 4	77 ± 7	27 ± 3	65 ± 3

These calculations are used in a basic sediment transport model. Using an advective-settling model, deposition is predicted along the centerline of the flume and is compared to the experimental deposition for all four cases (Zong and Nepf, 2010). First order trends are compared between the modeled and actual sediment. When the mean bed stress is less than the critical shear stress, the probability of deposition maxes out, $p = 1$. The areas of constant deposition indicate areas where

the local velocity is low and producing low local bed shear stress. If the critical shear stress was shifted, then the values of p would change accordingly to unity more often (if critical shear stress increased) or less than unity for increasing distance (if critical shear stress decreased).

For Case 1, the experimental data show elevated deposition upstream of the vegetation patch, and a peak in deposition immediately after the patch that remained elevated relative to the control for almost a meter (Figure 4-1). The deposition is decreased, and stays lower than the control for the rest of the flume. The patterns visible in the model, however, are different in parts. There is increasing sediment deposition predicted before the patch, net deposition above the modeled control deposition consistent with the actual trend. The maximum of deposition is predicted downstream of the patch, but continues for an extra 2 meters before the sediment deposition decreased significantly. Moreover, according to the modeled deposition for Case 1, modeled deposition remains much higher than the predicted deposition for the control experiment. Only after $x = 10D$ does the modeled deposition for Case 1 go below the modeled deposition for the control experiment. This is in contrast to the trend in the actual data, where from $x > 3D$, the actual deposition for Case 1 is less than the deposition for the control.

For Case 2, the experimental data show elevated deposition upstream of the vegetation patch. The lowest deposition is within the patch. There is a peak in deposition after the patch that remains elevated relative to the control for almost 4 meters (Figure 4-1). The deposition decreases and stays near the control, or just

below, for the rest of the flume. There is low sediment deposition predicted before the patch, but it is elevated relative to the modeled control, which is consistent with the experimental data. The maximum deposition is predicted for the patch, but it continues for an extra 3 meters (x = 17.1D) before the sediment deposition is slowly decreased. Moreover, the predicted deposition for Case 2 remains elevated above the predicted deposition for the control experiment for the entire length of the flume due to diminished velocity for x/D = 14 downstream of the patch. On the other hand, the actual deposition results fluctuate above and below the control deposition.

For Case 3, the experimental data show a decreasing deposition approaching the patch of vegetation upstream (Figure 4-1). Immediately downstream of the patch, there is decreased deposition, and it remains relatively uniform for the remainder of the patch. For Case 4, the experimental data demonstrate variable deposition before the vegetation patch (Figure 4-1). The deposition remains relatively uniform for the remainder of the patch, except for a small dip towards the end of the flume. For both Cases 3 & 4, the model predicts uniform deposition over the entire length of the flume. This is because the measured flow characteristics do not exceed the critical shear stress (ψ_{cr} = 0.23). The modeled deposition for Case 3 remains at the modeled deposition for the control experiment, similar the actual experimental data. The modeled deposition for Case 4 remains almost equal to the modeled deposition for the control experiment, just slightly below the modeled control deposition. The model predicts constant deposition because it only accounts

for changes in local bed stress based on the local mean flow; there is no dependence on turbulence. The differences between the trends observed in the modeled and experimental data indicate that deposition should not be solely dependant on the local bed shear stress.

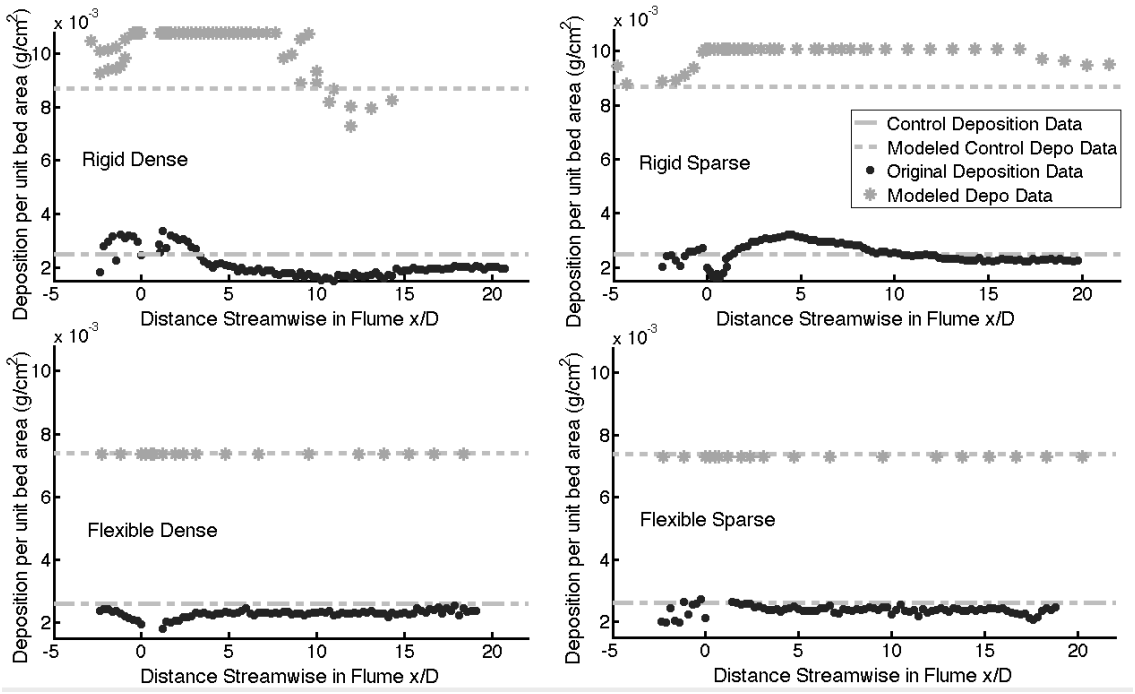

Figure 4-1. Predicted sediment deposition along the centerline of the flume for each case given the measured flow characteristics using an advective settling model (Zong and Nepf, 2010). The x-axis is streamwise distance along the flume; the y-axis is the net deposition per unit bed area.

By considering both the total horizontal velocity and the *TKE* for each case, interesting trends are revealed in the experiments. The flow measurements can be categorized into four areas based on the flow characteristics relative to control measurements (Figure 4-2). The four quadrants are: high mean velocity and high

TKE (upper right quadrant); high mean velocity and low *TKE* (lower right quadrant); low mean velocity and low *TKE* (lower left quadrant); and low mean velocity and high *TKE* (upper left quadrant). The data are colored by the significant deposition at each location.

The rigid dense patch, Case 1, has the largest variability in measured mean velocity with the TKE reaching a maximum of 2Uo and 0.2TKEo. The rigid sparse patch, Case 2, has a relatively restricted range of values for the horizontal velocity and *TKE*, ranging from 0.5Uo to 1.4Uo and zero *TKEo* to 0.05*TKEo*. The flexible dense patch, Case 3, has a wide range in TKE from 0.01TKEo to 0.15*TKEo*, and a small range in horizontal velocity from 0.8Uo to 1.4Uo. The flexible sparse patch, Case 4, is clustered around the measured control values, with a small range similar to Case 3 except the range in TKE is smaller from 0.015TKEo to 0.1*TKEo*.

Overall, for all the four cases, there is little enhanced deposition relative to the control experiments, only for Case 1 & 2 is there enhanced deposition, which is enhanced for less than 25% of the data points (Figure 4-2). The rigid dense patch, Case 1, has the largest amount of deposition; the majority of this deposition occurs in quadrant III, where both TKE and horizontal velocity are below the initial values (Figure 4-2). The rigid sparse patch has enhanced deposition also in quadrant III. The flexible patches of both densities have no enhanced deposition relative to the control experiment. Overall, enhanced deposition appears to occur when $U \leq 0.5Uo$ and when $TKE \leq TKE_o$.

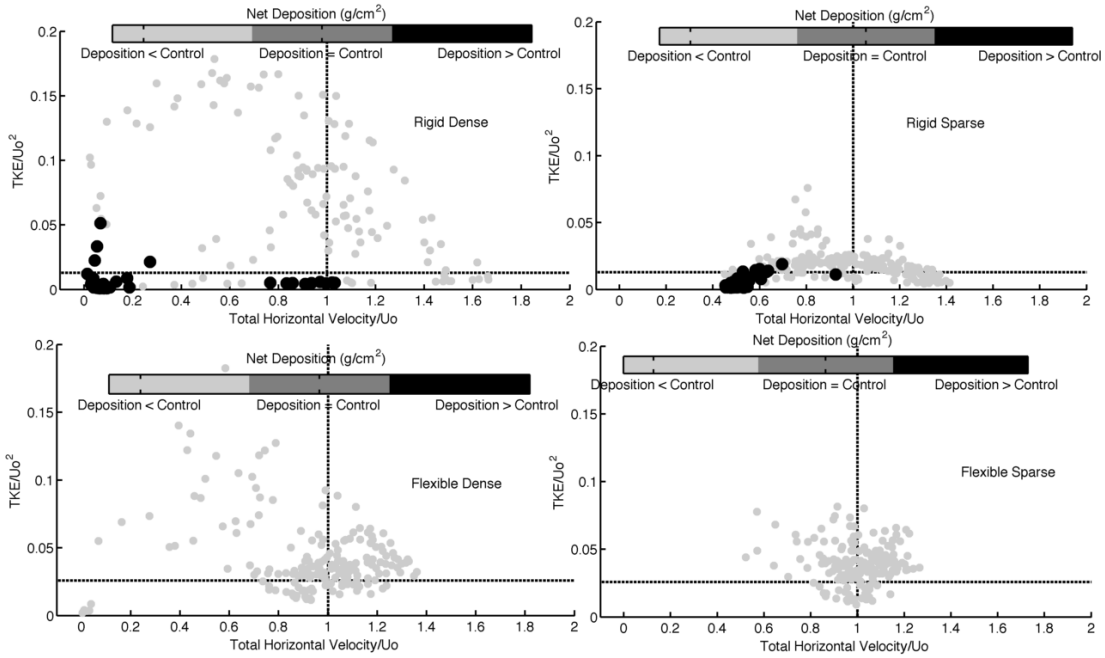

Figure 4-2. Horizontal velocity versus turbulence kinetic energy colored and scaled by the net deposition. The x-axis is total horizontal velocity relative to initial velocity; the y-axis is TKE/U_o^2 for each graph. The points on each graph are colored and sized by the net deposition relative to the control experiment (where deposition is either greater than the control experiment, less than the control experiment, or within the standard deviation of the control experiment). The dashed black lines are the flow measurements from the control experiment.

The location within the flume of the enhanced deposition fits into a specific spatial pattern (Figure 4-3). The enhanced deposition occurs almost entirely in the L_1 region, the steady wake region. It is in this region that both velocity and turbulence are depressed, relative to the open channel control. The flexible vegetation patch has no steady wake region downstream of the patch, $L_1 = 0$. This would explain why there is no enhanced deposition in the flexible submerged patches.

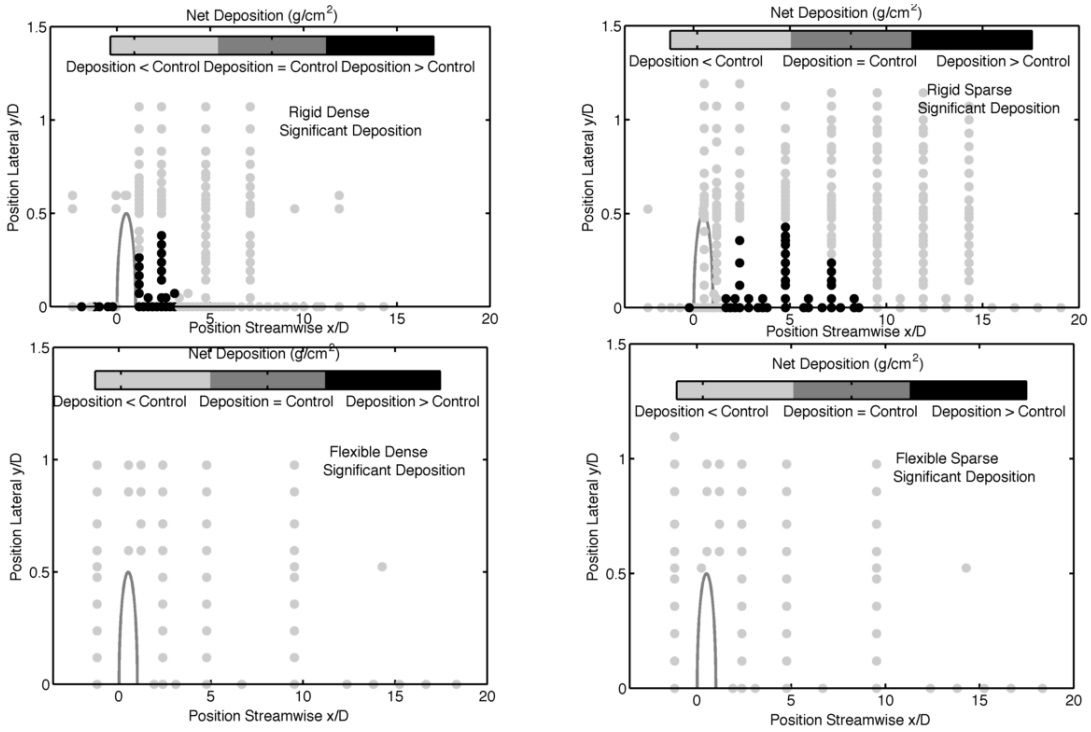

Figure 4-3. Locations in the flume where the deposition is measured, colored by significant deposition relative to the control position where deposition is either greater than the control experiment, less than the control experiment, or within the standard deviation of the control experiment). The graphs are the plan view half of the flume, with the x and y-axis the streamwise and lateral position normalized by the diameter of the patch. The location of the patch is indicated by the semicircle.

Chapter 5 Conclusions & Future Work

Enhanced sediment deposition occurs primarily in the steady wake region downstream of the patch of vegetation. In this region, both mean velocity and turbulence are depressed relative to the open channel flow. In fact, for enhanced deposition to occur, mean velocity has to be less than or equal to half the open channel velocity, and turbulence must be less than or equal to the free stream turbulence. The patches comprised of the rigid emergent plants have a steady wake region immediately downstream of the patch where the mean flow and the turbulence satisfy these requirements. However, the patches comprised of the flexible submerged vegetation have no steady wake region downstream of the patch. In addition, there are very few locations where turbulence and mean velocity fall below the suggested requirements for enhanced deposition. Thus, it makes sense that this is an overall lack of enhanced deposition for the flexible cases.

When the total deposition is extrapolated for the reach of the flume, there appears to be no net enhanced deposition relative to the control experiments. The presence of a patch of vegetation merely redistributes sediment around the flume. There are local changes in net deposition relative to the control, where the steady wake region has enhanced deposition. But on the larger scale of the reach of the flume, there is no net enhanced deposition. The local enhanced deposition in the steady wake region agrees with previous research. In the field during the preliminary stages of vegetation colonization, vegetation is often found in a circular

patches (Sand-Jensen and Madsen, 1992). But over time, these patches have been shown to grow predominantly in the downstream direction (Sand-Jensen and Madsen, 1992; Schnauder and Moggridge, 2009). Since suspended sediment typically contains fine sediment especially organics, the enhanced deposition in the steady wake region would be preferential to fine rather than coarse sediment. This project supports the conclusion that patches experiencing a steady wake region will preferentially deposit sediment in that region enabling easier colonization because of the decreased flow, decreased turbulence, and increased deposition of fine sediment.

Increasing grain size would lower the critical shear stress value to a minimum at medium grained sand (d = 0.3 mm) and then increase the critical shear value to ψ_{cr} = 0.065 (Julien, 2010). Decreasing the ψ_{cr} value would mean it is easier to initiate motion of sediment given constant bed shear stress and local velocity. If all things remain equal otherwise, then this should decrease the area of enhanced deposition because it's easier to entrain sediment. I would hypothesize that with increasing grain size, the effect of turbulence on sediment deposition should decrease.

Future research should be focused on verifying the stipulations discussed above. For patches of vegetation with a predicted steady wake region, is there an enhanced sediment deposition? In addition, if there is enhanced sediment deposition in the steady wake region, does it correspond to the stipulated low values of mean velocity and turbulence? For the flexible vegetation, it would be

interesting to investigate if there are ever cases that experience enhanced deposition. If the upstream velocity is increased, there may be a steady wake region that develops downstream of the patch. If the size of the patch is increased, the wake recovery length is delayed because the lateral and vertical turbulence structures take longer to reach the centerline of the flume downstream of the patch because the flow field scales on the patch size. It would be interesting to investigate the deposition behind a rigid submerged patch rather than emergent behavior, which would also have vertical turbulence structures similar to those seen in the flexible submerged cases. It could even be possible to construct a flexible vegetation patch where the canopy height is at the free surface equal to the water depth. All of these cases could be investigate to see if the proposed argument for enhanced sediment deposition remains valid.

References

Anderson, R.S. and Anderson, S.P., 2011. Rivers, Geomorphology: The Mechanics and Chemistry of Landscapes. Cambridge University Press.

Bos, A.R., Bouma, T.J., Kort, G.L.J. and van Katwijk, M.M., 2007. Ecosystem Engineering by Annual Intertidal Seagrass Beds: Sediment Accretion and Modification. Estuarine Coastal and Shelf Science, 74: 344-348.

Bouma, T.J. et al., 2007. Spatial Flow and Sedimentation Patterns within Patches of Epibenthic Structures: Combining field, Flume and Modeling Experiments. Continental Shelf Research, 27: 1020-1045.

Boyer, C., Roy, A.G. and Best, J.L., 2006. Dynamics of a river channel confluence with discordant beds: flow turbulence, bed load sediment transport, and bed morphology. Journal of Geophysical Research, 111.

Chen, Z., Ortiz, A.C., Zong, L.J. and Nepf, H., 2012 The wake structure behind a porous obstruction with implications for deposition near a finite patch of emergent vegetation. Water Resources Research (In review): 41.

Christiansen, T., Wiberg, P.L. and Milligan, T.G., 2000. Flow and sediment transport on a tidal salt marsh surface. Estuarine Coastal and Shelf Science, 50(3): 315-331.

Church, M., 2006. Bed material transport and morphology of alluvial river channels. Annual Review of Earth and Planetary Science, 34: 325-354.

Ciraolo, G., Ferreri, G.B. and La Loggia, G., 2006. Flow resistance of Posidonia oceanica in shallow water. Journal of Hydraulic Research, 44(2): 189-202.

Corenblit, D., Tabacchi, E., Steiger, J. and Gurnell, A.M., 2007. Reciprocal interactions and adjustments between fluvial landforms and vegetation dynamics in river corridors: a review of complementary approaches. Earth Science Reviews, 84: 56-86.

Dade, W.B. and Friend, P.F., 1998. Grain-size, sediment-transport regime, and channel slope in alluvial rivers. Geology, 106(6): 661-676.

Engelund, F. and Fredsoe, J., 1976. A sedment transport model for straight alluvial channels. Nord. Hydrology, 7: 293-306.

Folkard, A.M., 2005. Hydrodynamics of model Posidonia oceanica patches in shallow water. Limnology and Oceanography, 50(5).

Follett, E.M. and Nepf, H.M., 2012. Sediment patterns near a model patch of reedy emergent vegetation. Geomorphology (In review).

Ghisalberti, M. and Nepf, H., 2006. The structure of the shear layer in flows over rigid and flexible canopies. Environmental Fluid Mechanics, 6(3): 277-301.

Hendriks, I.E., Sintes, T., Bouma, T.J. and Duarte, C.M., 2008. Experimental assessment and modeling evaluation of the effects of the seagrass Posidonia oceanica on flow and particle trapping. Marine Ecology-Progress Series, 356: 163-173.

Hussein, H.J. and Martinuzzi, R.J., 1996. Energy balance for turbulent flow around a surface mounted cube placed in a channel. Physics of Fluids, 8.

Julien, P.Y., 2010. Incipient Motion, Erosion and Sedimentation. Cambridge University Press, Cambridge
Kemp, J., Harper, D. and Crosa, G., 2000. The habitat-scale ecohydraulics of rivers. Ecological Engineering, 16: 17-29.
Luhar, M., Rominger, J. and Nepf, H., 2008. Interaction between flow, transport and vegetation spatial structure. Environmental Fluid Mechanics, 8(5-6): 423-439.
Madsen, O.S., Sediment Characteristics, Mechanics of Sediment Transport in Steady Flow. Massachusetts Institute of Technology.
Madsen, O.S. and Grant, W.D., 1976. Quantitative Description of Sediment Transport by Waves, International Conference on Coastal Engineering.
Manhart, M., 1998. Vortex Shedding from a Hemisphere in a Turbulent Boundary Layer. Theoretical and Computational Fluid Dynamics, 12: 1-28.
Mazda, Y. et al., 1997. Drag force due to vegetation in mangrove swamps. Mangroves and Salt Marshes, I: 193-199.
Murphy, E., Ghisalberti, M. and Nepf, H., 2007. Model and laboratory study of dispersion in flows with submerged vegetation. Water Resources Research, 43(5).
Murphy, E., Ghisalberti, M. and Nepf, H.M., 2006. Longitudinal dispersion in vegetated channels. In: R.M.L. Ferreira, C.T.L. Alves, G.A.B. Leal and A.H. Cardoso (Editors), River Flow 2006, Vols 1 and 2. Proceedings and Monographs in Engineering, Water and Earth Sciences, pp. 613-621.
Murray, A.B. and Paola, C., 2003. Modelling the effect of vegetation on channel pattern in bedload rivers. Earth Surface Processes and Landforms, 28: 131-143.
Naden, P., Rameshwaran, P., Mountford, O. and Robertson, C., 2006. The Influence of Macrophyte Growth, Typical of Eutrophic Conditions, on River Flow Velocities and Turbulence Production. Hydrological Processes, 20: 3915-3938.
Nelson, J.M., Shreve, R.L., McLean, S.R. and Drake, T.G., 1995. Role of near-bed turbulence structure in bed load transport and bed form mechanics. Water Resources Research, 31(2071-2086).
Nepf, H., 2012. Flow and Transport in Regions with Aquatic Vegetation. Annual Review of Fluid Mechanics, 44: 123-142.
Nepf, H. and Ghisalberti, M., 2008. Flow and transport in channels with submerged vegetation. Acta Geophysica, 56(3): 753-777.
Neumeier, U., 2007. Velocity and turbulence variations at the edge of saltmarshes. Continental Shelf Research, 27(8): 1046-1059.
Norberg, C., 1994. An experimental investigation of the flow around a circular cylinder: influence of aspect ratio. Journal of Fluid Mechanics, 258: 287-316.
Peralta, G., van Duren, L.A., Morris, E.P. and Bouma, T.J., 2008. Consequences of shoot density and stiffness for ecosystem engineering by benthic

macrophytes in flow dominated areas: a hydrodynamic flume study. Marine Ecology-Progress Series, 368: 103-115.
Pollen, N. and Simon, A., 2005. Estimating the mechanical effects of riparian vegetation on stream bank stability using a fiber bundle model. Water Resources Research, 2005(41).
Ratnam, G.S. and Vengadesan, S., 2007. Performance of two equation turbulence models for prediction of flow and heat transfer over a wall mounted cube. International Journal of Heat and Mass Transfer, 51: 2834-2846.
Rodrigues, S. et al., 2006. Flow and sediment dynamics in the vegetated secondary channels of an anabranching river: The Loire River (France). Sedimentary Geology, 186(1-2): 89-109.
Rominger, J. and Nepf, H., 2011. Flow Adjustment and Interior Flow Associated with a Rectangular Porous Obstruction. Journal of Fluid Mechanics, 680: 636-659.
Rominger, J.T., Lightbody, A.F. and Nepf, H.M., 2010. Effects of Added Vegetation on Sand Bar Stability and Stream Hydrodynamics. Journal of Hydraulic Engineering-Asce, 136(12): 994-1002.
Sand-Jensen, K. and Madsen, T.V., 1992. Patch Dynamics of the Stream Macrophyte, *Callitriche cophocarpa*. Freshwater Biology, 27: 277-282.
Savory, E. and Toy, N., 1986. The Flow regime in the turbulent near wake of a hemisphere. Experiments in Fluids, 4: 181-188.
Schnauder, I. and Moggridge, H.L., 2009. Vegetation and hydraulic-morphological interactions at the individual plant, patch and channel scale. Aquatic Sciences, 71: 318-330.
Tal, M. and Paola, C., 2007. Dynamic single-thread channels maintained by the interaction of flow and vegetation. Geology, 35(4).
Temmerman, S. et al., 2005. Impact of vegetation on flow routing and sedimentation patterns: Three-dimensional modeling for a tidal marsh. Journal of Geophysical Research-Earth Surface, 110(F4).
Vandenbruwaene, W. et al., 2011. Flow Interaction with Dynamic Vegetation Patches: Implications for Biogeomorphic Evolution of a Tidal Landscape. Journal of Geophysical Research, 116.
Williams, J.J., Thorne, P.D. and Heathershaw, A.D., 1989. Measurements of turbulence in the benthic boundary layer over a gravel bed. Sedimentology, 36: 959-971.
Zong, L.J. and Nepf, H., 2010. Flow and deposition in and around a finite patch of vegetation. Geomorphology, 116(3-4): 363-372.
Zong, L.J. and Nepf, H., 2011. Vortex development behind a finite porous obstruction in a channel, Journal of Fluid Mechanics.

Appendix

The appendix contains 12 tables of the raw velocity and deposition data along the centerline of the flume for each experiment including the control experiments.

Table 1. Rigid Control Case – Raw velocity data along centerline of flume with measured standard deviation.

Rigid Control									
X Position		**Ux**		**Urms**		**Vrms**		**Wrms**	
Value (cm)	**Error (cm)**	**Value (cm/s)**	**Error (cm/s)**	**Value (cm/s)**	**Error (cm/s)**	**Value (cm/s)**	**Error (cm/s)**	**Value (cm/s)**	**Error (cm/s)**
-95	1	8.9	0.1	1.4	0.3	1.2	0.3	0.6	0.3
-95	1	9.3	0.1	1.4	0.3	1.0	0.3	0.7	0.3
-50	1	9.4	0.1	1.5	0.3	0.9	0.3	0.6	0.3
-50	1	9.3	0.1	1.3	0.3	0.8	0.3	0.6	0.3
0	1	9.4	0.1	1.6	0.3	0.9	0.3	0.6	0.3
0	1	9.3	0.1	1.3	0.3	0.7	0.3	0.5	0.3
30	1	9.4	0.1	1.3	0.3	0.7	0.3	0.5	0.3
50	1	9.4	0.1	1.3	0.3	0.8	0.3	0.5	0.3
80	1	9.6	0.1	1.3	0.3	0.7	0.3	0.5	0.3
130	1	9.6	0.1	1.3	0.3	0.7	0.3	0.5	0.3
200	1	9.5	0.1	1.3	0.3	0.6	0.3	0.4	0.3
280	1	9.8	0.1	1.3	0.3	0.6	0.3	0.4	0.3
300	1	9.6	0.1	1.4	0.3	0.7	0.3	0.5	0.3
300	1	9.3	0.1	1.4	0.3	0.7	0.3	0.5	0.3
300	1	8.9	0.1	1.8	0.3	1.0	0.3	0.7	0.3
300	1	9.0	0.1	1.7	0.3	0.8	0.3	0.5	0.3
400	1	9.4	0.1	1.3	0.3	0.6	0.3	0.4	0.3

X Position Value (cm)	Ux Error (cm)	Urms Value (cm/s)	Vrms Error (cm/s)	Wrms Value (cm/s)	X Position Value (cm)	Ux Error (cm)	Urms Value (cm/s)	Vrms Error (cm/s)	Wrms Value (cm/s)
520	1	9.6	0.1	1.3	0.3	0.6	0.3	0.4	0.3
580	1	9.4	0.1	1.3	0.3	0.6	0.3	0.5	0.3
640	1	9.5	0.1	1.3	0.3	0.7	0.3	0.5	0.3
700	1	9.5	0.1	1.4	0.3	0.7	0.3	0.5	0.3
770	1	9.4	0.1	1.5	0.3	0.7	0.3	0.5	0.3

Table 2. Rigid Control – Raw deposition data along centerline of flume with measured standard deviation.

Rigid Control			
X Position		Net Deposition	
Value (cm)	Error (cm)	Value (g/cm2)	Error (g/cm2)
-100	1	0.0017	0.0001
-50	1	0.0025	0.0001
-10	1	0.0025	0.0001
30	1	0.0026	0.0001
70	1	0.0025	0.0001
110	1	0.0025	0.0001
150	1	0.0025	0.0001
190	1	0.0025	0.0001
230	1	0.0025	0.0001
270	1	0.0025	0.0001
300	1	0.0024	0.0001
340	1	0.0025	0.0001
380	1	0.0026	0.0001
420	1	0.0026	0.0001
460	1	0.0025	0.0001
500	1	0.0025	0.0001
540	1	0.0025	0.0001
580	1	0.0025	0.0001
600	1	0.0025	0.0001
620	1	0.0025	0.0001
640	1	0.0026	0.0001
660	1	0.0025	0.0001
680	1	0.0025	0.0001
700	1	0.0025	0.0001
720	1	0.0024	0.0001
740	1	0.0024	0.0001

X Position Value (cm)	Net Deposition Error (cm)	X Position Value (cm)	Net Deposition Error (cm)
760	1	0.0025	0.0001
780	1	0.0024	0.0001
800	1	0.0024	0.0001
820	1	0.0024	0.0001
830	1	0.0025	0.0001
840	1	0.0025	0.0001

Table 3. Case 1 – Raw velocity data along centerline of flume with measured standard deviation.

Rigid Dense – Case 1									
X Position		Ux		Urms		Vrms		Wrms	
Value (cm)	Error (cm)	Value (cm/s)	Error (cm/s)	Value (cm/s)	Error (cm/s)	Value (cm/s)	Error (cm/s)	Value (cm/s)	Error (cm/s)
-120	1	8.9	0.1	0.7	0.3	0.7	0.3	0.4	0.3
-100	1	9.1	0.1	0.7	0.3	0.6	0.3	0.4	0.3
-100	1	9.8	0.1	0.7	0.3	0.6	0.3	0.4	0.3
-80	1	9.1	0.1	0.7	0.3	0.6	0.3	0.4	0.3
-80	1	9.7	0.1	0.7	0.3	0.6	0.3	0.4	0.3
-60	1	9.0	0.1	0.7	0.3	0.6	0.3	0.4	0.3
-60	1	9.6	0.1	0.7	0.3	0.6	0.3	0.4	0.3
-50	1	9.6	0.1	0.7	0.3	0.6	0.3	0.4	0.3
-40	1	8.8	0.1	0.6	0.3	0.6	0.3	0.4	0.3
-40	1	9.4	0.1	0.6	0.3	0.5	0.3	0.4	0.3
-20	1	8.1	0.1	0.7	0.3	0.5	0.3	0.4	0.3
-20	1	8.6	0.1	0.6	0.3	0.5	0.3	0.4	0.3
-15	1	7.7	0.1	0.7	0.3	0.5	0.3	0.4	0.3
-10	1	7.2	0.1	0.7	0.3	0.5	0.3	0.4	0.3
-10	1	7.8	0.1	0.7	0.3	0.5	0.3	0.4	0.3
-5	1	6.3	0.1	0.7	0.3	0.5	0.3	0.3	0.3
-5	1	7.1	0.1	0.6	0.3	0.5	0.3	0.4	0.3
-2	1	5.5	0.1	0.7	0.3	0.5	0.3	0.3	0.3
-2	1	6.1	0.1	0.7	0.3	0.5	0.3	0.4	0.3
45	1	1.5	0.1	0.6	0.3	0.6	0.3	0.3	0.3
45	1	1.5	0.1	0.6	0.3	0.6	0.3	0.3	0.3
45	1	1.1	0.1	0.7	0.3	0.6	0.3	0.3	0.3
50	1	0.9	0.1	0.4	0.3	0.3	0.3	0.2	0.3
50	1	0.9	0.1	0.4	0.3	0.4	0.3	0.2	0.3
55	1	0.9	0.1	0.3	0.3	0.3	0.3	0.2	0.3
55	1	0.8	0.1	0.3	0.3	0.3	0.3	0.2	0.3
60	1	0.8	0.1	0.3	0.3	0.3	0.3	0.2	0.3

X Position		Ux		Urms		Vrms		Wrms	
Value	Error	Value	Error	Value	Value	Error	Value	Error	Value
(cm)	(cm)	(cm/s)	(cm/s)	(cm/s)	(cm)	(cm)	(cm/s)	(cm/s)	(cm/s)
60	1	0.9	0.1	0.3	0.3	0.2	0.3	0.2	0.3
65	1	0.7	0.1	0.3	0.3	0.2	0.3	0.1	0.3
70	1	0.7	0.1	0.3	0.3	0.3	0.3	0.2	0.3
70	1	0.8	0.1	0.3	0.3	0.3	0.3	0.2	0.3
80	1	0.5	0.1	0.3	0.3	0.3	0.3	0.2	0.3
80	1	0.6	0.1	0.3	0.3	0.3	0.3	0.2	0.3
90	1	0.6	0.1	0.3	0.3	0.4	0.3	0.1	0.3
100	1	0.4	0.1	0.3	0.3	0.4	0.3	0.1	0.3
100	1	0.4	0.1	0.3	0.3	0.7	0.3	0.1	0.3
100	1	0.3	0.1	0.5	0.3	0.8	0.3	0.2	0.3
110	1	0.3	0.1	0.3	0.3	0.9	0.3	0.1	0.3
110	1	0.4	0.1	0.4	0.3	0.7	0.3	0.2	0.3
120	1	0.1	0.1	0.5	0.3	1.4	0.3	0.2	0.3
130	1	-0.6	0.1	1.2	0.3	2.7	0.3	0.7	0.3
140	1	-0.7	0.1	1.3	0.3	2.7	0.3	0.8	0.3
140	1	-0.9	0.1	1.3	0.3	2.6	0.3	0.8	0.3
150	1	-0.5	0.1	1.5	0.3	2.9	0.3	0.8	0.3
160	1	-0.2	0.1	2.0	0.3	3.5	0.3	0.9	0.3
160	1	0.2	0.1	2.0	0.3	3.7	0.3	0.9	0.3
170	1	0.9	0.1	2.5	0.3	4.0	0.3	0.9	0.3
180	1	2.8	0.1	2.8	0.3	4.4	0.3	0.9	0.3
190	1	2.0	0.1	2.5	0.3	3.9	0.3	0.9	0.3
200	1	2.5	0.1	2.6	0.3	3.8	0.3	0.9	0.3
200	1	5.0	0.1	3.0	0.3	4.6	0.3	1.0	0.3
200	1	4.9	0.1	2.5	0.3	4.7	0.3	1.0	0.3
210	1	5.3	0.1	2.4	0.3	4.7	0.3	1.0	0.3
220	1	3.5	0.1	3.0	0.3	3.9	0.3	0.9	0.3
230	1	6.8	0.1	2.8	0.3	4.4	0.3	1.0	0.3
240	1	6.0	0.1	2.6	0.3	4.1	0.3	0.9	0.3

X Position		Ux		Urms		Vrms		Wrms	
Value (cm)	Error (cm)	Value (cm/s)	Error (cm/s)	Value (cm/s)	Value (cm)	Error (cm)	Value (cm/s)	Error (cm/s)	Value (cm/s)
250	1	7.4	0.1	2.0	0.3	4.0	0.3	0.9	0.3
260	1	7.5	0.1	2.1	0.3	3.9	0.3	0.9	0.3
280	1	8.2	0.1	2.0	0.3	3.7	0.3	0.9	0.3
300	1	8.5	0.1	1.9	0.3	3.5	0.3	0.9	0.3
300	1	8.0	0.1	1.8	0.3	3.3	0.3	0.9	0.3
320	1	8.1	0.1	1.9	0.3	3.1	0.3	0.9	0.3
340	1	9.4	0.1	1.6	0.3	3.0	0.3	0.9	0.3
360	1	9.2	0.1	1.7	0.3	2.8	0.3	0.8	0.3
380	1	10.0	0.1	1.7	0.3	2.9	0.3	0.8	0.3
380	1	8.8	0.1	1.7	0.3	2.7	0.3	0.8	0.3
400	1	8.6	0.1	2.0	0.3	2.7	0.3	0.8	0.3
420	1	10.0	0.1	1.7	0.3	2.5	0.3	0.8	0.3
420	1	9.7	0.1	1.5	0.3	2.5	0.3	0.8	0.3
450	1	10.5	0.1	1.7	0.3	2.5	0.3	0.8	0.3
460	1	10.2	0.1	1.5	0.3	2.3	0.3	0.8	0.3
500	1	11.1	0.1	1.6	0.3	2.1	0.3	0.8	0.3
500	1	10.6	0.1	1.7	0.3	2.1	0.3	0.8	0.3
550	1	10.7	0.1	1.5	0.3	1.9	0.3	0.7	0.3
600	1	10.5	0.1	1.3	0.3	1.6	0.3	0.7	0.3

Table 4. Case 1 – Raw deposition data along centerline of flume for each replicate with measured standard deviation and the mean of the replicates.

Rigid Dense – Case 1									
X Position		Net Deposition Replicate 1		Net Deposition Replicate 2		Net Deposition Replicate 3		Mean Net Deposition	
Value (cm)	Error (cm)	Value (g/cm2)	Error (g/cm2)	Value (g/cm2)	Error (g/cm2)	Value (g/cm2)	Error (g/cm2)	Value (g/cm2)	Error (g/cm2)
-100	3	0.0021	0.0001	0.0024	0.0001	0.0010	0.0001	0.0018	0.0007
-90	3	0.0029	0.0001	0.0036	0.0001	0.0019	0.0001	0.0028	0.0008
-80	3	0.0031	0.0001	0.0037	0.0001	0.0021	0.0001	0.0030	0.0008
-70	3	0.0032	0.0001	0.0040	0.0001	0.0023	0.0001	0.0032	0.0009
-60	3	0.0020	0.0001	0.0026	0.0001	0.0022	0.0001	0.0022	0.0003
-50	3	0.0032	0.0001	0.0039	0.0001	0.0025	0.0001	0.0032	0.0007
-40	3	0.0032	0.0001	0.0037	0.0001	0.0024	0.0001	0.0031	0.0006
-30	3	0.0032	0.0001	0.0038	0.0001	0.0025	0.0001	0.0032	0.0007
-20	3	0.0032	0.0001	0.0037	0.0001	0.0026	0.0001	0.0032	0.0006
-10	3	0.0031	0.0001	0.0032	0.0001	0.0026	0.0001	0.0030	0.0003
0	3	0.0026	0.0001	0.0024	0.0001	0.0024	0.0001	0.0025	0.0001
42	3	0.0029	0.0001	0.0028	0.0001	-	-	0.0029	0.0001
43	3	-	-	-	-	0.0026	0.0001	0.0026	-
50	3	0.0036	0.0001	0.0033	0.0001	0.0032	0.0001	0.0034	0.0002
60	3	0.0032	0.0001	0.0029	0.0001	0.0021	0.0001	0.0027	0.0005
70	3	0.0033	0.0001	0.0030	0.0001	0.0033	0.0001	0.0032	0.0001
80	3	0.0032	0.0001	0.0031	0.0001	0.0031	0.0001	0.0031	0.0001
90	3	0.0031	0.0001	0.0030	0.0001	0.0030	0.0001	0.0030	0.0001
100	3	0.0032	0.0001	0.0032	0.0001	0.0029	0.0001	0.0031	0.0002
110	3	0.0030	0.0001	0.0031	0.0001	0.0028	0.0001	0.0030	0.0002
120	3	0.0030	0.0001	0.0029	0.0001	0.0024	0.0001	0.0028	0.0003
130	3	0.0028	0.0001	0.0027	0.0001	0.0026	0.0001	0.0027	0.0001
140	3	0.0026	0.0001	0.0025	0.0001	0.0022	0.0001	0.0024	0.0002
150	3	0.0024	0.0001	0.0022	0.0001	0.0021	0.0001	0.0022	0.0002

X Position		Net Deposition Replicate 1		Net Deposition Replicate 2		Net Deposition Replicate 3		Mean Net Deposition	
Value (cm)	Error (cm)	Value (g/cm2)	Error (g/cm2)	Value (g/cm2)	Error (g/cm2)	Value (g/cm2)	Error (g/cm2)	Value (g/cm2)	Error (g/cm2)
160	3	0.0022	0.0001	0.0022	0.0001	0.0020	0.0001	0.0021	0.0001
170	3	0.0021	0.0001	0.0019	0.0001	0.0020	0.0001	0.0020	0.0001
180	3	0.0023	0.0001	0.0020	0.0001	0.0021	0.0001	0.0021	0.0001
190	3	0.0023	0.0001	0.0020	0.0001	0.0021	0.0001	0.0021	0.0002
200	3	0.0023	0.0001	0.0020	0.0001	0.0020	0.0001	0.0021	0.0002
210	3	0.0021	0.0001	0.0021	0.0001	0.0020	0.0001	0.0021	0.0001
220	3	0.0020	0.0001	0.0019	0.0001	0.0021	0.0001	0.0020	0.0001
230	3	0.0019	0.0001	0.0016	0.0001	0.0020	0.0001	0.0018	0.0002
240	3	0.0020	0.0001	0.0019	0.0001	0.0021	0.0001	0.0020	0.0001
250	3	-	-	0.0019	0.0001	0.0019	0.0001	0.0019	0.0000
260	3	0.0020	0.0001	0.0017	0.0001	0.0020	0.0001	0.0019	0.0002
270	3	0.0019	0.0001	0.0016	0.0001	0.0020	0.0001	0.0019	0.0002
280	3	0.0020	0.0001	0.0018	0.0001	0.0021	0.0001	0.0019	0.0002
290	3	0.0019	0.0001	0.0015	0.0001	0.0021	0.0001	0.0018	0.0003
300	3	0.0019	0.0001	0.0017	0.0001	0.0021	0.0001	0.0019	0.0002
310	3	0.0020	0.0001	0.0016	0.0001	0.0021	0.0001	0.0019	0.0003
320	3	0.0017	0.0001	0.0015	0.0001	0.0021	0.0001	0.0018	0.0003
330	3	0.0015	0.0001	0.0016	0.0001	0.0021	0.0001	0.0017	0.0003
340	3	0.0019	0.0001	0.0015	0.0001	0.0020	0.0001	0.0018	0.0003
350	3	0.0019	0.0001	0.0016	0.0001	0.0019	0.0001	0.0018	0.0002
360	3	-	-	0.0015	0.0001	0.0021	0.0001	0.0018	0.0005
370	3	0.0016	0.0001	0.0013	0.0001	0.0021	0.0001	0.0016	0.0004
380	3	0.0016	0.0001	0.0016	0.0001	0.0022	0.0001	0.0018	0.0003
390	3	0.0014	0.0001	0.0015	0.0001	0.0021	0.0001	0.0017	0.0004
400	3	0.0015	0.0001	0.0016	0.0001	0.0021	0.0001	0.0018	0.0003
410	3	0.0015	0.0001	0.0015	0.0001	0.0020	0.0001	0.0016	0.0003
420	3	0.0015	0.0001	0.0013	0.0001	0.0021	0.0001	0.0016	0.0004
430	3	0.0013	0.0001	0.0015	0.0001	0.0018	0.0001	0.0015	0.0002

X Position		Net Deposition Replicate 1		Net Deposition Replicate 2		Net Deposition Replicate 3		Mean Net Deposition	
Value (cm)	Error (cm)	Value (g/cm2)	Error (g/cm2)	Value (g/cm2)	Error (g/cm2)	Value (g/cm2)	Error (g/cm2)	Value (g/cm2)	Error (g/cm2)
440	3	0.0015	0.0001	0.0012	0.0001	0.0020	0.0001	0.0016	0.0004
450	3	0.0016	0.0001	0.0013	0.0001	0.0019	0.0001	0.0016	0.0003
460	3	0.0014	0.0001	0.0011	0.0001	0.0020	0.0001	0.0015	0.0004
470	3	0.0016	0.0001	0.0015	0.0001	0.0020	0.0001	0.0017	0.0002
480	3	0.0016	0.0001	0.0015	0.0001	0.0019	0.0001	0.0017	0.0002
490	3	0.0017	0.0001	0.0014	0.0001	0.0019	0.0001	0.0017	0.0003
500	3	0.0017	0.0001	0.0013	0.0001	0.0018	0.0001	0.0016	0.0002
510	3	0.0019	0.0001	0.0014	0.0001	0.0020	0.0001	0.0018	0.0003
520	3	0.0018	0.0001	0.0013	0.0001	0.0020	0.0001	0.0017	0.0003
530	3	0.0016	0.0001	0.0014	0.0001	0.0020	0.0001	0.0017	0.0003
540	3	0.0018	0.0001	0.0013	0.0001	0.0020	0.0001	0.0017	0.0003
550	3	0.0019	0.0001	0.0013	0.0001	0.0020	0.0001	0.0017	0.0004
560	3	0.0020	0.0001	0.0015	0.0001	0.0019	0.0001	0.0018	0.0003
570	3	0.0019	0.0001	0.0013	0.0001	0.0019	0.0001	0.0017	0.0003
580	3	0.0017	0.0001	0.0012	0.0001	0.0019	0.0001	0.0016	0.0003
590	3	0.0019	0.0001	0.0014	0.0001	0.0019	0.0001	0.0017	0.0003
600	3	0.0017	0.0001	0.0014	0.0001	0.0020	0.0001	0.0017	0.0003
610	3	-	-	-	-	0.0020	0.0001	0.0020	-
620	3	-	-	-	-	0.0019	0.0001	0.0019	-
630	3	-	-	-	-	0.0019	0.0001	0.0019	-
640	3	-	-	-	-	0.0019	0.0001	0.0019	-
650	3	-	-	-	-	0.0020	0.0001	0.0020	-
660	3	-	-	-	-	0.0019	0.0001	0.0019	-
670	3	-	-	-	-	0.0019	0.0001	0.0019	-
680	3	-	-	-	-	0.0019	0.0001	0.0019	-
690	3	-	-	-	-	0.0020	0.0001	0.0020	-
700	3	-	-	-	-	0.0020	0.0001	0.0020	-
710	3	-	-	-	-	0.0020	0.0001	0.0020	-
720	3	-	-	-	-	0.0019	0.0001	0.0019	-

X Position		Net Deposition Replicate 1		Net Deposition Replicate 2		Net Deposition Replicate 3		Mean Net Deposition	
Value (cm)	Error (cm)	Value (g/cm2)	Error (g/cm2)	Value (g/cm2)	Error (g/cm2)	Value (g/cm2)	Error (g/cm2)	Value (g/cm2)	Error (g/cm2)
730	3	-	-	-	-	0.0020	0.0001	0.0020	-
740	3	-	-	-	-	0.0020	0.0001	0.0020	-
750	3	-	-	-	-	0.0021	0.0001	0.0021	-
760	3	-	-	-	-	0.0020	0.0001	0.0020	-
770	3	-	-	-	-	0.0020	0.0001	0.0020	-
780	3	-	-	-	-	0.0020	0.0001	0.0020	-
790	3	-	-	-	-	0.0020	0.0001	0.0020	-
800	3	-	-	-	-	0.0021	0.0001	0.0021	-
810	3	-	-	-	-	0.0020	0.0001	0.0020	-
820	3	-	-	-	-	0.0019	0.0001	0.0019	-
830	3	-	-	-	-	0.0020	0.0001	0.0020	-
840	3	-	-	-	-	0.0020	0.0001	0.0020	-
850	3	-	-	-	-	0.0020	0.0001	0.0020	-
860	3	-	-	-	-	0.0020	0.0001	0.0020	-
870	3	-	-	-	-	0.0020	0.0001	0.0020	-

Table 5. Case 2 – Raw velocity data along centerline of flume with measured standard deviation.

Rigid Sparse – Case 2									
X Position		Ux		Urms		Vrms		Wrms	
Value (cm)	Error (cm)	Value (cm/s)	Error (cm/s)	Value (cm/s)	Error (cm/s)	Value (cm/s)	Error (cm/s)	Value (cm/s)	Error (cm/s)
-200	1	9.16	0.1	0.9	0.3	0.6	0.3	0.4	0.3
-180	1	9.69	0.1	0.9	0.3	0.6	0.3	0.4	0.3
-100	1	9.61	0.1	0.9	0.3	0.6	0.3	0.4	0.3
-70	1	9.57	0.1	1.0	0.3	0.6	0.3	0.4	0.3
-50	1	9.42	0.1	1.0	0.3	0.6	0.3	0.4	0.3
-30	1	9.20	0.1	1.0	0.3	0.6	0.3	0.4	0.3
-10	1	8.70	0.1	1.2	0.3	0.6	0.3	0.5	0.3
-5	1	8.28	0.1	1.1	0.3	0.6	0.3	0.5	0.3
-2	1	7.85	0.1	1.0	0.3	0.6	0.3	0.5	0.3
-1	1	8.26	0.1	1.0	0.3	0.6	0.3	0.5	0.3
2.5	1	8.13	0.1	1.8	0.3	1.4	0.3	0.7	0.3
6	1	8.32	0.1	1.8	0.3	1.7	0.3	0.7	0.3
16	1	7.47	0.1	2.7	0.3	2.4	0.3	0.8	0.3
23	1	7.42	0.1	2.3	0.3	2.1	0.3	0.8	0.3
33	1	6.97	0.1	1.7	0.3	1.6	0.3	0.7	0.3
40	1	6.10	0.1	1.8	0.3	1.8	0.3	0.7	0.3
44	1	5.62	0.1	1.4	0.3	1.3	0.3	0.6	0.3
45	1	6.14	0.1	1.4	0.3	1.2	0.3	0.6	0.3
45	1	5.48	0.1	1.3	0.3	1.2	0.3	0.6	0.3
45	1	5.96	0.1	1.4	0.3	1.2	0.3	0.6	0.3
50	1	4.92	0.1	0.9	0.3	0.9	0.3	0.4	0.3
50	1	5.59	0.1	1.0	0.3	0.8	0.3	0.5	0.3
60	1	5.22	0.1	0.8	0.3	0.6	0.3	0.3	0.3
70	1	4.39	0.1	0.5	0.3	0.5	0.3	0.2	0.3
70	1	5.08	0.1	0.6	0.3	0.4	0.3	0.3	0.3
80	1	5.08	0.1	0.7	0.3	0.4	0.3	0.3	0.3
84	1	5.05	0.1	0.4	0.3	0.3	0.3	0.2	0.3

X Position		Ux		Urms		Vrms		Wrms	
Value	Error	Value	Error	Value	Value	Error	Value	Error	Value
(cm)	(cm)	(cm/s)	(cm/s)	(cm/s)	(cm)	(cm)	(cm/s)	(cm/s)	(cm/s)
90	1	4.43	0.1	0.4	0.3	0.3	0.3	0.2	0.3
100	1	4.80	0.1	0.4	0.3	0.3	0.3	0.2	0.3
100	1	4.99	0.1	0.4	0.3	0.3	0.3	0.2	0.3
120	1	4.60	0.1	0.3	0.3	0.4	0.3	0.2	0.3
120	1	5.06	0.1	0.6	0.3	0.3	0.3	0.2	0.3
140	1	4.99	0.1	0.5	0.3	0.3	0.3	0.2	0.3
150	1	4.34	0.1	0.4	0.3	0.3	0.3	0.2	0.3
160	1	4.89	0.1	0.5	0.3	0.3	0.3	0.2	0.3
200	1	4.41	0.1	0.5	0.3	0.5	0.3	0.2	0.3
200	1	4.91	0.1	0.4	0.3	0.4	0.3	0.1	0.3
200	1	4.92	0.1	0.5	0.3	0.4	0.3	0.2	0.3
240	1	4.83	0.1	0.6	0.3	0.5	0.3	0.2	0.3
250	1	4.46	0.1	0.5	0.3	0.8	0.3	0.2	0.3
280	1	4.88	0.1	0.6	0.3	0.6	0.3	0.2	0.3
300	1	4.73	0.1	0.6	0.3	1.0	0.3	0.4	0.3
300	1	5.04	0.1	0.5	0.3	0.6	0.3	0.2	0.3
320	1	5.03	0.1	0.7	0.3	0.8	0.3	0.4	0.3
350	1	4.97	0.1	0.9	0.3	1.2	0.3	0.5	0.3
360	1	5.48	0.1	1.0	0.3	1.2	0.3	0.5	0.3
400	1	5.94	0.1	1.3	0.3	1.5	0.3	0.6	0.3
400	1	5.47	0.1	0.7	0.3	1.0	0.3	0.4	0.3
400	1	5.74	0.1	1.0	0.3	1.2	0.3	0.5	0.3
450	1	6.22	0.1	1.2	0.3	1.3	0.3	0.6	0.3
450	1	6.37	0.1	1.3	0.3	1.3	0.3	0.5	0.3
500	1	6.59	0.1	1.2	0.3	1.2	0.3	0.5	0.3
500	1	6.72	0.1	1.3	0.3	1.3	0.3	0.6	0.3
500	1	6.43	0.1	1.2	0.3	1.2	0.3	0.5	0.3
550	1	6.56	0.1	1.2	0.3	1.2	0.3	0.5	0.3
550	1	7.39	0.1	1.4	0.3	1.1	0.3	0.6	0.3

X Position		Ux		Urms		Vrms		Wrms	
Value (cm)	Error (cm)	Value (cm/s)	Error (cm/s)	Value (cm/s)	Value (cm)	Error (cm)	Value (cm/s)	Error (cm/s)	Value (cm/s)
600	1	7.49	0.1	1.2	0.3	1.3	0.3	0.6	0.3
600	1	7.44	0.1	1.3	0.3	1.2	0.3	0.6	0.3
650	1	7.75	0.1	1.2	0.3	1.2	0.3	0.5	0.3
700	1	8.57	0.1	1.2	0.3	1.2	0.3	0.5	0.3
750	1	8.93	0.1	1.2	0.3	1.1	0.3	0.5	0.3
800	1	8.98	0.1	1.0	0.3	1.0	0.3	0.5	0.3
850	1	9.13	0.1	1.2	0.3	0.9	0.3	0.5	0.3
900	1	9.08	0.1	1.1	0.3	0.8	0.3	0.5	0.3

Table 6. Case 2 – Raw deposition data along centerline of flume for each replicate with measured standard deviation and the mean of the replicates.

Rigid Sparse – Case 2									
X Position		Net Deposition Replicate 1		Net Deposition Replicate 2		Net Deposition Replicate 3		Mean Net Deposition	
Value (cm)	Error (cm)	Value (g/cm2)	Error (g/cm2)	Value (g/cm2)	Error (g/cm2)	Value (g/cm2)	Error (g/cm2)	Value (g/cm2)	Error (g/cm2)
-100	3	0.0021	0.0001	0.0028	0.0001	0.0012	0.0001	0.0020	0.0008
-90	3	0.0024	0.0001	0.0028	0.0001	0.0020	0.0001	0.0024	0.0004
-80	3	0.0022	0.0001	0.0026	0.0001	0.0026	0.0001	0.0025	0.0002
-70	3	0.0022	0.0001	0.0023	0.0001	0.0022	0.0001	0.0023	0.0000
-60	3	0.0014	0.0001	0.0020	0.0001	0.0027	0.0001	0.0020	0.0006
-50	3	0.0020	0.0001	0.0022	0.0001	0.0031	0.0001	0.0024	0.0006
-40	3	0.0024	0.0001	0.0024	0.0001	0.0029	0.0001	0.0026	0.0003
-30	3	0.0024	0.0001	0.0025	0.0001	0.0029	0.0001	0.0026	0.0003
-20	3	0.0025	0.0001	0.0025	0.0001	0.0029	0.0001	0.0027	0.0002
-10	3	0.0026	0.0001	0.0026	0.0001	0.0029	0.0001	0.0027	0.0002
0	3	0.0015	0.0001	0.0017	0.0001	0.0028	0.0001	0.0020	0.0007
5	3	-	-	-	-	0.0018	0.0001	0.0018	-
11	3	-	-	-	-	0.0017	0.0001	0.0017	-
18	3	-	-	-	-	0.0016	0.0001	0.0016	-
22	3	-	-	-	-	0.0018	0.0001	0.0018	-
28	3	-	-	-	-	0.0016	0.0001	0.0016	-
35	3	-	-	-	-	0.0018	0.0001	0.0018	-
42	3	0.0022	0.0001	0.0025	0.0001	-	-	0.0023	0.0002
43	3	-	-	-	-	0.0020	0.0001	0.0020	-
50	3	0.0025	0.0001	0.0027	0.0001	0.0020	0.0001	0.0024	0.0004
60	3	0.0025	0.0001	0.0027	0.0001	0.0025	0.0001	0.0025	0.0001
70	3	0.0026	0.0001	0.0029	0.0001	0.0025	0.0001	0.0027	0.0002
80	3	0.0027	0.0001	0.0029	0.0001	0.0026	0.0001	0.0027	0.0002
90	3	0.0027	0.0001	0.0030	0.0001	0.0027	0.0001	0.0028	0.0001
100	3	0.0029	0.0001	0.0031	0.0001	0.0029	0.0001	0.0030	0.0001

X Position		Net Deposition Replicate 1		Net Deposition Replicate 2		Net Deposition Replicate 3		Mean Net Deposition	
Value (cm)	Error (cm)	Value (g/cm2)	Error (g/cm2)	Value (g/cm2)	Value (cm)	Error (cm)	Value (g/cm2)	Error (g/cm2)	Value (g/cm2)
110	3	0.0029	0.0001	0.0031	0.0001	0.0029	0.0001	0.0030	0.0001
120	3	0.0029	0.0001	0.0030	0.0001	0.0032	0.0001	0.0030	0.0001
130	3	0.0029	0.0001	0.0032	0.0001	0.0031	0.0001	0.0031	0.0002
140	3	0.0029	0.0001	0.0032	0.0001	0.0030	0.0001	0.0031	0.0002
150	3	0.0029	0.0001	0.0033	0.0001	0.0030	0.0001	0.0031	0.0002
160	3	0.0030	0.0001	0.0033	0.0001	0.0030	0.0001	0.0031	0.0002
170	3	0.0031	0.0001	0.0033	0.0001	0.0031	0.0001	0.0031	0.0001
180	3	0.0031	0.0001	0.0033	0.0001	0.0033	0.0001	0.0032	0.0001
190	3	0.0031	0.0001	0.0033	0.0001	0.0032	0.0001	0.0032	0.0001
200	3	0.0030	0.0001	0.0033	0.0001	0.0031	0.0001	0.0031	0.0002
210	3	0.0030	0.0001	0.0034	0.0001	0.0030	0.0001	0.0031	0.0002
220	3	0.0030	0.0001	0.0033	0.0001	0.0029	0.0001	0.0031	0.0002
230	3	0.0029	0.0001	0.0032	0.0001	0.0030	0.0001	0.0030	0.0002
240	3	0.0029	0.0001	0.0032	0.0001	0.0030	0.0001	0.0030	0.0001
250	3	0.0028	0.0001	0.0031	0.0001	0.0029	0.0001	0.0029	0.0002
260	3	0.0028	0.0001	0.0031	0.0001	0.0029	0.0001	0.0029	0.0002
270	3	0.0029	0.0001	0.0032	0.0001	0.0029	0.0001	0.0030	0.0002
280	3	0.0028	0.0001	0.0032	0.0001	0.0028	0.0001	0.0030	0.0002
290	3	0.0028	0.0001	0.0032	0.0001	0.0027	0.0001	0.0029	0.0002
300	3	0.0028	0.0001	0.0031	0.0001	0.0028	0.0001	0.0029	0.0001
310	3	0.0027	0.0001	0.0031	0.0001	0.0027	0.0001	0.0028	0.0002
320	3	0.0028	0.0001	0.0030	0.0001	0.0027	0.0001	0.0028	0.0002
330	3	0.0027	0.0001	0.0030	0.0001	0.0027	0.0001	0.0028	0.0002
340	3	0.0028	0.0001	0.0031	0.0001	0.0026	0.0001	0.0028	0.0002
350	3	0.0026	0.0001	0.0029	0.0001	0.0026	0.0001	0.0027	0.0002
360	3	0.0025	0.0001	0.0028	0.0001	0.0026	0.0001	0.0026	0.0002
370	3	0.0024	0.0001	0.0028	0.0001	0.0026	0.0001	0.0026	0.0002
380	3	0.0024	0.0001	0.0027	0.0001	0.0024	0.0001	0.0025	0.0002
390	3	0.0025	0.0001	0.0028	0.0001	0.0024	0.0001	0.0026	0.0002

X Position		Net Deposition Replicate 1		Net Deposition Replicate 2		Net Deposition Replicate 3		Mean Net Deposition	
Value (cm)	Error (cm)	Value (g/cm2)	Error (g/cm2)	Value (g/cm2)	Value (cm)	Error (cm)	Value (g/cm2)	Error (g/cm2)	Value (g/cm2)
400	3	0.0025	0.0001	0.0028	0.0001	0.0024	0.0001	0.0026	0.0002
410	3	0.0025	0.0001	0.0028	0.0001	0.0023	0.0001	0.0025	0.0002
420	3	0.0025	0.0001	0.0028	0.0001	0.0024	0.0001	0.0025	0.0002
430	3	0.0024	0.0001	0.0028	0.0001	0.0024	0.0001	0.0025	0.0002
440	3	0.0024	0.0001	0.0026	0.0001	0.0023	0.0001	0.0024	0.0002
450	3	0.0024	0.0001	0.0026	0.0001	0.0023	0.0001	0.0025	0.0002
460	3	0.0023	0.0001	0.0026	0.0001	0.0024	0.0001	0.0024	0.0002
470	3	0.0024	0.0001	0.0026	0.0001	0.0023	0.0001	0.0024	0.0001
480	3	0.0024	0.0001	0.0026	0.0001	0.0024	0.0001	0.0024	0.0001
490	3	0.0024	0.0001	0.0026	0.0001	0.0024	0.0001	0.0025	0.0001
500	3	0.0024	0.0001	0.0026	0.0001	0.0024	0.0001	0.0025	0.0001
510	3	0.0024	0.0001	0.0025	0.0001	0.0024	0.0001	0.0024	0.0001
520	3	0.0023	0.0001	0.0025	0.0001	0.0023	0.0001	0.0023	0.0001
530	3	0.0022	0.0001	0.0025	0.0001	0.0023	0.0001	0.0023	0.0002
540	3	0.0022	0.0001	0.0025	0.0001	0.0023	0.0001	0.0023	0.0001
550	3	0.0022	0.0001	0.0025	0.0001	0.0023	0.0001	0.0023	0.0002
560	3	-	-	-	-	0.0023	0.0001	0.0023	-
570	3	-	-	-	-	0.0023	0.0001	0.0023	-
580	3	-	-	-	-	0.0022	0.0001	0.0022	-
590	3	-	-	-	-	0.0022	0.0001	0.0022	-
600	3	-	-	-	-	0.0023	0.0001	0.0023	-
610	3	-	-	-	-	0.0023	0.0001	0.0023	-
620	3	-	-	-	-	0.0022	0.0001	0.0022	-
630	3	-	-	-	-	0.0022	0.0001	0.0022	-
640	3	-	-	-	-	0.0022	0.0001	0.0022	-
650	3	-	-	-	-	0.0023	0.0001	0.0023	-
660	3	-	-	-	-	0.0023	0.0001	0.0023	-
670	3	-	-	-	-	0.0023	0.0001	0.0023	-
680	3	-	-	-	-	0.0023	0.0001	0.0023	-

X Position		Net Deposition Replicate 1		Net Deposition Replicate 2		Net Deposition Replicate 3		Mean Net Deposition	
Value (cm)	Error (cm)	Value (g/cm2)	Error (g/cm2)	Value (g/cm2)	Value (cm)	Error (cm)	Value (g/cm2)	Error (g/cm2)	Value (g/cm2)
690	3	-	-	-	-	0.0023	0.0001	0.0023	-
700	3	-	-	-	-	0.0023	0.0001	0.0023	-
710	3	-	-	-	-	0.0022	0.0001	0.0022	-
720	3	-	-	-	-	0.0022	0.0001	0.0022	-
730	3	-	-	-	-	0.0023	0.0001	0.0023	-
740	3	-	-	-	-	0.0023	0.0001	0.0023	-
750	3	-	-	-	-	0.0023	0.0001	0.0023	-
760	3	-	-	-	-	0.0023	0.0001	0.0023	-
770	3	-	-	-	-	0.0023	0.0001	0.0023	-
780	3	-	-	-	-	0.0022	0.0001	0.0022	-
790	3	-	-	-	-	0.0023	0.0001	0.0023	-
800	3	-	-	-	-	0.0023	0.0001	0.0023	-
810	3	-	-	-	-	0.0022	0.0001	0.0022	-
820	3	-	-	-	-	0.0022	0.0001	0.0022	-
830	3	-	-	-	-	0.0022	0.0001	0.0022	-

Table 7. Flexible Control – Raw velocity data along centerline of flume with measured standard deviation.

Flexible Control											
X Position		Z Position		Ux		Urms		Vrms		Wrms	
Value (cm)	Error (cm)	Value (cm)	Error (cm)	Value (cm/s)	Error (cm/s)	Value (cm/s)	Error (cm/s)	Value (cm/s)	Error (cm/s)	Value (cm/s)	Error (cm/s)
-95	1	15.0	0.5	7.8	0.1	1.5	0.3	1.3	0.3	0.8	0.3
-95	1	10.0	0.5	7.7	0.1	1.4	0.3	1.2	0.3	0.8	0.3
-95	1	6.0	0.5	7.1	0.1	1.5	0.3	1.3	0.3	0.7	0.3
-50	1	15.0	0.5	8.2	0.1	1.4	0.3	1.1	0.3	0.7	0.3
-50	1	15.0	0.5	8.1	0.1	1.3	0.3	1.0	0.3	0.7	0.3
-50	1	10.0	0.5	7.6	0.1	1.5	0.3	1.2	0.3	0.7	0.3
-50	1	10.0	0.5	7.9	0.1	1.4	0.3	1.2	0.3	0.8	0.3
-50	1	6.0	0.5	7.4	0.1	1.5	0.3	1.1	0.3	0.7	0.3
-50	1	6.0	0.5	7.2	0.1	1.6	0.3	1.3	0.3	0.7	0.3
0	1	15.0	0.5	8.2	0.1	1.3	0.3	1.0	0.3	0.6	0.3
0	1	10.0	0.5	7.2	0.1	1.5	0.3	1.1	0.3	0.6	0.3
0	1	6.0	0.5	7.3	0.1	1.3	0.3	1.0	0.3	0.6	0.3
10	1	6.0	0.5	8.0	0.1	1.4	0.3	1.1	0.3	0.6	0.3
30	1	15.0	0.5	8.2	0.1	1.4	0.3	1.0	0.3	0.6	0.3
30	1	10.0	0.5	7.4	0.1	1.5	0.3	1.1	0.3	0.6	0.3
50	1	15.0	0.5	8.1	0.1	1.4	0.3	1.0	0.3	0.6	0.3
50	1	10.0	0.5	7.9	0.1	1.3	0.3	1.0	0.3	0.6	0.3
50	1	6.0	0.5	8.0	0.1	1.3	0.3	1.0	0.3	0.6	0.3
80	1	15.0	0.5	7.9	0.1	1.6	0.3	0.9	0.3	0.5	0.3
80	1	10.0	0.5	7.7	0.1	1.3	0.3	0.9	0.3	0.6	0.3
80	1	6.0	0.5	8.2	0.1	1.2	0.3	0.9	0.3	0.5	0.3
130	1	15.0	0.5	7.8	0.1	1.6	0.3	0.9	0.3	0.5	0.3
130	1	10.0	0.5	7.7	0.1	1.3	0.3	0.9	0.3	0.5	0.3
130	1	6.0	0.5	8.3	0.1	1.2	0.3	0.8	0.3	0.5	0.3
200	1	15.0	0.5	8.1	0.1	1.5	0.3	0.8	0.3	0.5	0.3

X Position		Z Position		Ux		Urms		Vrms		Wrms	
Value (cm)	Error (cm)	Value (cm)	Error (cm)	Value (cm/s)	Error (cm/s)	Value (cm)	Error (cm)	Value (cm)	Error (cm)	Value (cm/s)	Error (cm/s)
200	1	10.0	0.5	7.1	0.1	1.5	0.3	0.9	0.3	0.5	0.3
200	1	6.0	0.5	8.6	0.1	1.1	0.3	0.7	0.3	0.5	0.3
280	1	15.0	0.5	8.1	0.1	1.4	0.3	0.8	0.3	0.4	0.3
280	1	10.0	0.5	8.4	0.1	1.2	0.3	0.7	0.3	0.5	0.3
280	1	6.0	0.5	7.9	0.1	1.2	0.3	0.7	0.3	0.4	0.3
300	1	15.0	0.5	8.4	0.1	1.1	0.3	0.6	0.3	0.4	0.3
300	1	15.0	0.5	8.0	0.1	1.1	0.3	0.7	0.3	0.4	0.3
300	1	14.0	0.5	8.3	0.1	1.1	0.3	0.7	0.3	0.4	0.3
300	1	13.0	0.5	8.0	0.1	1.1	0.3	0.7	0.3	0.4	0.3
300	1	12.0	0.5	8.0	0.1	1.3	0.3	0.9	0.3	0.5	0.3
300	1	11.0	0.5	8.1	0.1	1.7	0.3	1.7	0.3	0.5	0.3
300	1	10.0	0.5	8.1	0.1	1.4	0.3	1.1	0.3	0.5	0.3
300	1	9.0	0.5	8.2	0.1	1.2	0.3	1.1	0.3	0.5	0.3
300	1	8.0	0.5	8.5	0.1	1.1	0.3	0.7	0.3	0.4	0.3
300	1	7.0	0.5	8.3	0.1	1.1	0.3	0.7	0.3	0.4	0.3
300	1	6.0	0.5	8.0	0.1	1.1	0.3	0.7	0.3	0.4	0.3
300	1	6.0	0.5	8.3	0.1	1.1	0.3	0.7	0.3	0.4	0.3
300	1	5.0	0.5	7.8	0.1	1.1	0.3	0.7	0.3	0.4	0.3
300	1	4.0	0.5	7.6	0.1	1.1	0.3	0.8	0.3	0.4	0.3
300	1	3.0	0.5	7.1	0.1	1.2	0.3	0.8	0.3	0.4	0.3
300	1	2.0	0.5	6.9	0.1	1.1	0.3	0.8	0.3	0.4	0.3
300	1	1.0	0.5	6.8	0.1	1.2	0.3	0.9	0.3	0.4	0.3
300	1	0.0	0.5	5.8	0.1	1.1	0.3	0.9	0.3	0.3	0.3
300	1	-1.0	0.5	0.0	0.1	0.1	0.3	0.0	0.3	0.0	0.3
400	1	15.0	0.5	8.1	0.1	1.5	0.3	0.8	0.3	0.4	0.3
400	1	10.0	0.5	8.6	0.1	1.5	0.3	1.0	0.3	0.5	0.3
400	1	6.0	0.5	8.1	0.1	1.1	0.3	0.7	0.3	0.4	0.3
520	1	15.0	0.5	8.2	0.1	1.5	0.3	0.8	0.3	0.4	0.3
520	1	10.0	0.5	7.8	0.1	1.6	0.3	1.1	0.3	0.5	0.3
520	1	6.0	0.5	7.8	0.1	1.2	0.3	0.7	0.3	0.4	0.3

X Position		Z Position		Ux		Urms		Vrms		Wrms	
Value (cm)	Error (cm)	Value (cm)	Error (cm)	Value (cm/s)	Error (cm/s)	Value (cm)	Error (cm)	Value (cm)	Error (cm)	Value (cm/s)	Error (cm/s)
580	1	15.0	0.5	8.0	0.1	1.6	0.3	0.9	0.3	0.4	0.3
580	1	10.0	0.5	7.8	0.1	1.3	0.3	0.6	0.3	0.4	0.3
580	1	6.0	0.5	7.8	0.1	1.1	0.3	0.7	0.3	0.4	0.3
640	1	15.0	0.5	7.8	0.1	1.7	0.3	0.9	0.3	0.4	0.3
640	1	10.0	0.5	8.2	0.1	1.4	0.3	0.8	0.3	0.4	0.3
640	1	6.0	0.5	7.8	0.1	1.4	0.3	0.8	0.3	0.5	0.3
640	1	6.0	0.5	8.2	0.1	1.0	0.3	0.6	0.3	0.4	0.3
700	1	15.0	0.5	8.0	0.1	1.6	0.3	0.7	0.3	0.4	0.3
700	1	10.0	0.5	8.2	0.1	1.5	0.3	0.9	0.3	0.5	0.3
700	1	6.0	0.5	8.2	0.1	1.5	0.3	0.8	0.3	0.5	0.3
700	1	6.0	0.5	7.9	0.1	1.5	0.3	0.8	0.3	0.5	0.3
770	1	15.0	0.5	7.9	0.1	1.6	0.3	0.8	0.3	0.4	0.3
770	1	10.0	0.5	8.0	0.1	1.6	0.3	0.9	0.3	0.5	0.3
770	1	6.0	0.5	8.0	0.1	1.3	0.3	0.8	0.3	0.5	0.3

Table 8. Flexible Control – Raw deposition data along centerline of flume with measured standard deviation.

Flexible Control			
X Position		Net Deposition	
Value (cm)	Error (cm)	Value (g/cm2)	Error (g/cm2)
-100	1	0.0021	0.0001
-50	1	0.0024	0.0001
-10	1	0.0024	0.0001
30	1	0.0027	0.0001
70	1	0.0027	0.0001
110	1	0.0027	0.0001
150	1	0.0026	0.0001
190	1	0.0026	0.0001
230	1	0.0027	0.0001
270	1	0.0027	0.0001
300	1	0.0028	0.0001
340	1	0.0026	0.0001
380	1	0.0026	0.0001
420	1	0.0028	0.0001
460	1	0.0027	0.0001
500	1	0.0025	0.0001
540	1	0.0026	0.0001
580	1	0.0026	0.0001
600	1	0.0026	0.0001
620	1	0.0026	0.0001
640	1	0.0027	0.0001
660	1	0.0027	0.0001
680	1	0.0026	0.0001
700	1	0.0025	0.0001
720	1	0.0026	0.0001

X Position		Net Deposition	
Value (cm)	Error (cm)	Value (cm)	Error (cm)
740	1	0.0026	0.0001
760	1	0.0025	0.0001
780	1	0.0026	0.0001
800	1	0.0026	0.0001
820	1	0.0023	0.0001
830	1	0.0025	0.0001
840	1	0.0024	0.0001

Table 9. Case 3 – Raw velocity data along centerline with measured standard deviation.

Flexible Dense – Case 3											
X Position		Z Position		Ux		Urms		Vrms		Wrms	
Value (cm)	Error (cm)	Value (cm)	Error (cm)	Value (cm/s)	Error (cm/s)	Value (cm/s)	Error (cm/s)	Value (cm/s)	Error (cm/s)	Value (cm/s)	Error (cm/s)
-95	1	15.0	0.5	7.3	0.1	1.5	0.3	1.2	0.3	0.8	0.3
-95	1	10.0	0.5	7.2	0.1	1.6	0.3	1.3	0.3	0.8	0.3
-95	1	6.0	0.5	7.6	0.1	1.4	0.3	1.4	0.3	0.7	0.3
-50	1	15.0	0.5	7.5	0.1	1.4	0.3	1.0	0.3	0.7	0.3
-50	1	15.0	0.5	7.2	0.1	1.6	0.3	1.2	0.3	0.7	0.3
-50	1	10.0	0.5	7.0	0.1	1.6	0.3	1.1	0.3	0.7	0.3
-50	1	10.0	0.5	8.0	0.1	1.3	0.3	1.1	0.3	0.7	0.3
-50	1	6.0	0.5	7.1	0.1	1.5	0.3	1.2	0.3	0.6	0.3
-50	1	6.0	0.5	7.1	0.1	1.4	0.3	1.2	0.3	0.6	0.3
0	1	15.0	0.5	7.3	0.1	1.3	0.3	1.0	0.3	0.6	0.3
0	1	15.0	0.5	7.4	0.1	1.4	0.3	0.9	0.3	0.6	0.3
0	1	10.0	0.5	6.7	0.1	1.5	0.3	1.1	0.3	0.6	0.3
0	1	10.0	0.5	7.6	0.1	1.5	0.3	1.2	0.3	0.7	0.3
0	1	6.0	0.5	6.2	0.1	1.1	0.3	1.0	0.3	0.5	0.3
10	1	15.0	0.5	7.8	0.1	1.4	0.3	1.0	0.3	0.6	0.3
10	1	10.0	0.5	5.7	0.1	2.9	0.3	1.3	0.3	0.6	0.3
10	1	6.0	0.5	0.3	0.1	0.5	0.3	0.4	0.3	0.1	0.3
22	1	15.0	0.5	9.3	0.1	1.8	0.3	1.3	0.3	0.6	0.3
22	1	10.0	0.5	7.7	0.1	2.3	0.3	1.6	0.3	0.6	0.3
22	1	6.0	0.5	4.7	0.1	1.3	0.3	0.9	0.3	0.4	0.3
30	1	15.0	0.5	9.0	0.1	1.5	0.3	1.0	0.3	0.6	0.3
30	1	10.0	0.5	7.1	0.1	1.8	0.3	1.1	0.3	0.5	0.3
30	1	6.0	0.5	0.1	0.1	0.2	0.3	0.2	0.3	0.1	0.3
50	1	15.0	0.5	9.4	0.1	1.5	0.3	0.9	0.3	0.6	0.3
50	1	15.0	0.5	10.7	0.1	1.8	0.3	1.4	0.3	0.6	0.3
50	1	10.0	0.5	4.6	0.1	2.3	0.3	1.6	0.3	0.8	0.3
50	1	10.0	0.5	6.3	0.1	2.7	0.3	1.8	0.3	0.8	0.3

X Position		Z Position		Ux		Urms		Vrms		Wrms	
Value (cm)	Error (cm)	Value (cm)	Error (cm)	Value (cm/s)	Error (cm/s)	Value (cm)	Error (cm)	Value (cm)	Error (cm)	Value (cm/s)	Error (cm/s)
50	1	6.0	0.5	-0.2	0.1	0.5	0.3	0.4	0.3	0.2	0.3
50	1	6.0	0.5	0.0	0.1	0.4	0.3	0.3	0.3	0.2	0.3
80	1	15.0	0.5	7.9	0.1	2.1	0.3	1.5	0.3	0.8	0.3
80	1	10.0	0.5	3.5	0.1	2.8	0.3	2.7	0.3	1.0	0.3
80	1	6.0	0.5	-0.5	0.1	1.7	0.3	1.8	0.3	1.0	0.3
100	1	15.0	0.5	7.8	0.1	2.2	0.3	1.5	0.3	0.8	0.3
100	1	10.0	0.5	3.2	0.1	3.4	0.3	2.4	0.3	0.9	0.3
100	1	6.0	0.5	1.3	0.1	1.9	0.3	2.1	0.3	1.0	0.3
130	1	15.0	0.5	5.6	0.1	2.2	0.3	1.8	0.3	0.9	0.3
130	1	10.0	0.5	5.1	0.1	1.8	0.3	2.0	0.3	0.9	0.3
130	1	6.0	0.5	2.9	0.1	1.5	0.3	1.9	0.3	0.9	0.3
200	1	15.0	0.5	5.8	0.1	1.5	0.3	1.3	0.3	0.7	0.3
200	1	15.0	0.5	3.1	0.1	2.2	0.3	1.2	0.3	0.8	0.3
200	1	10.0	0.5	5.5	0.1	1.3	0.3	1.6	0.3	0.7	0.3
200	1	10.0	0.5	3.7	0.1	3.0	0.3	1.4	0.3	0.8	0.3
200	1	6.0	0.5	4.8	0.1	1.4	0.3	1.4	0.3	0.8	0.3
200	1	6.0	0.5	5.7	0.1	1.4	0.3	1.2	0.3	0.7	0.3
280	1	15.0	0.5	6.2	0.1	1.3	0.3	0.9	0.3	0.6	0.3
280	1	10.0	0.5	7.0	0.1	1.3	0.3	1.1	0.3	0.7	0.3
280	1	6.0	0.5	5.9	0.1	1.3	0.3	1.1	0.3	0.6	0.3
400	1	15.0	0.5	6.7	0.1	1.2	0.3	0.8	0.3	0.5	0.3
400	1	15.0	0.5	7.3	0.1	1.2	0.3	0.8	0.3	0.5	0.3
400	1	10.0	0.5	7.1	0.1	1.2	0.3	1.0	0.3	0.6	0.3
400	1	10.0	0.5	6.7	0.1	1.7	0.3	0.9	0.3	0.6	0.3
400	1	6.0	0.5	6.4	0.1	1.1	0.3	0.9	0.3	0.5	0.3
400	1	6.0	0.5	6.2	0.1	1.2	0.3	0.8	0.3	0.5	0.3
520	1	15.0	0.5	7.1	0.1	1.1	0.3	0.7	0.3	0.4	0.3
520	1	10.0	0.5	7.5	0.1	1.1	0.3	1.0	0.3	0.5	0.3
520	1	6.0	0.5	6.9	0.1	1.1	0.3	0.9	0.3	0.5	0.3
580	1	15.0	0.5	7.4	0.1	1.0	0.3	0.7	0.3	0.4	0.3

X Position		Z Position		Ux		Urms		Vrms		Wrms	
Value (cm)	Error (cm)	Value (cm)	Error (cm)	Value (cm/s)	Error (cm/s)	Value (cm)	Error (cm)	Value (cm)	Error (cm)	Value (cm/s)	Error (cm/s)
580	1	10.0	0.5	7.3	0.1	1.0	0.3	0.8	0.3	0.4	0.3
580	1	6.0	0.5	7.0	0.1	1.1	0.3	0.8	0.3	0.5	0.3
640	1	15.0	0.5	7.5	0.1	1.0	0.3	0.6	0.3	0.4	0.3
640	1	10.0	0.5	7.5	0.1	1.0	0.3	0.7	0.3	0.4	0.3
640	1	6.0	0.5	7.0	0.1	1.1	0.3	0.8	0.3	0.4	0.3
700	1	15.0	0.5	7.4	0.1	1.0	0.3	0.6	0.3	0.4	0.3
700	1	10.0	0.5	7.6	0.1	1.3	0.3	0.7	0.3	0.4	0.3
700	1	6.0	0.5	7.0	0.1	1.0	0.3	0.8	0.3	0.4	0.3
770	1	15.0	0.5	7.5	0.1	1.0	0.3	0.6	0.3	0.4	0.3
770	1	10.0	0.5	7.3	0.1	1.7	0.3	0.8	0.3	0.5	0.3
770	1	6.0	0.5	7.0	0.1	1.0	0.3	0.7	0.3	0.4	0.3

Table 10. Case 3 – Raw deposition data along centerline for each replicate with measured standard deviation and the mean of the replicates.

Flexible Dense – Case 3											
X Position		Z Position		Ux		Urms		Vrms		Wrms	
Value (cm)	Error (cm)	Value (cm)	Error (cm)	Value (cm/s)	Error (cm/s)	Value (cm/s)	Error (cm/s)	Value (cm/s)	Error (cm/s)	Value (cm/s)	Error (cm/s)
-95	1	15.0	0.5	7.3	0.1	1.5	0.3	1.2	0.3	0.8	0.3
-95	1	10.0	0.5	7.2	0.1	1.6	0.3	1.3	0.3	0.8	0.3
-95	1	6.0	0.5	7.6	0.1	1.4	0.3	1.4	0.3	0.7	0.3
-50	1	15.0	0.5	7.5	0.1	1.4	0.3	1.0	0.3	0.7	0.3
-50	1	15.0	0.5	7.2	0.1	1.6	0.3	1.2	0.3	0.7	0.3
-50	1	10.0	0.5	7.0	0.1	1.6	0.3	1.1	0.3	0.7	0.3
-50	1	10.0	0.5	8.0	0.1	1.3	0.3	1.1	0.3	0.7	0.3
-50	1	6.0	0.5	7.1	0.1	1.5	0.3	1.2	0.3	0.6	0.3
-50	1	6.0	0.5	7.1	0.1	1.4	0.3	1.2	0.3	0.6	0.3
0	1	15.0	0.5	7.3	0.1	1.3	0.3	1.0	0.3	0.6	0.3
0	1	15.0	0.5	7.4	0.1	1.4	0.3	0.9	0.3	0.6	0.3
0	1	10.0	0.5	6.7	0.1	1.5	0.3	1.1	0.3	0.6	0.3
0	1	10.0	0.5	7.6	0.1	1.5	0.3	1.2	0.3	0.7	0.3
0	1	6.0	0.5	6.2	0.1	1.1	0.3	1.0	0.3	0.5	0.3
10	1	15.0	0.5	7.8	0.1	1.4	0.3	1.0	0.3	0.6	0.3
10	1	10.0	0.5	5.7	0.1	2.9	0.3	1.3	0.3	0.6	0.3
10	1	6.0	0.5	0.3	0.1	0.5	0.3	0.4	0.3	0.1	0.3
22	1	15.0	0.5	9.3	0.1	1.8	0.3	1.3	0.3	0.6	0.3
22	1	10.0	0.5	7.7	0.1	2.3	0.3	1.6	0.3	0.6	0.3
22	1	6.0	0.5	4.7	0.1	1.3	0.3	0.9	0.3	0.4	0.3
30	1	15.0	0.5	9.0	0.1	1.5	0.3	1.0	0.3	0.6	0.3
30	1	10.0	0.5	7.1	0.1	1.8	0.3	1.1	0.3	0.5	0.3
30	1	6.0	0.5	0.1	0.1	0.2	0.3	0.2	0.3	0.1	0.3
50	1	15.0	0.5	9.4	0.1	1.5	0.3	0.9	0.3	0.6	0.3
50	1	15.0	0.5	10.7	0.1	1.8	0.3	1.4	0.3	0.6	0.3
50	1	10.0	0.5	4.6	0.1	2.3	0.3	1.6	0.3	0.8	0.3

X Position		Z Position		Ux		Urms		Vrms		Wrms	
Value (cm)	Error (cm)	Value (cm)	Error (cm)	Value (cm/s)	Error (cm/s)	Value (cm)	Error (cm)	Value (cm)	Error (cm)	Value (cm/s)	Error (cm/s)
50	1	10.0	0.5	6.3	0.1	2.7	0.3	1.8	0.3	0.8	0.3
50	1	6.0	0.5	-0.2	0.1	0.5	0.3	0.4	0.3	0.2	0.3
50	1	6.0	0.5	0.0	0.1	0.4	0.3	0.3	0.3	0.2	0.3
80	1	15.0	0.5	7.9	0.1	2.1	0.3	1.5	0.3	0.8	0.3
80	1	10.0	0.5	3.5	0.1	2.8	0.3	2.7	0.3	1.0	0.3
80	1	6.0	0.5	-0.5	0.1	1.7	0.3	1.8	0.3	1.0	0.3
100	1	15.0	0.5	7.8	0.1	2.2	0.3	1.5	0.3	0.8	0.3
100	1	10.0	0.5	3.2	0.1	3.4	0.3	2.4	0.3	0.9	0.3
100	1	6.0	0.5	1.3	0.1	1.9	0.3	2.1	0.3	1.0	0.3
130	1	15.0	0.5	5.6	0.1	2.2	0.3	1.8	0.3	0.9	0.3
130	1	10.0	0.5	5.1	0.1	1.8	0.3	2.0	0.3	0.9	0.3
130	1	6.0	0.5	2.9	0.1	1.5	0.3	1.9	0.3	0.9	0.3
200	1	15.0	0.5	5.8	0.1	1.5	0.3	1.3	0.3	0.7	0.3
200	1	15.0	0.5	3.1	0.1	2.2	0.3	1.2	0.3	0.8	0.3
200	1	10.0	0.5	5.5	0.1	1.3	0.3	1.6	0.3	0.7	0.3
200	1	10.0	0.5	3.7	0.1	3.0	0.3	1.4	0.3	0.8	0.3
200	1	6.0	0.5	4.8	0.1	1.4	0.3	1.4	0.3	0.8	0.3
200	1	6.0	0.5	5.7	0.1	1.4	0.3	1.2	0.3	0.7	0.3
280	1	15.0	0.5	6.2	0.1	1.3	0.3	0.9	0.3	0.6	0.3
280	1	10.0	0.5	7.0	0.1	1.3	0.3	1.1	0.3	0.7	0.3
280	1	6.0	0.5	5.9	0.1	1.3	0.3	1.1	0.3	0.6	0.3
400	1	15.0	0.5	6.7	0.1	1.2	0.3	0.8	0.3	0.5	0.3
400	1	15.0	0.5	7.3	0.1	1.2	0.3	0.8	0.3	0.5	0.3
400	1	10.0	0.5	7.1	0.1	1.2	0.3	1.0	0.3	0.6	0.3
400	1	10.0	0.5	6.7	0.1	1.7	0.3	0.9	0.3	0.6	0.3
400	1	6.0	0.5	6.4	0.1	1.1	0.3	0.9	0.3	0.5	0.3
400	1	6.0	0.5	6.2	0.1	1.2	0.3	0.8	0.3	0.5	0.3
520	1	15.0	0.5	7.1	0.1	1.1	0.3	0.7	0.3	0.4	0.3
520	1	10.0	0.5	7.5	0.1	1.1	0.3	1.0	0.3	0.5	0.3

X Position		Z Position		Ux		Urms		Vrms		Wrms	
Value (cm)	Error (cm)	Value (cm)	Error (cm)	Value (cm/s)	Error (cm/s)	Value (cm)	Error (cm)	Value (cm)	Error (cm)	Value (cm/s)	Error (cm/s)
520	1	6.0	0.5	6.9	0.1	1.1	0.3	0.9	0.3	0.5	0.3
580	1	15.0	0.5	7.4	0.1	1.0	0.3	0.7	0.3	0.4	0.3
580	1	10.0	0.5	7.3	0.1	1.0	0.3	0.8	0.3	0.4	0.3
580	1	6.0	0.5	7.0	0.1	1.1	0.3	0.8	0.3	0.5	0.3
640	1	15.0	0.5	7.5	0.1	1.0	0.3	0.6	0.3	0.4	0.3
640	1	10.0	0.5	7.5	0.1	1.0	0.3	0.7	0.3	0.4	0.3
640	1	6.0	0.5	7.0	0.1	1.1	0.3	0.8	0.3	0.4	0.3
700	1	15.0	0.5	7.4	0.1	1.0	0.3	0.6	0.3	0.4	0.3
700	1	10.0	0.5	7.6	0.1	1.3	0.3	0.7	0.3	0.4	0.3
700	1	6.0	0.5	7.0	0.1	1.0	0.3	0.8	0.3	0.4	0.3
770	1	15.0	0.5	7.5	0.1	1.0	0.3	0.6	0.3	0.4	0.3
770	1	10.0	0.5	7.3	0.1	1.7	0.3	0.8	0.3	0.5	0.3
770	1	6.0	0.5	7.0	0.1	1.0	0.3	0.7	0.3	0.4	0.3

Table 11. Case 4 – Raw velocity data along centerline of flume with standard deviation given.

Flexible Sparse – Case 4											
X Position		Z Position		Ux		Urms		Vrms		Wrms	
Value (cm)	Error (cm)	Value (cm)	Error (cm)	Value (cm/s)	Error (cm/s)	Value (cm/s)	Error (cm/s)	Value (cm/s)	Error (cm/s)	Value (cm/s)	Error (cm/s)
-95	1	15.0	0.5	7.3	0.1	1.5	0.3	1.2	0.3	0.8	0.3
-95	1	10.0	0.5	7.2	0.1	1.6	0.3	1.3	0.3	0.8	0.3
-95	1	6.0	0.5	7.6	0.1	1.4	0.3	1.4	0.3	0.7	0.3
-50	1	15.0	0.5	7.5	0.1	1.4	0.3	1.0	0.3	0.7	0.3
-50	1	15.0	0.5	7.2	0.1	1.6	0.3	1.2	0.3	0.7	0.3
-50	1	10.0	0.5	7.0	0.1	1.6	0.3	1.1	0.3	0.7	0.3
-50	1	10.0	0.5	8.0	0.1	1.3	0.3	1.1	0.3	0.7	0.3
-50	1	6.0	0.5	7.1	0.1	1.5	0.3	1.2	0.3	0.6	0.3
-50	1	6.0	0.5	7.1	0.1	1.4	0.3	1.2	0.3	0.6	0.3
0	1	15.0	0.5	7.3	0.1	1.3	0.3	1.0	0.3	0.6	0.3
0	1	15.0	0.5	7.4	0.1	1.4	0.3	0.9	0.3	0.6	0.3
0	1	10.0	0.5	6.7	0.1	1.5	0.3	1.1	0.3	0.6	0.3
0	1	10.0	0.5	7.6	0.1	1.5	0.3	1.2	0.3	0.7	0.3
0	1	6.0	0.5	6.2	0.1	1.1	0.3	1.0	0.3	0.5	0.3
10	1	15.0	0.5	7.8	0.1	1.4	0.3	1.0	0.3	0.6	0.3
10	1	10.0	0.5	5.7	0.1	2.9	0.3	1.3	0.3	0.6	0.3
10	1	6.0	0.5	0.3	0.1	0.5	0.3	0.4	0.3	0.1	0.3
22	1	15.0	0.5	9.3	0.1	1.8	0.3	1.3	0.3	0.6	0.3
22	1	10.0	0.5	7.7	0.1	2.3	0.3	1.6	0.3	0.6	0.3
22	1	6.0	0.5	4.7	0.1	1.3	0.3	0.9	0.3	0.4	0.3
30	1	15.0	0.5	9.0	0.1	1.5	0.3	1.0	0.3	0.6	0.3
30	1	10.0	0.5	7.1	0.1	1.8	0.3	1.1	0.3	0.5	0.3
30	1	6.0	0.5	0.1	0.1	0.2	0.3	0.2	0.3	0.1	0.3
50	1	15.0	0.5	9.4	0.1	1.5	0.3	0.9	0.3	0.6	0.3
50	1	15.0	0.5	10.7	0.1	1.8	0.3	1.4	0.3	0.6	0.3
50	1	10.0	0.5	4.6	0.1	2.3	0.3	1.6	0.3	0.8	0.3

X Position		Z Position		Ux		Urms		Vrms		Wrms	
Value (cm)	Error (cm)	Value (cm)	Error (cm)	Value (cm/s)	Error (cm/s)	Value (cm/s)	Error (cm/s)	Value (cm/s)	Error (cm/s)	Value (cm/s)	Error (cm/s)
50	1	10.0	0.5	6.3	0.1	2.7	0.3	1.8	0.3	0.8	0.3
50	1	6.0	0.5	-0.2	0.1	0.5	0.3	0.4	0.3	0.2	0.3
50	1	6.0	0.5	0.0	0.1	0.4	0.3	0.3	0.3	0.2	0.3
80	1	15.0	0.5	7.9	0.1	2.1	0.3	1.5	0.3	0.8	0.3
80	1	10.0	0.5	3.5	0.1	2.8	0.3	2.7	0.3	1.0	0.3
80	1	6.0	0.5	-0.5	0.1	1.7	0.3	1.8	0.3	1.0	0.3
100	1	15.0	0.5	7.8	0.1	2.2	0.3	1.5	0.3	0.8	0.3
100	1	10.0	0.5	3.2	0.1	3.4	0.3	2.4	0.3	0.9	0.3
100	1	6.0	0.5	1.3	0.1	1.9	0.3	2.1	0.3	1.0	0.3
130	1	15.0	0.5	5.6	0.1	2.2	0.3	1.8	0.3	0.9	0.3
130	1	10.0	0.5	5.1	0.1	1.8	0.3	2.0	0.3	0.9	0.3
130	1	6.0	0.5	2.9	0.1	1.5	0.3	1.9	0.3	0.9	0.3
200	1	15.0	0.5	5.8	0.1	1.5	0.3	1.3	0.3	0.7	0.3
200	1	15.0	0.5	3.1	0.1	2.2	0.3	1.2	0.3	0.8	0.3
200	1	10.0	0.5	5.5	0.1	1.3	0.3	1.6	0.3	0.7	0.3
200	1	10.0	0.5	3.7	0.1	3.0	0.3	1.4	0.3	0.8	0.3
200	1	6.0	0.5	4.8	0.1	1.4	0.3	1.4	0.3	0.8	0.3
200	1	6.0	0.5	5.7	0.1	1.4	0.3	1.2	0.3	0.7	0.3
280	1	15.0	0.5	6.2	0.1	1.3	0.3	0.9	0.3	0.6	0.3
280	1	10.0	0.5	7.0	0.1	1.3	0.3	1.1	0.3	0.7	0.3
280	1	6.0	0.5	5.9	0.1	1.3	0.3	1.1	0.3	0.6	0.3
400	1	15.0	0.5	6.7	0.1	1.2	0.3	0.8	0.3	0.5	0.3
400	1	15.0	0.5	7.3	0.1	1.2	0.3	0.8	0.3	0.5	0.3
400	1	10.0	0.5	7.1	0.1	1.2	0.3	1.0	0.3	0.6	0.3
400	1	10.0	0.5	6.7	0.1	1.7	0.3	0.9	0.3	0.6	0.3
400	1	6.0	0.5	6.4	0.1	1.1	0.3	0.9	0.3	0.5	0.3
400	1	6.0	0.5	6.2	0.1	1.2	0.3	0.8	0.3	0.5	0.3
520	1	15.0	0.5	7.1	0.1	1.1	0.3	0.7	0.3	0.4	0.3
520	1	10.0	0.5	7.5	0.1	1.1	0.3	1.0	0.3	0.5	0.3

X Position		Z Position		Ux		Urms		Vrms		Wrms	
Value (cm)	**Error (cm)**	**Value (cm)**	**Error (cm)**	**Value (cm/s)**	**Error (cm/s)**	**Value (cm/s)**	**Error (cm/s)**	**Value (cm/s)**	**Error (cm/s)**	**Value (cm/s)**	**Error (cm/s)**
520	1	6.0	0.5	6.9	0.1	1.1	0.3	0.9	0.3	0.5	0.3
580	1	15.0	0.5	7.4	0.1	1.0	0.3	0.7	0.3	0.4	0.3
580	1	10.0	0.5	7.3	0.1	1.0	0.3	0.8	0.3	0.4	0.3
580	1	6.0	0.5	7.0	0.1	1.1	0.3	0.8	0.3	0.5	0.3
640	1	15.0	0.5	7.5	0.1	1.0	0.3	0.6	0.3	0.4	0.3
640	1	10.0	0.5	7.5	0.1	1.0	0.3	0.7	0.3	0.4	0.3
640	1	6.0	0.5	7.0	0.1	1.1	0.3	0.8	0.3	0.4	0.3
700	1	15.0	0.5	7.4	0.1	1.0	0.3	0.6	0.3	0.4	0.3
700	1	10.0	0.5	7.6	0.1	1.3	0.3	0.7	0.3	0.4	0.3
700	1	6.0	0.5	7.0	-	1.0	-	0.8	-	0.4	-
770	1	15.0	0.5	7.5	-	1.0	-	0.6	-	0.4	-
770	1	10.0	0.5	7.3	-	1.7	-	0.8	-	0.5	-
770	1	6.0	0.5	7.0	-	1.0	-	0.7	-	0.4	-

Table 12. Case 4 – Raw deposition data along centerline for each replicate with standard deviation given.

Flexible Sparse – Case 4									
X Position		Net Deposition Replicate 1		Net Deposition Replicate 2		Net Deposition Replicate 3		Mean Net Deposition	
Value (cm)	Error (cm)	Value (g/cm^2)	Error (g/cm^2)	Value (g/cm^2)	Error (g/cm^2)	Value (g/cm^2)	Error (g/cm^2)	Value (g/cm^2)	Error (g/cm^2)
-100	3	0.0023	0.0001	0.0019	0.0001	0.0018	0.0001	0.0020	0.0002
-90	3	0.0008	0.0001	0.0025	0.0001	0.0027	0.0001	0.0020	0.0010
-80	3	0.0019	0.0001	0.0026	0.0001	0.0028	0.0001	0.0024	0.0004
-70	3	0.0006	0.0001	0.0026	0.0001	0.0030	0.0001	0.0020	0.0013
-60	3	0.0009	0.0001	0.0024	0.0001	0.0026	0.0001	0.0020	0.0009
-50	3	0.0022	0.0001	0.0027	0.0001	0.0031	0.0001	0.0026	0.0004
-40	3	0.0012	0.0001	0.0026	0.0001	0.0029	0.0001	0.0022	0.0009
-30	3	0.0021	0.0001	0.0026	0.0001	0.0030	0.0001	0.0026	0.0004
-20	3	0.0022	0.0001	0.0026	0.0001	0.0029	0.0001	0.0026	0.0004
-10	3	0.0025	0.0001	0.0027	0.0001	0.0030	0.0001	0.0027	0.0002
0	3	0.0009	0.0001	0.0027	0.0001	0.0028	0.0001	0.0021	0.0011
2	3	0.0013	0.0001	-	-	-	-	0.0013	-
3	3	-	-	0.0023	0.0001	0.0026	0.0001	0.0024	0.0002
6	3	0.0013	0.0001	0.0024	0.0001	0.0024	0.0001	0.0020	0.0006
9	3	0.0014	0.0001	0.0024	0.0001	0.0024	0.0001	0.0021	0.0006
12	3	0.0013	0.0001	0.0025	0.0001	0.0023	0.0001	0.0020	0.0006
15	3	-	-	0.0024	0.0001	0.0024	0.0001	0.0024	0.0000
16	3	0.0015	0.0001	-	-	-	-	0.0015	-
18	3	-	-	0.0022	0.0001	0.0022	0.0001	0.0022	0.0000
19	3	0.0012	0.0001	-	-	-	-	0.0012	-
22	3	0.0012	0.0001	0.0023	0.0001	0.0024	0.0001	0.0020	0.0007
25	3	-	-	0.0023	0.0001	0.0023	0.0001	0.0023	0.0000
26	3	0.0010	0.0001	-	-	-	-	0.0010	-
28	3	-	-	0.0023	0.0001	0.0021	0.0001	0.0022	0.0001
29	3	0.0018	0.0001	-	-	-	-	0.0018	-
31	3	-	-	0.0021	0.0001	0.0024	0.0001	0.0022	0.0002

X Position		Net Deposition Replicate 1		Net Deposition Replicate 2		Net Deposition Replicate 3		Mean Net Deposition	
Value (cm)	Error (cm)	Value (g/cm2)	Error (g/cm2)	Value (g/cm2)	Error (g/cm2)	Value (g/cm2)	Error (g/cm2)	Value (g/cm2)	Error (g/cm2)
33	3	0.0021	0.0001	-	-	-	-	0.0021	-
35	3	0.0018	0.0001	0.0024	0.0001	0.0022	0.0001	0.0022	0.0003
39	3	0.0008	0.0001	0.0021	0.0001	0.0020	0.0001	0.0016	0.0007
42	3	-	-	0.0024	0.0001	-	-	0.0024	-
43	3	-	-	-	-	0.0022	0.0001	0.0022	-
44	3	0.0017	0.0001	-	-	-	-	0.0017	-
45	3	-	-	0.0026	0.0001	0.0026	0.0001	0.0026	0.0001
50	3	0.0007	0.0001	0.0032	0.0001	0.0033	0.0001	0.0024	0.0015
60	3	0.0018	0.0001	0.0029	0.0001	0.0032	0.0001	0.0026	0.0008
70	3	0.0023	0.0001	0.0027	0.0001	0.0029	0.0001	0.0026	0.0003
80	3	0.0022	0.0001	0.0027	0.0001	0.0028	0.0001	0.0026	0.0003
90	3	0.0023	0.0001	0.0026	0.0001	0.0028	0.0001	0.0026	0.0003
100	3	0.0024	0.0001	0.0026	0.0001	0.0028	0.0001	0.0026	0.0002
110	3	0.0022	0.0001	0.0026	0.0001	0.0027	0.0001	0.0025	0.0002
120	3	0.0023	0.0001	0.0026	0.0001	0.0027	0.0001	0.0025	0.0002
130	3	0.0022	0.0001	0.0025	0.0001	0.0026	0.0001	0.0024	0.0002
140	3	0.0022	0.0001	0.0025	0.0001	0.0025	0.0001	0.0024	0.0002
150	3	0.0021	0.0001	0.0026	0.0001	0.0025	0.0001	0.0024	0.0003
160	3	0.0023	0.0001	0.0024	0.0001	0.0025	0.0001	0.0024	0.0001
170	3	0.0021	0.0001	0.0025	0.0001	0.0024	0.0001	0.0023	0.0002
180	3	0.0022	0.0001	0.0025	0.0001	0.0025	0.0001	0.0024	0.0002
190	3	0.0022	0.0001	0.0025	0.0001	0.0026	0.0001	0.0024	0.0002
200	3	0.0024	0.0001	0.0025	0.0001	0.0026	0.0001	0.0025	0.0001
210	3	0.0023	0.0001	0.0024	0.0001	0.0025	0.0001	0.0024	0.0001
220	3	0.0022	0.0001	0.0024	0.0001	0.0025	0.0001	0.0024	0.0002
230	3	0.0021	0.0001	0.0024	0.0001	0.0026	0.0001	0.0023	0.0003
240	3	0.0021	0.0001	0.0024	0.0001	0.0026	0.0001	0.0024	0.0003

X Position		Net Deposition Replicate 1		Net Deposition Replicate 2		Net Deposition Replicate 3		Mean Net Deposition	
Value (cm)	Error (cm)	Value (g/cm2)	Error (g/cm2)	Value (g/cm2)	Error (g/cm2)	Value (g/cm2)	Error (g/cm2)	Value (g/cm2)	Error (g/cm2)
250	3	0.0022	0.0001	0.0024	0.0001	0.0025	0.0001	0.0024	0.0002
260	3	0.0021	0.0001	0.0026	0.0001	0.0026	0.0001	0.0024	0.0003
270	3	0.0022	0.0001	0.0025	0.0001	0.0026	0.0001	0.0025	0.0003
280	3	-	-	0.0024	0.0001	0.0026	0.0001	0.0025	0.0001
290	3	0.0020	0.0001	0.0024	0.0001	0.0025	0.0001	0.0023	0.0003
300	3	0.0017	0.0001	0.0025	0.0001	0.0026	0.0001	0.0023	0.0005
310	3	0.0021	0.0001	0.0025	0.0001	0.0026	0.0001	0.0024	0.0003
320	3	0.0020	0.0001	0.0025	0.0001	0.0026	0.0001	0.0024	0.0003
330	3	0.0019	0.0001	0.0026	0.0001	0.0026	0.0001	0.0024	0.0004
340	3	0.0022	0.0001	0.0025	0.0001	0.0025	0.0001	0.0024	0.0002
350	3	0.0020	0.0001	0.0025	0.0001	0.0026	0.0001	0.0024	0.0003
360	3	0.0019	0.0001	0.0026	0.0001	0.0027	0.0001	0.0024	0.0004
370	3	0.0023	0.0001	0.0026	0.0001	0.0025	0.0001	0.0025	0.0002
380	3	0.0022	0.0001	0.0026	0.0001	0.0026	0.0001	0.0024	0.0002
390	3	0.0020	0.0001	0.0026	0.0001	0.0026	0.0001	0.0024	0.0003
400	3	0.0021	0.0001	0.0027	0.0001	0.0026	0.0001	0.0025	0.0003
410	3	0.0022	0.0001	0.0026	0.0001	0.0026	0.0001	0.0025	0.0002
420	3	0.0017	0.0001	0.0026	0.0001	0.0025	0.0001	0.0023	0.0005
430	3	0.0021	0.0001	0.0026	0.0001	0.0025	0.0001	0.0024	0.0003
440	3	-	-	0.0026	0.0001	0.0025	0.0001	0.0026	0.0001
450	3	0.0020	0.0001	0.0026	0.0001	0.0025	0.0001	0.0024	0.0003
460	3	0.0019	0.0001	0.0025	0.0001	0.0025	0.0001	0.0023	0.0003
470	3	0.0020	0.0001	0.0026	0.0001	0.0025	0.0001	0.0024	0.0003
480	3	0.0014	0.0001	0.0026	0.0001	0.0025	0.0001	0.0022	0.0006
490	3	0.0022	0.0001	0.0026	0.0001	0.0025	0.0001	0.0024	0.0002
500	3	0.0020	0.0001	0.0025	0.0001	0.0024	0.0001	0.0023	0.0003

X Position		Net Deposition Replicate 1		Net Deposition Replicate 2		Net Deposition Replicate 3		Mean Net Deposition	
Value (cm)	Error (cm)	Value (g/cm2)	Error (g/cm2)	Value (g/cm2)	Error (g/cm2)	Value (g/cm2)	Error (g/cm2)	Value (g/cm2)	Error (g/cm2)
510	3	0.0020	0.0001	0.0026	0.0001	0.0025	0.0001	0.0024	0.0003
520	3	0.0021	0.0001	0.0026	0.0001	0.0025	0.0001	0.0024	0.0003
530	3	0.0022	0.0001	0.0026	0.0001	0.0025	0.0001	0.0024	0.0002
540	3	0.0021	0.0001	0.0025	0.0001	0.0025	0.0001	0.0024	0.0003
550	3	0.0018	0.0001	0.0026	0.0001	0.0026	0.0001	0.0023	0.0004
560	3	0.0022	0.0001	0.0026	0.0001	0.0025	0.0001	0.0024	0.0002
570	3	0.0023	0.0001	0.0025	0.0001	0.0024	0.0001	0.0024	0.0001
580	3	0.0021	0.0001	0.0025	0.0001	0.0025	0.0001	0.0024	0.0002
590	3	0.0021	0.0001	0.0025	0.0001	0.0025	0.0001	0.0024	0.0002
600	3	0.0022	0.0001	0.0025	0.0001	0.0025	0.0001	0.0024	0.0002
610	3	0.0021	0.0001	0.0025	0.0001	0.0025	0.0001	0.0024	0.0002
620	3	0.0023	0.0001	0.0025	0.0001	0.0025	0.0001	0.0024	0.0001
630	3	0.0023	0.0001	0.0025	0.0001	0.0024	0.0001	0.0024	0.0001
640	3	0.0025	0.0001	0.0025	0.0001	0.0024	0.0001	0.0024	0.0001
650	3	0.0023	0.0001	0.0025	0.0001	0.0025	0.0001	0.0024	0.0001
660	3	0.0023	0.0001	0.0025	0.0001	0.0024	0.0001	0.0024	0.0001
670	3	0.0024	0.0001	0.0025	0.0001	0.0024	0.0001	0.0024	0.0000
680	3	0.0022	0.0001	0.0024	0.0001	0.0025	0.0001	0.0024	0.0002
690	3	0.0020	0.0001	0.0025	0.0001	0.0024	0.0001	0.0023	0.0003
700	3	0.0019	0.0001	0.0025	0.0001	0.0024	0.0001	0.0023	0.0004
710	3	0.0019	0.0001	0.0024	0.0001	0.0024	0.0001	0.0023	0.0003
720	3	0.0019	0.0001	0.0024	0.0001	0.0025	0.0001	0.0023	0.0003
730	3	0.0014	0.0001	0.0024	0.0001	0.0025	0.0001	0.0021	0.0006
740	3	0.0017	0.0001	-	-	0.0024	0.0001	0.0021	0.0005
750	3	0.0019	0.0001	-	-	0.0024	0.0001	0.0021	0.0004
760	3	0.0022	0.0001	-	-	0.0025	0.0001	0.0023	0.0002
770	3	-	-	-	-	0.0024	0.0001	0.0024	-
780	3	-	-	-	-	0.0024	0.0001	0.0024	-

X Position		Net Deposition Replicate 1		Net Deposition Replicate 2		Net Deposition Replicate 3		Mean Net Deposition	
Value (cm)	Error (cm)	Value (g/cm2)	Error (g/cm2)	Value (g/cm2)	Error (g/cm2)	Value (g/cm2)	Error (g/cm2)	Value (g/cm2)	Error (g/cm2)
790	3	-	-	-	-	0.0025	0.0001	0.0025	-